TÉCNICO LISBOA

Modelling and experimenting thermal energy storage through the use of PCM in low thermal inertia office

Duarte Pedro Vicente Drumond de Abreu

Thesis to obtain the Master of Science Degree in

Mechanical Engineering

Supervisors: Dr. Rui Pedro da Costa Neto
Dr. Laura Elena Aelenei

Examination Committee

Chairperson: Prof. Edgar Caetano Fernandes
Supervisor: Dr. Rui Pedro da Costa Neto
Member of the Committee: Prof. Carlos Augusto Santos Silva

November 2018

«E o mundo não tem metade
Porque nunca está inteiro (...)»

Uma viagem à Índia, Gonçalo M. Tavares

Acknowledgments

First and foremost, I have to thank my parents Maria Irene and Duarte Drumond for their love and support throughout my life. Thank you both for being caring and teaching me the values of life. My sister Rita deserves my wholehearted thanks as well.

I would like to sincerely thank my thesis advisers, Dr. Rui Costa Neto and Dr. Laura Aelenei, for their continued guidance and precious advices in the course of this thesis. Their patience and encouragement were vital to me.

My gratitude extends as well to Prof. João Gomes Ferreira for borrowing his infrared camera (*Fluke TiR27*), to Engineer Ricardo Gomes for his time devoted to teach me some basics on *EnergyPlus*® and *P*rof. Carlos Silva for funding this thesis consumables.

To my dear friend António Jacques, thank you for this journey which has lasted since we were five years old and will certainly extend for many years to come.

One last thank you to Gonçalo Silva, the best companionship I could have had during these last months.

Resumo

No âmbito desta tese, foram testadas trinta placas *DuPont Energain*® dentro dum contentor situado em Oeiras, Portugal, e caracterizado pela sua baixa inércia térmica. As placas têm um ponto de fusão à volta dos $21.7°C$ e foram instaladas numa estrutura feita especificamente para este trabalho que lhes permitiu estarem suspensas. O seu desempenho foi testado experimentalmente durante o mês de agosto (verão) e posteriormente, com o auxílio destes dados medidos, validada através do uso de *software* de simulação energética em edifícios como o *EnergyPlus*®. Em termos experimentais, foi observado que estas placas têm a capacidade de adiar por três horas picos máximos de temperatura sentidos dentro do contentor em relação aos picos máximos de temperatura exterior. Ainda neste trabalho, foi realizada uma análise de sensibilidade recorrendo ao modelo de *EnergyPlus*®validado anteriormente. Esta análise permitiu observar que peso parâmetros como o ponto de fusão, o nível de ventilação noturna, a espessura, quantidade e localização das placas podem ter no seu desempenho. O melhor cenário encontrado para este caso específico acabou por ser o uso de quarenta e oito placas com um ponto de fusão de $20°C$ e com $10\,mm$ de espessura. Por último mas não menos importante, um simples estudo económico permitiu perceber que apesar das placas demorarem actualmente trinta e dois anos a recuperar o investimento inicial, dentro de alguns anos, quando começarem a ser produzidas em massa, este pode baixar drasticamente para cinco anos.

Palavras-chave: Material de mudança de fase, Inércia térmica, Sistemas de armazenamento de energia térmica, *EnergyPlus*®

Abstract

Within the scope of this thesis, thirty *DuPont Energain*® thermal mass boards were tested inside a shipping container located in Oeiras, Portugal. These phase change material (PCM) boards have a $21.7°C$ melting point and they were experimented during August (Summer) as internal mass due to a structure specifically designed for this project. Results showed that these latent heat storage systems induced an indoor peak temperatures shift of three hours and a slight indoor temperatures reduction. An *EnergyPlus*® model was validated using measured data and several parametric studies were made using this model. In this case, it was found that the best solution for this low thermal inertia enclosure was incorporating forty eight panels with $10\,mm$ of thickness and a melting point of $20°C$. Although these panels have a payback period of thirty two years, in the future it can fall into a more acceptable value of five years.

Keywords: Phase change material, Thermal inertia, Thermal energy storage systems, Buildings applications, *EnergyPlus*®

Contents

List of Tables

List of Figures

Nomenclature

Other Symbols

Δp	Pressure rise $[Pa]$
$\dot{Q}$	Volume flow $\left[dm^3 \cdot s^{-1}\right]$
η	Efficiency $\left[W \cdot W^{-1}\right]$
P_e	Electrical power input $[W]$
SFP	Specific fan power $\left[dm^3 \cdot W^{-1} \cdot s^{-1}\right]$

Physical Variables

ρ	Volumetric mass density $\left[kg \cdot m^{-3}\right]$
A	Surface area $\left[m^2\right]$
L	Length $[m]$
m	Mass of the material $[kg]$
V	Volume $\left[m^3\right]$
v	Velocity $\left[m \cdot s^{-1}\right]$

Thermal Energy Variables

Δh	Number of hours $[h]$
Δh_m	Latent heat of fusion or enthalpy of fusion $\left[J \cdot kg^{-1}\right]$
Δh_r	Heat of reaction or enthalpy of reaction $\left[J \cdot kg^{-1}\right]$
λ	Kappa value or thermal mass value $\left[J \cdot m^{-2} \cdot K^{-1}\right]$
a_m	Fraction of melted material $\left[kg \cdot kg^{-1}\right]$
a_r	Fraction of reacted material $\left[kg \cdot kg^{-1}\right]$
c_p	Specific heat capacity $\left[J \cdot kg^{-1} \cdot K^{-1}\right]$

h_{conv}	Convective heat transfer coefficient $\left[W \cdot m^{-2} \cdot K^{-1}\right]$
h_{rad}	Radiative heat transfer coefficient $\left[W \cdot m^{-2} \cdot K^{-1}\right]$
I	Thermal inertia $\left[J \cdot m^{-2} \cdot K^{-1} \cdot s^{-1/2}\right]$
k	Thermal conductivity $\left[W \cdot m^{-1} \cdot K^{-1}\right]$
Q	Heat stored $[J]$
R	Thermal resistance $\left[K \cdot W^{-1}\right]$
R_{cond}	Thermal resistance for conduction $\left[K \cdot W^{-1}\right]$
R_{conv}	Thermal resistance for convection $\left[K \cdot W^{-1}\right]$
R_{rad}	Thermal resistance for radiation $\left[K \cdot W^{-1}\right]$
T_i, T_f	Initial and final temperature $[K]$
U	Overal heat transfer coefficient $\left[W \cdot m^{-2} \cdot K^{-1}\right]$

Glossary

BS Biological Storage

CES Chemical Energy Storage

CondFD Conduction Finite Difference

COP Coefficient of Performance

CTF Conduction Transfer Function

CVRMSE Coefficient of Variation of the Root Mean Square Error

DSC Differential Scanning Calorimetry

HVAC Heating, Ventilation and Air Conditioning

LHTES Latent Heat Thermal Energy Storage

MAE Mean Absolute Error

MDF Medium Density Fiberboard

ME Maximum Error

MES Mechanical Energy Storage

MS Magnetic Storage

NMBE Normalised Mean Bias Error

NPV Net Present Value

PCM Phase Change Material

PMV Predicted Mean Vote

PV Present Value

PVC Polyvinyl Chloride

PVC-P Plasticized Polyvinyl Chloride

RMSE Root Mean Square Error

SAP Standard Assessment Procedure

SBEM Simplified Building Energy Model

TES Thermal Energy Storage

Chapter 1

Introduction

1.1 Motivation

As the years go by, the world is becoming more energy dependent, planet Earth is running out of fossil fuels and CO_2 emissions are rising faster than ever. Climate change went from theory to reality in few years and humanity is now facing problems such as variation in precipitation patterns, stronger and intenser hurricanes, rises in sea level due to slumps in the amount of ice in the Arctic and overheating temperatures.

By 2050, heating and cooling demand are expected to present values $2.1 - 2.3$ and $3.8 - 4.5$ times higher than the ones registered in 2010 (Gi et al., 2018, [1]) as a result of a $2°C$ rise in mean ground temperatures (Clarke et al., 2018, [2]). In 2010, residential and commercial buildings used 32% and 33% of their total energy consumption for space heating whereas cooling spent more than 2% and 7%. Between now and 2050, residential and commercial buildings are expected to increase their energy consumption by 75% and 83% from $16\,PWh$ and $6\,PWh$ to $28\,PWh$ and $11\,PWh$ respectively (Ürge-Vorsatz et al., 2015, [3]).

In search of a solution for these energy needs growth and decrease in resources trends, new and cleaner energy systems have being built and tested over the years. However, some of those such as solar and wind power are intermittent energy sources which require backup electricity solutions (Schrag, 2018, [4]).

Given this picture, thermal energy storage (TES) systems are assuming an innovative and promising potential to store the excess energy in buildings and release it when needed and consequently discard the use of heat, ventilation and air conditioning (HVAC) or thermal insulators. These systems absorb energy by latent heat storage when a phase change occurs (melting) and discharge it when temperatures fall to a level in which the solidification process can be completed. For this reason, they are commonly named phase change materials (PCM).

1.2 Objectives

Nowadays, some PCM are being incorporated in floors, internal walls, exterior walls, ceilings or used as internal mass systems. These materials have been tested with different specifications and in diversified climates.

The aim of this thesis is to study a specific PCM board, *DuPont Energain®* thermal mass system, and observe the effect it has on an extremely low inertia building in terms of thermal comfort, indoor temperatures reduction, temperatures fluctuation and peak temperatures delay. For this purpose, thirty PCM boards will be installed as internal mass of a shipping container located in Oeiras, Portugal.

Furthermore, this scenario should be modelled and validated using *EnergyPlus®* software in order to perform several parametric studies that could provide an optimal solution for low inertia buildings located in zones with the same type of climate classification.

1.3 Thesis Outline

This thesis is divided into the following main groups: Background, Implementation, Results and discussion and Conclusions. In the first chapter, a review and a state of the art on the topics will be made. Then, in the second chapter, a detailed description on the shipping container structure, material, experimental set up, PCM boards used and the simulation inputs will be presented. In chapter 4, a brief overview of the experimental and simulations results will be displayed and, finally, chapter 5 will end this report by specifying some of the most important knowledges and conclusions learned in the course time of this thesis.

Chapter 2

Background

In this chapter, a state of the art on phase change material (PCM) is done. This chapter begins with a quick review of existing methods to achieve thermal comfort in buildings, indicating not only how this thermal comfort is reached in a passive way but also some types of thermal energy storage. Then a PCM literature review is made evidencing what it is, how it works, its properties, its classification and its building applications. A review on some studies about dynamic simulation of PCMs is also made. In the end, a section is dedicated to recalling some aspects about verification and validation.

2.1 Thermal energy storage

A building can be represented as a thermodynamic system with a balance between energy storage, energy consumption and energy production in that building. This balance is influenced by external (outdoor temperature, wind speed, radiation, sky temperature) and internal solicitations (indoor heat source, ventilation, air conditioning, heating) and also by thermal resistance and heat capacity of a building's envelope (fig. 2.1). For specified conditions, such as climatic, air exchange rate, room size, wall thickness, occupation rate and activity, the indoor air temperature is related to building's thermal resistance and heat capacity [5].

To achieve thermal comfort inside a building, there are three main cooling/heating strategies: active, passive and hybrid. In an active cooling/heating strategy, thermal comfort is dependent of conventional sources of energy, thus using this type of strategy will not only increase the energy consumption but also greenhouse gas emissions. An example of an active cooling/heating strategy is a heating, ventilation and air conditioning system (HVAC). On the other hand, in a passive cooling/heating strategy, only renewable types of energy are used and in consequence there is an improvement of energy conservation, energy efficiency and also in terms of sustainability of the building. The definition of an ideal energy conservation building states that the indoor air temperature should achieve the thermal comfort without heating or air conditioning [6] or, in other words, in a passive way. According to Dincer et al. [7], there are many energy

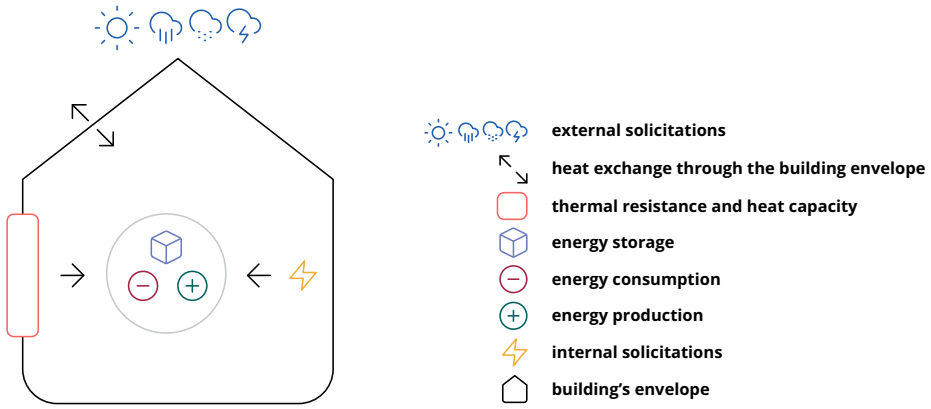

Figure 2.1: Energy balance in a building.

storage systems such as mechanical energy storage (MES), chemical energy storage (CES), biological storage (BS), magnetic storage (MS) and thermal energy storage (TES).

As solar energy is not available at all times, TES systems are used to solve the mismatch between energy supply and energy demand and there are three primary ways to store this type of energy: (a) sensible heat storage, (b) latent heat storage and (c) thermochemical energy storage. In sensible heat storage, thermal energy is saved by changing the temperature of the material. The amount of stored heat, Q, depends on the heat capacity of the material, c_p, the mass of the material, m, and a change between the initial temperature, T_i, and the final one, T_f (eq. 2.1 and fig. 2.2(a)).

$$Q = \int_{T_i}^{T_f} mc_p dT = m\bar{c}_p \left(T_f - T_i\right) , \tag{2.1}$$

In latent heat storage, thermal energy is stored by a reversible phase change in the storage material. Although sensible heat is present in this process, the term which contains the fraction of melted material, a_m, and the latent heat of fusion per unit mass, Δh_m, still predominates (eq. 2.2 and fig. 2.2(b)).

$$Q = \int_{T_i}^{T_m} mc_p dT + ma_m \Delta h_m + \int_{T_m}^{T_f} mc_p dT \approx ma_m \Delta h_m , \tag{2.2}$$

In thermochemical heat storage, thermal energy is stored or released by a reversible endothermic or exothermic reaction process. The amount of heat stored depends on the mass of the material, m, the fraction of material that reacted, a_r, and the heat of reaction per unit mass, Δh_r (eq. 2.3 and fig. 2.2(c)) [8].

$$Q = a_r m \Delta h_r . \tag{2.3}$$

Given these types of TES, latent heat storage is preferable since it provides much higher energy storage density with a lower temperature variation when compared with the sensible heat storage method. Furthermore, thermochemical heat storage technology is at an early stage [9].

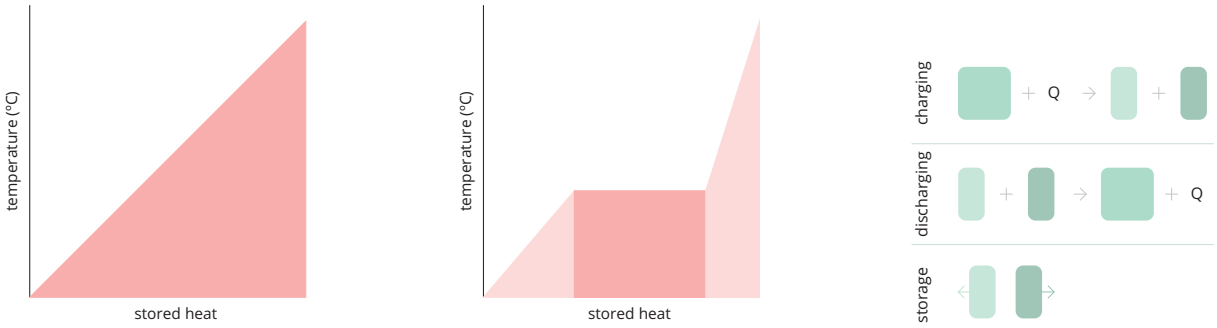

(a) sensible heat storage (b) latent heat storage (c) thermochemical energy storage

Figure 2.2: Methods of thermal energy storage (TES)

2.2 Phase change material

To take advantage of the latent heat storage, the so-called phase change materials (PCM) are used. These materials absorb or release latent thermal energy when there is a change in state. Although it is commonly called a latent heat storage material, it can also store thermal energy in sensible heat.

A PCM can be chosen by its melting/solidifying point or range in order to satisfy the thermal comfort needs. When the melting point is achieved a phase change occurs and the solid PCM becomes liquid by absorbing latent heat. When there is an outdoor temperature drop to the freezing point, the liquid PCM turns solid by releasing the latent heat previously absorbed to the environment and increasing its temperature.

PCMs are a great add-on to lightweight buildings as they increase thermal mass and thus thermal inertia to a building [6]. According to some studies [10], a wall of $25mm$ thickness with PCM can store an equivalent quantity of energy as a $420mm$ thick concrete wall and therefore a PCM wall is better in terms of thermal energy storage efficiency and thermal comfort than a concrete wall [11].

2.2.1 PCM properties

In order to be used in the design of passive latent heat thermal energy storage (LHTES) systems, PCMs should have specific thermophysical, kinetic, chemical, economic and environmental properties. The most important are summarized in the figure 2.3.

Thermophycal speaking, PCMs must fulfil several characteristics. They should have high latent heat of fusion per unit of mass or volume since this means smaller quantities of the material can absorb or release greater quantities of energy allowing lighter building's constructions. High thermal conductivity, k, is another requirement as it leads to faster thermal responses. PCMs should also exhibit no segregation properties in order to maintain the material mixed and in good operating conditions. Moreover, PCMs must keep their shape during phase transition and so having small volume change is a desirable feature. Having high specific heat capacity, c_p, and volumetric mass density, ρ, is another demand since it leads

thermophysical	kinetic	chemical	economic	environment
1 high latent heat of fusion 2 no segregation 3 high thermal conductivity and good heat transfer 4 small volume change on phase change 5 high specific heat capacity 6 suitable phase change temperature in the desired operating temperature range; favourable phase equilibrium 7 congruent melting 8 small vapour pressure at operating temperature	9 little or non-supercooling of the liquid phase 10 high nucleation rate 11 high rate of crystallization 12 long term thermal stability	13 complete reversible melt/freeze cycles 14 no corrosiveness, nontoxic 15 compability with construction materials 16 no flammable	17 abundant 18 cost effective	19 embodied energy 20 recycle potential 21 low environmental impact

Figure 2.3: PCM properties [5, 12].

to a large thermal inertia, I, of the material (eq. (2.6)). Furthermore, PCMs should have a congruent melting to preserve the composition between phase change and small vapour pressures which conducts to a smaller evaporation rate of the material.

In terms of their kinetic properties, PCMs should not suffer from supercooling which means that to solidify the material it must not be at a temperature underneath the melting point. A high supercooling would result in an inappropriate heat extraction. These materials should also create a new structure rapidly when a new phase is triggered by small temperature variations (high nucleation and crystallization rates). On top of that, stability during freezing and melting is important to make heat storage properly [13].

In terms of chemical properties, PCMs should have complete reversible melt/freeze cycles so that no changes in storage capacity occur. Additionally, no corrosiveness, non toxicity and compatibility with construction materials are important to integrate PCMs into buildings. No flammability is another requisite as PCMs are usually exposed to high temperatures.

In terms of economic properties, PCMs should be abundant and cost effective to encourage its use. In terms of environmental properties, PCMs should not require high quantities of energy to be produced, should be recyclable and its production should not have much environmental impact.

2.2.2 PCM classification, advantages and disadvantages

Although the most common PCM type used in building's cooling and heating strategies is a solid-liquid type, it can also be solid-solid, gas-solid and gas-liquid [12]. Furthermore, solid-liquid PCMs can be classified into three main groups: organic, inorganic and eutectic. Figure 2.4 presents not only this classification but also some of the advantages and disadvantages for each type.

The most widely studied and used type of PCMs is the paraffin organic [15] and so its defects are being analysed. A research of nanoinclusions in n-hexadecane alkane PCM in liquid and solid state using cop-

Figure 2.4: PCM classification, advantages and disadvantages [5, 12–14].

per nanowire (CuNWs), multi walled carbon nanotubes (MWCNTs) and graphene nanoplatelets (GNPs) have been made. This investigation showed that the PCM thermal conductivity increases with the concentration of CuNWs, MWCNTs and GNPs, decreases with temperature and stabilizes some degrees below the freezing point [16].

2.3 PCM in building: applications

2.3.1 PCM in building: materials

Hawes et al. [17] concluded that there are three principal ways to integrate PCM in buildings: incorporation, immersion and encapsulation.

In incorporation, the PCM in liquid or powdered form is mixed with materials used in construction such as gypsum, concrete or plaster. This is the most low-priced method of including PCM into building's materials and no further equipment is necessary.

In immersion, the construction material absorbs the melted PCM by capillarity action. In both techniques, there are leakage problems specially after a certain number of thermal cycles and in some cases compatibility issues with construction materials may appear [18].

However, PCM are mostly incorporated into buildings after being encapsulated. In encapsulation, the

PCM is coated or surrounded by a shell. According to Jacob et al. [19], encapsulation classification depends on capsule's diameter: nano-encapsulation $(\varnothing < 1\mu m)$, micro-encapsulation $(1\mu m < \varnothing < 1mm)$ and macro-encapsulation $(1mm < \varnothing < 1cm)$. Although macro-encapsulation is the most widely used type of encapsulation [20], several problems have been reported for this type such as low thermal conductivity and solidification at edges [21]. Micro-encapsulation and nano-encapsulation increase the heat exchange rate [22], decrease PCM reactivity, control volume changes and prevent leakages [23].

Nowadays there are already several PCM commercially manufactured in distinct ways. According to Kenisarin et al. [24], a company called *Teappcm*® produces PCM encapsulated in polyolefin and polypropylene. The capsules can be spheres, cylinders or parallelepiped $1.2\,mm$ thick layers filled with appropriately $180\,ml$ of PCM. On the other hand, *EPS Ltd.*® manufactures spheric $3\,mm$ thick capsules made of stainless steel with a radius of $50\,mm$.

2.3.2 PCM in building: components

In spite of the fact that PCM can be integrated into any element of a building envelope, the most common integrations of PCM are in walls, floors, ceilings, roofs and windows [12]. These integrations into building envelope are usually achieved using wallboards constituted of diverse materials.

Shilei et al. [25, 26] used capric acid and lauric acid PCM to incorporate into a gypsum $400\,mm$ long, $400\,mm$ wide and $9.5\,mm$ thick wallboard for further wall installation, whereas Athienitis et al. [27] studied another type of gypsum board to incorporate in walls, this time soaked into liquid butyl stearate PCM.

In some cases, aluminium boards and other structures were used to incorporate PCM. Kuznik et al. [28] tested cubical cells made of polish aluminium with an internal width and length of $50\,mm$ (Microbat®). One of the faces of this cube was $2\,mm$ thick in order to provide a better heat transfer due to its low thermal resistance. Moreover, Lai et al. [29] proved that aluminium honeycomb wallboards could be effective latent heat storage systems without suffering from heat stratification. In total, the honeycomb wallboard was $100\,mm$ high, $100\,mm$ long and $25.4\,mm$ thick which was thermal and physically suitable to be incorporated in a building wall. Nonetheless, Ahmad et al. [30] experimented a different system constituted by fiber cement, plywood, Polyvinyl Chloride (PVC) panel and PCM in a cell. The idea was to incorporate these cells in walls letting PCM store solar energy while protecting them of external aggressions by a layer of PVC.

In addition to wallboards, in some cases PCM can be integrated directly into concrete. One of those was the specially modified concrete (Mopcon®) in which micro-capsules of Micronal® PCM (5% of PCM by weight) were imbued into fresh typical concrete used to build the walls of one cubicle with $2\,m \times 2\,m \times 3\,m$ [31]. Entrop et al. [32] studied a similar type of concrete with micro-encapsulated PCM, this time in floors. This type of concrete was designed and manufactured with the aim of not affecting its mechanical strength.

Notwithstanding those, some researches even studied PCM cylinders fixed inside bricks which could

reduce the total heat flux by 17.55% [33] and the energy consumption by 15% [34]. Others [35] studied directly immersed PCM into brick pores which could result in a 180° phase temperature delay. Silva et al. [36] tested a brick wall in which PCM were introduced by macro-encapsulation and resulted in an average peak temperatures reduction of $3.5^{\circ}C$. In addition to these, trombe walls, shutters or window blinds [37] and translucent walls [38–40] examples of installation of PCM into building components.

Whether wallboards or other construction materials are used, PCM are integrated into these elements by the methods described in subsection 2.3.1. According to Soares et al. [5], some factors influence the effectiveness of wallboards such as the method used to integrate PCM, the orientation of the wall, climatic conditions, direct solar gains, internal gains, colour of the surface, ventilation rate, PCM chosen, temperatures at which phase change occurs and the latent heat capacity per unit area of the wall.

2.4 PCM in buildings: dynamic simulation

In order to evaluate the effect of using PCM in building components, in the overall thermal behaviour of the building, simulations tools can be used such as BLAST, BSim, DeST, DOE, ECOTECT, Ener-Win, Energy Express, Energy-10, EnergyPlus, eQUEST, ESP-r, IDA-ICE, IES, HAP, HEED, PowerDomus, SUNREL, Tas, TRACE, TRNSYS, among others. From these, EnergyPlus, ESP-r and TRNSYS are the more reliable and versatile ones [5].

2.4.1 EnergyPlus simulations

Pedersen [41] simulated the performance of a $20cm$ thick layer of polystyrene insulation filled with 30% encapsulated octadecane (C18) paraffin PCM in all surfaces of a $140m^2$ building located both in Denver, CO, and Minneapolis, MN, USA, during summer months. The author made simulations of the building using conduction transfer function (CTF) without PCM, finite difference without PCM and finite difference with PCM. The simulations showed that CTF and finite difference without PCM present similar results and that finite difference with PCM improved thermal comfort. It can be concluded that *EnergyPlus*® can generate a simulation of PCMs in any location provided that the other aspects of a detailed energy simulation remain the same. No data was measured.

Shrestha et al. [42] studied the performance of a double wall configuration in a $253m^2$ building located in Oak Ridge, TN from 28^{th} to 31^{st} of May 2011. An *EnergyPlus*®simulation of the building with and without PCM installed in walls was made and data was measured. The walls were made of cellulose with 20% by weight microencapsulated PCM and conduction finite difference solution algorithm was used. The results showed a good agreement between measured and predicted data. Simulation results also showed a 5% reduction in the cooling load due to the use of PCM.

Tardieu et al. [43] made some tests on phase change material with the assistance of *EnergyPlus*®. Two cabins in New Zealand were tested. One of those did not have PCM and the other had an interior

gypsum panel with $27\,\%$ by weight of PCM Rubitherm® with a melting point between $18\,°C$ and $23\,°C$. Experimental results showed PCM reduced inner temperatures fluctuation by $4°C$ and the simulations carried out showed agreement with measured data.

Evola et al. [44] studied a honeycomb PCM panel which consists of paraffin spheres microencapsulated inside an aluminum structure. The panel developed at *French Scientific and Technical Centre for Building* had $20\,mm$ thickness and a melting range of $22\,°C$ to $28.5\,°C$. The effectiveness of the paraffin on thermal comfort was tested through *EnergyPlus*® models using a CondFD solution algorithm. Incorporating phase change materials translated into a reduction of operative temperatures by $2\,°C$. Moreover, night ventilation showed a high correlation with PCM boards performance. Simulation run period was set between the months of June and September using Lyon weather files. A time step of three minutes was considered.

Tabares-Velasco et al. [45] conducted some *EnergyPlus*® tests on several types of PCM such as PCM insulation ($20\,\%$ by weight of microencapsulated paraffin), PCM drywall ($30\,\%$ by weight of microencapsulated paraffin) and a concentrated thin PCM layer ($100\,\%$ by weight of microencapsulated paraffin). The main goal of these tests was to verify phase change material modules' accuracy instead of the benefits of including PCM in construction materials. Using CondFD (fully implicit) and CTF Heat Balance solution algorithms, the authors tested different values of time steps and node spacing. The two buildings model was located in Phoenix, AZ. For better results when including PCM in *EnergyPlus*®, it should be used a time step lower or equal than three minutes and a node grid spacing of one for accurate hourly values. Results can be affected when using PCM panels with high hysteresis values. Overall, CondFD presented verisimilitude values.

Evola et al. [46] studied an aluminium honeycomb panel with $60\,\%$ microencapsulated paraffin (Micronal T23®). Three wallboards were incorporated inside interior walls of a room with an area of $17.5\,m^2$. Chambery, France, and Catania, Italy, were the locations selected to run the model. Tests were performed during Summer time (June-September) and the main goal was to study the effect of this material in hot Mediterranean climate. *EnergyPlus*® model used a CondFD solution algorithm (fully implicit) with a two minute time step and a node spacing of two. Overall, although its performance highly depended on climate conditions, season and type, melting point and quantity, PCM lead to a greater thermal comfort, since surface temperatures reduced from $29.7°C$ to $28°C$ and temperatures amplitude went from $5.7°C$ to $2.9°C$.

Sage-Lauck et al. [47] carried out some experiments on microencapsulated PCM (BioPCM®). The tests were taken in a medium thermal inertia building in Portland, OR, USA, during the Summer period (1^{st} June - 30^{th} September). The *EnergyPlus*® model was validated using measured data. The Heat Balance algorithm used by the software had time step of one minute and a node spacing of three. Several scenarios were tested such as the effect of incorporating PCM on walls, their melting point temperatures and their location. It was concluded that PCM may not benefit from outside temperatures above $38\,°C$ as it hinders its solidification and therefore the latent heat release effectiveness. Moreover,

adding PCM resulted in a reduction of $1°C$ in peak temperatures. On the other hand, placing PCM in interior walls reduced overheat by 60% and PCM with a melting point below $25°C$ that had an adverse effect on thermal comfort.

Soares et al. [48] optimized *DuPont Energain*® drywalls (walls and ceiling) in residential rooms for different climates such as Seville, Spain (Csa), Coimbra, Portugal (Csb), Milan, Italy (Cfa), Paris, France (Cfb), Bucharest, Romania (Dfa), Warsaw, Polonia (Dfb), and Kiruna, Sweden (Dfc). Tests were carried out during a year, using a CondFD fully implicit scheme solution algorithm with a time step of three minutes. It was shown that the optimal PCM board thickness was $40\,mm$ in all cases. Moreover, a melting point of $22°C$-$26°C$ and $18°C$-$24°C$ should be chosen for Summer and Winter, respectively. It was also concluded that energy savings due to use of PCM boards were higher in warmer climates.

Jiao et al. [49] studied the effect of ventilation both with outdoor and indoor air on a room with PCM incorporated in ceiling, floor and walls. Furthermore, phase change temperature, PCM thickness and heat conductivity coefficient were also studied during the hottest Summer days in Shanghai, China. Results showed that a PCM layer with $27\,°C$, thin and with high conductivity values performs better for this weather. Night ventilation should also be considered given that it contributed to a better latent heat release.

Marin et al. [50] studied the effectiveness of Knauf plasterboard filled with 18% Micronal® PCM microcapsules with a melting point of $25°C$. These boards were incorporated in the inner part of exterior walls and roof of a building with an area of $5.76\,m^2$. To perform this study, the CondFD (fully implicit) Heat Balance solution algorithm was used with a time step of one minute and node spacing of three. Several cities were studied such as Brasilia, Brasil (Aw), Kuala Lumpur, Malaysia (Af), Singapore (Af), Albuquerque, NM, USA (BsK), Mexico, Mexico (BsK), New Delphi, India (BSh), Abu Dhabi, UAE (BWh), Calama, Chile (BWk), Brisbane, Australia (Cfa), Madrid, Spain (Cfa), Tokyo, Japan (Cfa), Berlin, Germany (Cfb), Johannesburg, South Africa (Cfb), Antofagasta, Chile (Csb), Auckland, New Zealand (Csb), Bogotá, Colombia (Csb), Concepcion, Chile (Csb), Quito, Ecuador (Csb), San Francisco, California, USA (Csb), Santiago de Chile, Chile (Csb), Chicago, IL, USA (Dfa), Montreal, Canada (Dfb), Moscow, Russia (Dfb), Stockholm, Sweden (Dfb), and Beijing, China (Dwa). Although it was observed that lightweight buildings benefited from incorporating PCM, there was still a time interval where thermal comfort was not met. In tropical climates such as the one present in Kuala Lumpur, installing PCM decreased the amount of hours thermal comfort was satisfied.

A NewMass® system was studied by Yang et al. [51]. This was a new type of PCM with a melting point of $21°C$ incorporated inside of a group of cylinders. These tubes were placed below the ceiling of two classrooms in the North-West London and measured data was used to validate the *EnergyPlus*® model. A CondFD was included in the software and the results showed that including this cooling system can save 36% of energy.

Saffari et al. [52] simulated a low thermal inertia building in Madrid, Spain (Csa) with an area of $48\,m^2$. PCM panels were installed in the inner part of exterior walls and ceiling. The panels studied were

compact storage modules filled with Rubitherm® organic PCM with melting point values of $23°C$, $25°C$ and $27°C$. These panels had thickness values of $5\,mm$ and $10\,mm$. Incorporating these cooling system resulted on cooling savings and the highest melting point panel had the best payback period with 2-3 years and 6-8 years for residential and office buildings respectively.

Jamil et al. [53] performed some experimental and simulation tests on a house located in Melbourne, Australia. The aim of this study was to understand the effect that a mat with polyfilm macroencapsulated fatty-acid organic PCM (BioPCM Q25®) had in terms of thermal comfort improvement. This PCM was installed in the ceiling of the building and had a melting point of $25°C$. Validation data was gathered from the 23^{rd} of January to the 13^{th} of March. When simulating with and without PCM, CondFD (with a time step of two minutes) and CTF solution algorithms were used. Moreover, a Ground Heat Transfer function were added to model energy transfer between ground and indoor floor. It was proven that this system reduced mean indoor temperatures by $1.1°C$ and that it could drop thermal discomfort hours by $34\,\%$. Furthermore, installing PCM in ceilings and walls instead of only ceilings increased the effectiveness of this cooling system.

Ozdenefe et al. [54] studied the thermal behaviour of a traditional building in Cyprus. This two-story building with an area of $186\,m^2$ had several rooms with different thermal inertia enclosures. All of these were tested with and without PCM. Tests were taken between the 1^{st} of May and the 31^{st} of October. The *EnergyPlus*® model used CTF and CondFD (fully implicit) solution algorithms. The PCM used was a polymer with 26% by weight microencapsulated in wallboards with a melting point of $26°C$. For all the scenarios, there was a maximum temperature reduction due to PCM incorporation. Moreover, it was seen that adding thermal capacity to a building translated into a decrease of the indoor temperature fluctuation. On the other hand, diminishing this thermal capacity results into a rise of the cooling energy demand.

Lei et al. [55] simulated a installation of PCM on the inner surfaces of exterior walls in a room in Singapore with an area of $9\,m^2$. The study was done in two different modalities: one that took weather from only a day (30^{th} of July) and other that used year-round weather data. Several melting points were considered for this cooling system with a thickness of $10\,mm$. For the CondFD algorithm, a time step of one minute and a space discretization of one were set. This experiment showed that PCM reduced heat gains by $4.5\,\%$ on the 30^{th} of July and an yearly reduction of $21\% - 32\%$.

Nghana et al. [56] tested the incorporation of PCM in a lightweight residential building at the British Columbia Institute of Technology Burnaby Campus. The mat paraffin BioPCM® with a melting point of $23\,°C$ was installed in the interior part of exterior walls. Results showed that PCM increased the heating demand savings by $57\,\%$ during Winter. On the other hand, no improvement in thermal comfort was registered during Summer nights, concluding that Winter season was the most appropriate for this latent release system.

Auzeby et al. [57] experimented two different weather files (real data and data from Prometheus Project) to simulate the effect that installing PCM had on a residential building located in England during Sum-

mer time. Four different scenarios were tested such as low insulation with and without PCM and high insulation with and without PCM. The PCM was a shape-stabilized compost of paraffin encapsulated by high density polyethylene. This cooling system was installed in external walls and it was proved that it was capable of reducing overheating by $20\% - 25\%$ when a high insulation scenario was set. In addition, it was shown that PCM were more effective on lightweight buildings than in the others since its impact was more evident.

Zhou et al. [58] made some experiments on *DuPont Energain*® thermal mass systems installed in a lightweight office in Birmingham, England. The office had an area of $96\,m^2$ and these boards were installed in both its external and internal walls. These panels had a thickness of $10\,mm$ and a yearly analysis was made focusing in Summer season (May-September). To model this scenario, CondFD and CTF solution algorithms were used. It was concluded that these type of cooling system suited well when their melting point was fairly higher than mean indoor temperatures with an optimal melting temperature range around $23°C - 24°C$. Furthermore, thermal conductivity of these materials should be upgraded since this improved their effectiveness. Results also showed that incorporating these boards in external walls rather than on internal fitted better in terms of thermal comfort. Nonetheless, installing PCM in both external and internal saved the cooling consumption in the hottest month by 20%.

Ramakrishnan et al. [59] ran some simulations on a house in Australia using different locations (Melbourne, Sydney, Brisbane and Perth). Below this house's ceiling, a BioPCM® was incorporated between the insulation and plasterboard. Experiments lasted two days (1^{st}-2^{nd} December). The melting points considered were $23°C$, $25°C$ and $27°C$ and PCM mat had thickness values of $3.75\,mm$, $7.5\,mm$, $12.5\,mm$, $21\,mm$ and $30\,mm$. Different values for night ventilation were also analysed. Studies showed that increasing PCM thickness could result in thermal comfort improvement but at the same time effective thermal energy storage efficiency could fall. The optimal night ventilation value for all the cities studied was $4\,ACH$ once it caused improvements in the storage efficiency in a range of 5%-33%.

Mi et al. [60] studied an office building in Shenyang, Zhengzhou, Changsha, Kunming and Hong Kong (China). Each floor of the high thermal inertia building modelled had an area of $646.58\,m^2$ and the PCM were installed in the interior layer of walls. The PCM used had a melting point of $27°C$ and it was sufficient to reduce higher temperatures. Energy savings during summer due to the use of PCM were $244.309\,kWh$, $1541.209\,kWh$, $2352.555\,kWh$, $1.803\,kWh$ and $2160.128\,kWh$ while for both Winter and Summer were $42987.73\,kWh$, $23141.05\,kWh$, $17845.04\,kWh$, $7843.72\,kWh$ and $3798.34\,kWh$ for Shenyang, Zhengzhou, Changsha, Kunming and Hong Kong, respectively. However, the payback was too high to make it a good investment.

Long et al. [61] studied the effect of PCM on two low thermal inertia enclosures ($0.8\,m^2$) located in Chengdu, China. One of these was tested with a $20\,mm$ thickness PCM layer on the inner layer of the external walls and the other without. Experimental data was measured in order to validate the *EnergyPlus*® model. The simulations were made with a run period of a year and the authors concluded that PCM did not have an impressive performance for hot summers. However, an average temperature

drop ($8.5°C$) could be verified as well as its delay due to the incorporation of PCM (3.25 hours). Moreover, PCM could decrease indoor surface temperatures ($9.8°C$).

This time Soares et al. [62] studied the *DuPont Energain*® thermal mass system for a high thermal inertia building in Kuwait. This building had an area of $48\,m^2$ and PCM boards were incorporated on inner surfaces of walls and ceiling. A sensitivity analysis on the PCM melting point and its thickness was carried out. The conclusion was that the $40\,mm$ thickness wallboard with a $24\,°C$ melting point was the best option since it resulted in the lowest energy cooling demand ($124\,kWh \cdot m^{-2} \cdot year^{-1}$). Nevertheless, the $20\,mm$ wallboard should be considered when costs are taken into account.

Alam et al. [63] studied the effect that BioPCM® had on an australian duplex located in Melbourne. PCM boards were installed in the ceiling with an area of $326\,m^2$. Simulations were taken between the 26^{th} of February and the 3^{rd} of March. A time step of two minutes was set for the CondFD solution algorithm. This add-on together with a free cooling application promoted a temperature reduction of $1.8\,°C$ during Summer when compared to the $0.5°C$ decrease obtained by using PCM in a passive way. Although there was also a considerable reduction of the indoor ceiling temperature, zone temperatures did not reduced proportionally. It was observed that this PCM suffered from poor solidification at night.

Devaux et al. [64] studied both a floor made of gypsum board with 24% by weight of PCM and walls and ceilings with *DuPont Energain*® wallboards. The studied house was located in Tamaki Campus of University of Auckland, New Zealand. The building was a low thermal inertia house with an area of $7\,m^2$ and the simulation was made using a run period from the 7^{th} to the 16^{th} of September. It was concluded that there was a peak load shifting ($2.5\% - 9\%$), a cost saving of 42% and an energy saving of 32%.

Kharbouch et al. [65] investigated the impact that the incorporation of BioPCM™ in walls and ceiling of a house located in Morocco had on its cooling and heating thermal energy demand. The PCM fabricated by Phase Change Energy Solutions Company consisted of a macroencapsulated material available in five different melting temperatures ($21°C$, $23°C$, $25°C$, $27°C$, $29°C$) and two distinct surface density or quantity such as $2.7\,kg \cdot m^2$ and $4.9\,kg \cdot m^2$ which correspond to a thickness of $10\,mm$ and $15\,mm$. The residential building modelled by *EnergyPlus*® had seven rooms and the authors tested it in six different Moroccan climate zones: Tangier, Fes, Ifrane, Marrakech, Errachidia and Agadir. In terms of cooling and heating savings, the optimum melting temperature fell within the range of $21°C$ and $25°C$. Indeed, the warmer the climate the higher the melting point temperature. In the same way, the optimum PCM surface density was $4.9\,kg \cdot m^2$, both for walls and ceiling. On the other hand, in terms of cost-effectiveness optimisation results, the best option was using a PCM with a surface density of $2.7\,kg \cdot m^2$ and a melting temperature of $25°C$ or $27°C$.

For the purpose of comparing further results of this thesis with previous research outcomes aforementioned, a summary table condense their information on PCM type, installation, simulation inputs and respective conclusions (table 2.1).

Table 2.1: Dynamic *EnergyPlus*® simulations.

Info	PCM	Installation	Simulation	Conclusions
year: 2007 **citation:** [41]	**name:** octadecane **model:** — **formula:** $C_{18}H_{38}$ **type:** paraffin (organic) **wt%:** 30 **melt. point** $(^{\circ}C)$**:** 28 **integration:** encapsulation **o.m.:** polystyrene insulation **thk. (mm):** 200	**surfaces:** walls **space:** building **area:** $140\,m^2$ **city:** Denver, USA; Minneapolis, USA **period:** June, July, August, September **season:** Summer	**algorithms:** CTF, CondFD **schemes:** — **time step:** — **nodes:** — **validation:** ○	-simulation of the PCM can be made in any location -accurate accounting for the phase change enthalpy
year: 2011 **citation:** [42]	**name:** fire-resistive PCM **model:** — **formula:** — **type:** organic **wt%:** 20 **melt. point** $(^{\circ}C)$**:** 27.5-31.5 **integration:** microencapsulation **o.m.:** cellulose **thk. (mm):** 180, 102	**surfaces:** interior layer of walls, attic floor **space:** building **area:** $253\,m^2$ **city:** Oak Ridge, USA **period:** 28^{th} May-31^{st} May 2011 **season:** Spring	**algorithms:** CondFD **schemes:** — **time step:** — **nodes:** — **validation:** ●	-good agreement between measured and predicted heat flux -5% reduction in the cooling load due to PCM
year: 2011 **citation:** [43]	**name:** RT 21 **model:** Rubitherm® GmbH RT 21 **formula:** $C_{17}H_{34}$ **type:** paraffin (organic) **wt%:** 27 **melt. point** $(^{\circ}C)$**:** 18-23 **integration:** incorporation **o.m.:** gypsum **thk. (mm):** 4	**surfaces:** walls, ceiling **space:** building **area:** $6.76\,m^2$ **city:** Auckland, New Zealand **period:** 20^{th} February-4^{th} March **season:** Summer	**algorithms:** CondFD **schemes:** — **time step:** — **nodes:** — **validation:** ●	-good agreement between measured and predicted heat flux -4% reduction in indoor temperature fluctuation due to PCM -improvement on thermal inertia and on capturing solar energy
year: 2011 **citation:** [44]	**name:** octadecane **model:** honeycomb PCM panel **formula:** $C_{18}H_{38}$ **type:** paraffin (organic) **wt%:** — **melt. point** $(^{\circ}C)$**:** 27.6 **integration:** microencapsulation $(\varnothing = 5\mu m)$ **o.m.:** aluminium honeycomb structure **thk. (mm):** 20	**surfaces:** inside interior walls **space:** room **area:** $17.5m^2$ **city:** Lyon, France **period:** June-September **season:** Summer	**algorithms:** CondFD **schemes:** — **time step:** $3'$ **nodes:** — **validation:** ○	-night ventilation is highly important to remove latent heat -when choosing PCM panels a careful analysis of its type must be made
year: 2012 **citation:** [45]	**name:** distributed PCM in the insulation, distributed PCM in drywall, concentrated PCM **model:** — **formula:** — **type:** — **wt%:** 20, 30, 100 **melt. point** $(^{\circ}C)$**:** 29.4-29.6 **integration:** microencapsulation, microencapsulation, concentration **o.m.:** — **thk. (mm):** 105, 20, 5	**surfaces:** inside interior walls **space:** building **area:** $231m^2$ **city:** Phoenix, USA **period:** annual **season:** all	**algorithms:** CTF, CondFD **schemes:** — **time step:** $\leq 3'$ **nodes:** ≤ 3 (annual); ≤ 1 (hourly) **validation:** ○	-CondFD presents accurate results -PCM with strong hysteresis are not well modelled by *EnergyPlus*®

Table 2.1: Dynamic *EnergyPlus*® simulations.

Info	PCM	Installation	Simulation	Conclusions
year: 2013 **citation:** [46]	**name:** octadecane **model:** BASF Micronal® T23 **formula:** $C_{18}H_{38}$ **type:** paraffin (organic) **wt%:** 60 **melt. point** $(^{\circ}C)$**:** 27.6 **integration:** microencapsulation **o.m.:** aluminium honeycomb structure **thk. (mm):** 20	**surfaces:** three interior walls **space:** room **area:** $17.5m^2$ **city:** Chambery, France; Catania, Italy **period:** June-September **season:** Summer	**algorithms:** CondFD **schemes:** — **time step:** $2'$ **nodes:** 2 **validation:** ○	-PCM effectiveness depends on its type, melting point and quantity as well as climate and season type
year: 2014 **citation:** [47]	**name:** — **model:** BioPCM25® **formula:** — **type:** paraffin (organic) **wt%:** — **melt. point** $(^{\circ}C)$**:** 25 **integration:** microencapsulation **o.m.:** refined soy, palm kernel oils **thk. (mm):** —	**surfaces:** drywall and interior layer of interior walls **space:** apartment **area:** $145m^2$ **city:** Portland, USA **period:** 1^{st} June-30^{th} September **season:** Summer	**algorithms:** CondFD **schemes:** **time step:** $1'$ **nodes:** 3 **validation:** ●	-outside temperatures above $38^{\circ}C$ not allow night solidification -incorporating PCM may reduce peak temperatures by $1\,^{\circ}C$ -PCM on interior walls may reduce overheat by $60\,\%$ -melting point should be higher than $25\,^{\circ}C$ $(50\,\%$ overheat reduction); lower than that can make thermal comfort worst
year: 2014 **citation:** [48]	**name:** heptadecane **model:** *DuPont Energain*® thermal mass systems **formula:** $C_{17}H_{36}$ **type:** paraffin (organic) **wt%:** 60 **melt. point** $(^{\circ}C)$**:** 18, 20, 22, 24, 26, 28 **integration:** microencapsulation **o.m.:** ethylene based polymer, aluminium **thk. (mm):** 5.2	**surfaces:** walls, ceiling **space:** room **area:** $48\,m^2$ **city:** Seville, Spain; Coimbra, Portugal; Milan, Italy; Paris, France; Bucharest, Romania; Warsaw, Poland; Kiruna, Sweden **period:** annual **season:** all	**algorithms:** CondFD **schemes:** fully implicit **time step:** $1'$ **nodes:** 3 **validation:** ○	-optimum thickness is $40\,mm$ -warmer climate melting point range: $22\,^{\circ}C$-$26\,^{\circ}C$ -colder climates melting point range: $18\,^{\circ}c$ -$24\,^{\circ}C$ -energy savings higher in hot climates
year: 2015 **citation:** [49]	**name:** — **model:** — **formula:** — **type:** — **wt%:** — **melt. point** $(^{\circ}C)$**:** 25, 26, 27, 28 **integration:** **o.m.:** — **thk. (mm):** 20, 40, 60, 80	**surfaces:** ceiling, floor, walls **space:** room **area:** $16.32m^2$ **city:** Shanghai, China **period:** 19^{th} July - 7^{th} August **season:** Summer	**algorithms:** — **schemes:** — **time step:** — **nodes:** — **validation:** ○	-PCM with $27^{\circ}C$ melting point, thinner and with large thermal conductivity performs better for Summer days in Shanghai -night ventilation improves night's latent heat release

Table 2.1: Dynamic *EnergyPlus*® simulations.

Info	PCM	Installation	Simulation	Conclusions
year: 2016 **citation:** [50]	**name:** — **model:** Knauf plasterboard with Micronal® PCM **formula:** — **type:** — **wt%:** 18 **melt. point** $(^{\circ}C)$**:** 25 **integration:** microencapsulation **o.m.:** gypsum **thk. (mm):** 12.5	**surfaces:** exterior walls, roof **space:** building **area:** $5.76m^2$ **city:** Brasilia, Brasil; Kuala Lumpur, Malaysia; Singapore; Albuquerque, New Mexico, USA; Mexico, Mexico; New Delphi, India; Abu Dhabi, UAE; Calama, Chile; Brisbane, Australia; Madrid, Spain; Tokyo, Japan; Berlin, Germany; Johannesburg, South Africa; Antofagasta, Chile; Auckland, New Zealand; Bogotá, Colombia; Concepcion, Chile; Quito, Ecuador; San Francisco, California, USA; Santiago de Chile, Chile; Chicago, Illinois, USA; Montreal, Canada; Moscow, Russia; Stockholm, Sweden; Beijing, China **period:** annual **season:** all	**algorithms:** CondFD **schemes:** fully implicit **time step:** $1'$ **nodes:** 3 **validation:** ○	-energy savings are higher in lightweight buildings
year: 2016 **citation:** [51]	**name:** polyethylene glycol 600 **model:** NewMass® PCM cooling system with SP21 **formula:** $H(OC_2H_2)_n \cdot OH$ **type:** fatty acid (inorganic) **wt%:** **melt. point** $(^{\circ}C)$**:** 21 **integration:** incorporation **o.m.:** salt water, additives **thk. (mm):** —	**surfaces:** ceiling **space:** two classrooms **area:** — **city:** London, England **period:** 14^{th}July - 20^{th}July, 15^{th}September - 21^{st}September **season:** Summer	**algorithms:** CondFD **schemes:** CondFD **time step:** — **nodes:** — **validation:** ●	-36% energy savings
year: 2016 **citation:** [52]	**name:** RT 23, RT 25, RT 27 **model:** Rubitherm® CSM **formula:** — **type:** paraffin (organic) **wt%:** — **melt. point** $(^{\circ}C)$**:** $23, 25, 27$ **integration:** macroencapsulation **o.m.:** aluminium **thk. (mm):** $5, 10$	**surfaces:** exterior walls, roof **space:** building **area:** $48m^2$ **city:** Madrid, Spain **period:** annual **season:** all	**algorithms:** CondFD **schemes:** — **time step:** — **nodes:** — **validation:** ○	-considerable energy cooling savings -best payback for panels with a melting point of $27\ ^{\circ}C$ with 2-3 years and 6-8 years for residential and office buildings respectively

Table 2.1: Dynamic *EnergyPlus*® simulations.

Info	PCM	Installation	Simulation	Conclusions
year: 2016 **citation:** [53]	**name:** polyethylene glycol 600 **model:** BioPCM Q25® **formula:** $H(OC_2H_2)_n \cdot OH$ **type:** fatty-acid (organic) **wt%:** — **melt. point** $(^\circ C)$**:** 25 **integration:** macroencapsulation **o.m.:** mat with polyfilm **thk. (mm):** —	**surfaces:** walls, ceiling **space:** building **area:** $326\,m^2$ **city:** Melbourne, Australia **period:** 23^{rd}January - 13^{th}March **season:** Summer, Autumn	**algorithms:** CTF, CondFD **schemes:** — **time step:** $2'$ **nodes:** — **validation:** ●	-$1.1\,^\circ C$ mean indoor temperature reduction -$34\,\%$ reduction in thermal discomfort hours -installing PCM in ceilings and walls is more efficient than only ceilings
year: 2016 **citation:** [54]	**name:** p-Lattic acid **model:** — **formula:** $C_3H_6O_3$ **type:** paraffin (organic) **wt%:** 26 **melt. point** $(^\circ C)$**:** 26 **integration:** microencapsulation $\varnothing = 5\mu m$ **o.m.:** polymer wallboards **thk. (mm):** 15	**surfaces:** walls, ceiling **space:** building **area:** $186\,m^2$ **city:** Cyprus **period:** 1^{st}May - 31^{st}October **season:** Spring, Summer	**algorithms:** CTF, CondFD **schemes:** CondFD **time step:** $3'$ **nodes:** 3 **validation:** ●	-peak temperatures reduction -increasing thermal capacity reduces temperature fluctuation -decreasing thermal capacity increase cooling energy demand
year: 2016 **citation:** [55]	**name:** heptadecane **model:** — **formula:** $C_{18}H_{38}$ **type:** paraffin (organic) **wt%:** — **melt. point** $(^\circ C)$**:** 28 **integration:** — **o.m.:** — **thk. (mm):** 10	**surfaces:** exterior walls **space:** building **area:** $9\,m^2$ **city:** Singapore **period:** 30^{th}July, annual **season:** all	**algorithms:** CondFD **schemes:** **time step:** $1'$ **nodes:** 1 **validation:** ○	-peak temperatures reduction -reduction of heat gains by 4.5% on a single day -reduction of heat gains by $21\% - 32\%$ yearly
year: 2016 **citation:** [56]	**name:** — **model:** BioPCM23® **formula:** — **type:** paraffin (organic) **wt%:** — **melt. point** $(^\circ C)$**:** 23 **integration:** microencapsulation **o.m.:** — **thk. (mm):** —	**surfaces:** exterior walls **space:** building **area:** $192\,m^2$ **city:** Canada **period:** annual **season:** all	**algorithms:** CondFD **schemes:** **time step:** **nodes:** **validation:** ○	-$57\,\%$ heating savings during Winter -no thermal comfort improvement in Summer nights -this PCM is better for Winter than for Summer
year: 2016 **citation:** [57]	**name:** — **model:** — **formula:** — **type:** shape-stabilized paraffin (organic) **wt%:** — **melt. point** $(^\circ C)$**:** $23.1^\circ C$-$24^\circ C$ **integration:** encapsulation **o.m.:** high density polyethylene **thk. (mm):** 200	**surfaces:** exterior walls **space:** building **area:** $192\,m^2$ **city:** Nottinghamshire, England **period:** July **season:** Summer	**algorithms:** CondFD **schemes:** — **time step:** — **nodes:** — **validation:** ○	-overheating reduction

Table 2.1: Dynamic *EnergyPlus*® simulations.

Info	PCM	Installation	Simulation	Conclusions
year: 2016 **citation:** [58]	**name:** heptadecane **model:** *DuPont Energain*® thermal mass systems **formula:** $C_{17}H_{36}$ **type:** paraffin (organic) **wt%:** 60 **melt. point** $(^{\circ}C)$**:** 21.7 **integration:** microencapsulation **o.m.:** ethylene based polymer, aluminium **thk. (mm):** 10	**surfaces:** exterior walls, interior walls **space:** office building **area:** $96\,m^2$ **city:** Birmingham, England **period:** May-September **season:** Summer	**algorithms:** CondFD, CTF **schemes:** — **time step:** — **nodes:** — **validation:** ○	-PCM has a better performance in external walls than in interior walls in terms of energy savings
year: 2016 **citation:** [59]	**name:** — **model:** BioPCM® **formula:** — **type:** fatty acid **wt%:** — **melt. point** $(^{\circ}C)$**:** $23, 25, 27$ **integration:** macroencapsulation **o.m.:** — **thk. (mm):** $3.75,\ 7.5,\ 12.5,\ 21,\ 30$	**surfaces:** ceiling **space:** residential living room **area:** $16\,m^2$ **city:** Melbourne, Sydney, Brisbane, Perth (Australia) **period:** 1^{st}-2^{nd} December **season:** Summer	**algorithms:** CondFD **schemes:** **time step:** $1'$ **nodes:** — **validation:** ○	-peak temperatures reduction -daily fluctuation reduction -thermal comfort improvement $-30-50$ year payback
year: 2016 **citation:** [60]	**name:** — **model:** — **formula:** — **type:** — **wt%:** — **melt. point** $(^{\circ}C)$**:** 27 **integration:** incorporation **o.m.:** — **thk. (mm):** 10	**surfaces:** exterior walls **space:** building **area:** $182.46\,m^2$ **city:** Shenyang, Zhengzhou, Changsha, Kunming, Hong Kong (China) **period:** **season:**	**algorithms:** CondFD **schemes:** — **time step:** $2'$ **nodes:** — **validation:** ○	-peak temperatures reduction -payback makes the project not sustainable
year: 2017 **citation:** [61]	**name:** — **model:** — **formula:** — **type:** — **wt%:** — **melt. point** $(^{\circ}C)$**:** 18-26 **integration:** encapsulation **o.m.:** — **thk. (mm):** 20	**surfaces:** exterior walls **space:** enclosure **area:** $0.8\,m^2$ **city:** Chengdu, China **period:** annual **season:** all	**algorithms:** CondFD **schemes:** fully implicit **time step:** $3'$ **nodes:** 3 **validation:** ●	-peak temperatures reduction and delay -decrease of inner surfaces' temperatures -PCM did not have a good performance during hot Summers

Table 2.1: Dynamic *EnergyPlus*® simulations.

Info	PCM	Installation	Simulation	Conclusions
year: 2017 **citation:** [62]	**name:** heptadecane **model:** *DuPont Energain*® thermal mass systems **formula:** $C_{17}H_{36}$ **type:** paraffin (organic) **wt%:** 60 **melt. point** ($^{\circ}C$)**:** 18, 20, 22, 24, 26, 28, 30 **integration:** microencapsulation **o.m.:** ethylene based polymer, aluminium **thk. (mm):** 10, 15, 20, 25, 30, 35, 40	**surfaces:** exterior walls, ceiling **space:** building **area:** $48\,m^2$ **city:** Kuwait **period:** annual **season:** all	**algorithms:** CondFD **schemes:** — **time step:** $3'$ **nodes:** 1 **validation:** ○	-$40\,mm$ thickness with melting point of $24\,^{\circ}C$ performs better -peak temperatures drop by $5\,\%$ -annual energy savings -payback period of 50 years
year: 2017 **citation:** [63]	**name:** heptadecane **model:** BioPCM® **formula:** $C_{17}H_{36}$ **type:** paraffin (organic) **wt%:** — **melt. point** ($^{\circ}C$)**:** 22 **integration:** — **o.m.:** — **thk. (mm):**	**surfaces:** ceiling **space:** duplex house **area:** $326\,m^2$ **city:** Melbourne, Australia **period:** 26^{th}February-3^{rd}March **season:** Summer	**algorithms:** CondFD **schemes:** **time step:** $2'$ **nodes:** — **validation:** ○	-temperature reduction of $1.53^{\circ}C$ -considerable reduction of the indoor ceiling temperature
year: 2017 **citation:** [64]	**name:** heptadecane, — **model:** *DuPont Energain*® thermal mass systems, — **formula:** $C_{17}H_{36}$, — **type:** paraffin (organic), — **wt%:** 60, — **melt. point** ($^{\circ}C$)**:** 21.7, 24 **integration:** microencapsulation, — **o.m.:** ethylene based polymer, aluminium; gypsum **thk. (mm):** 5.2	**surfaces:** ceiling, walls, floor **space:** room **area:** $7\,m^2$ **city:** Auckland, New Zealand **period:** 7^{th}-16^{th} September **season:** Summer	**algorithms:** CondFD **schemes:** — **time step:** — **nodes:** — **validation:** ○	-peak load shifting -cost saving of $42\,\%$ -energy saving of $32\,\%$
year: 2018 **citation:** [65]	**name:** — **model:** BioPCM™ **formula:** — **type:** — **wt%:** — **melt. point** ($^{\circ}C$)**:** 21, 23, 23, 25, 27, 29 **integration:** macroencapsulation **o.m.:** — **thk. (mm):** 10, 15	**surfaces:** walls, ceiling **space:** building **area:** $100\,m^2$ **city:** Tangier, Fes, Ifrane, Marrakech, Errachidia, Agadir (Morocco) **period:** annual **season:** all	**algorithms:** CondFD **schemes:** fully implicit **time step:** $\leq 3'$ **nodes:** 1 **validation:** ○	-PCM with higher melting points suited better for warmer climates -PCM with lower melting points suited better for colder climates -melting point range of $[21, 25]\,^{\circ}C$ and a surface density of $4.9\,kg \cdot m^2$ performed better in terms of cooling/heating energy demand -melting point range of $[25, 27]\,^{\circ}C$ and a surface density of $2.7\,kg \cdot m^2$ performed better in terms of cost-effectiveness

wt% - percentage of PCM by weight of composite | **melt. point** - melting point | **o.m.** - others materials | **thk.** - thickness

2.5 Model validation

For the purpose of studying different scenarios that could not be experimentally tested or in the sense of doing a brief analysis on further experimental set ups, a validated model should be used.

According to Yang et al. [51], there are two metrics to validate an *EnergyPlus*® model which are the normalised mean bias error (NMBE) and the coefficient of variation of the root mean square error (CVRMSE).

The NMBE gauges the sum of the difference between every predicted, $(y_{simulated,i})$, and measured value, $(y_{measured,i})$, and divides it by the scalar multiplication of the mean hourly measured value $(\bar{y}_{measured})$ and the difference between the number of data points, (n), and the number of predictor variables, (p) (see equation 2.4). In order to have an accurate *EnergyPlus*® model, a NMBE value within a range from -10% to 10% is recommended.

$$NMBE = \frac{\sum_{i=1}^{n} (y_{simulated,i} - y_{measured,i})}{\bar{y}_{measured} \times (n-p)} \tag{2.4}$$

On the other hand, the CVRMSE describes the dispersion of a variable without recourse to its unit and the lower its value, the lower the residuals relative to simulated values. In the case of temperatures, this index is calculated by dividing the root mean square error (RMSE) by the mean hourly measured temperature (see equation 2.5). The model is said to be accurate when the CVRMSE value is within a range from -30% to 30%.

$$CVRMSE = \frac{1}{\bar{y}_{measured}} \times \sqrt{\frac{\sum_{i=1}^{n} (y_{simulated,i} - y_{measured,i})^2}{n-p-1}} \tag{2.5}$$

Nonetheless, despite of these metrics, most of the simulation studies above-mentioned (section 2.4.1) simply gauged the difference between predicted and measured temperatures and evaluated their verisimilitude [42, 43, 47, 53, 54, 61].

2.6 Thermal inertia

Nonetheless, integrating PCM into a building's envelope increases its thermal inertia. The thermal inertia or thermal mass (I) can be defined as the ability of a material to store heat and restore bit by bit. This thermal property depends on specific heat capacity, c_p, volumetric mass density, ρ, and thermal conductivity of the material, k (eq. (2.6)).

$$I = \sqrt{k \cdot \rho \cdot c_p} \tag{2.6}$$

For the purpose of ensuring thermal comfort in buildings, a high thermal inertia is desirable as it prevents overheating in Summer and keeps heat inside in Winter. In order to have a high thermal inertia, a material must have a high specific heat capacity so that the heat stored into every kilogram of material is maximized. The material should also have a high density value because it increases the amount of stored heat per volume of material. However, thermal conductivity should have a moderate value so that the rate heat flows in and out is in phase with the daily heating and cooling cycle of a building. Most of the construction materials used nowadays combine these three factors.

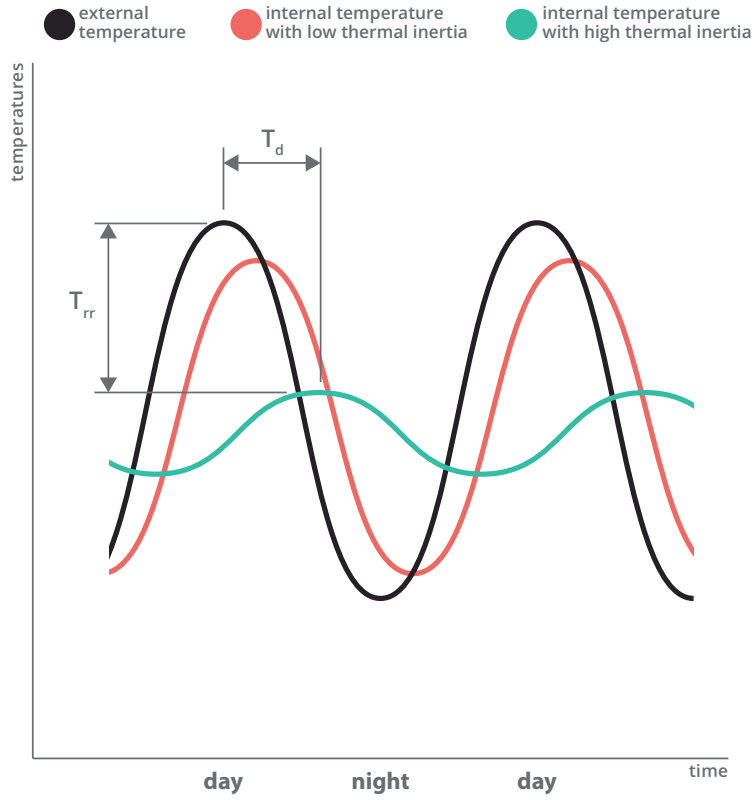

Figure 2.5: Stabilising effect of thermal inertia on internal temperature.

The higher the thermal inertia of a building, the higher peak temperatures delay, T_d, and the higher temperatures range reduction, T_{rr} (see figure 2.5). This shows thermal inertia has the ability to absorb and release heat enabling buildings to respond naturally to changing conditions and helping them to stabilize indoor temperatures. When used appropriately, thermal inertia and its stabilizing effect can prevent overheating and overcooling without the need to use active cooling/heating strategies (section 2.1).

Despite the ability to compute the thermal inertia of a surface using equation 2.6, the *Part L* of the *Building Regulations* and its associated compliance tools (*Standard Assessment Procedure* - SAP - and *Simplified Building Energy Model* - SBEM) use the kappa-value, λ, to account for thermal inertia. The kappa-value or thermal inertia value measures the heat capacity per square meter of the surface ($J \cdot m^{-2} \cdot K^{-1}$). To calculate the kappa-value of a surface, the thickness, L_i $[m]$, the volumetric mass density, ρ_i $\left[kg \cdot m^{-3}\right]$, and the specific heat capacity, c_{p_i} $\left[J \cdot kg^{-1} \cdot K^{-1}\right]$, of every i layer that composes the surface must be known (eq. (2.7)).

$$\lambda = \sum L_i \rho_i c_{p_i} \tag{2.7}$$

These values are measured starting from inner surface and stopping at which ever of the following conditions occur first:

1. halfway through the construction element;
2. an insulating layer ($k_i < 0.08\ W \cdot m^{-1} \cdot K^{-1}$);
3. a depth of $100\ mm$.

The kappa-values of every surface of a building are used to calculate the overall thermal mass parameter, TMP. This parameter is obtained by multiplying the surface area, A_j of each j surface by its kappa-value, λ_j, adding the results and dividing the total by the floor area, A_{floor} (eq. (2.8)).

$$TMP = \frac{\sum \lambda_j A_j}{A_{floor}} \tag{2.8}$$

This parameter accounts for the heat capacity per square meter of a building and it segments buildings according with its value [66]:

- low thermal inertia buildings — $TMP < 100\,kJ \cdot m^{-2} \cdot K^{-1}$
- medium thermal inertia buildings — $100 \leq TMP < 450\,kJ \cdot m^{-2} \cdot K^{-1}$
- high thermal inertia buildings — $TMP \geq 450\,kJ \cdot m^{-2} \cdot K^{-1}$

Chapter 3

Implementation

This chapter is split up into three main groups. Firstly, an overview on the PCM boards used, space in which they were installed and the respective geographic location is done. Secondly, there is a section that portrays the structure that sustains the PCM boards and reports experimental details. Finally, a segment which reports the model constraints.

3.1 Problem Formulation

3.1.1 Shipping container

The shipping container is catalogued by its model (*SP-TA-23A 20' Sea Container*) made by a company named *Shanghai Pacific International Container Co., LTD*. Although this model is currently discontinued, it has the same dimensions and it is made of the same material as another model made by the company [67]. A schematic representation of the shipping container and its surroundings can also be seen in figure 3.1. The dimensions of the shipping container were all measured considering its maximum and minimum exterior and interior limits. These dimensions are present in table 3.1.

Table 3.1: Dimensions of the shipping container [68].

lenght (mm)		width (mm)		height (mm)		tare (kg)
external	internal	external	internal	external	internal	
6058	5898	2438	2352	2591	2392	2220

Walls, roof and floor of the shipping container are all made of corten steel also known as weathering steel. This type of steel is widely used in shipping containers as it increases their resistance to atmospheric corrosion compared to others. Corten steel - EN 1.8967 (S355K2W) - has a thermal conductivity of $39\ W \cdot m^{-1} \cdot K^{-1}$, density of $7800\ kg \cdot m^{-3}$ and specific heat capacity of $470\ J \cdot m^{-1} \cdot K^{-1}$ [69]. All

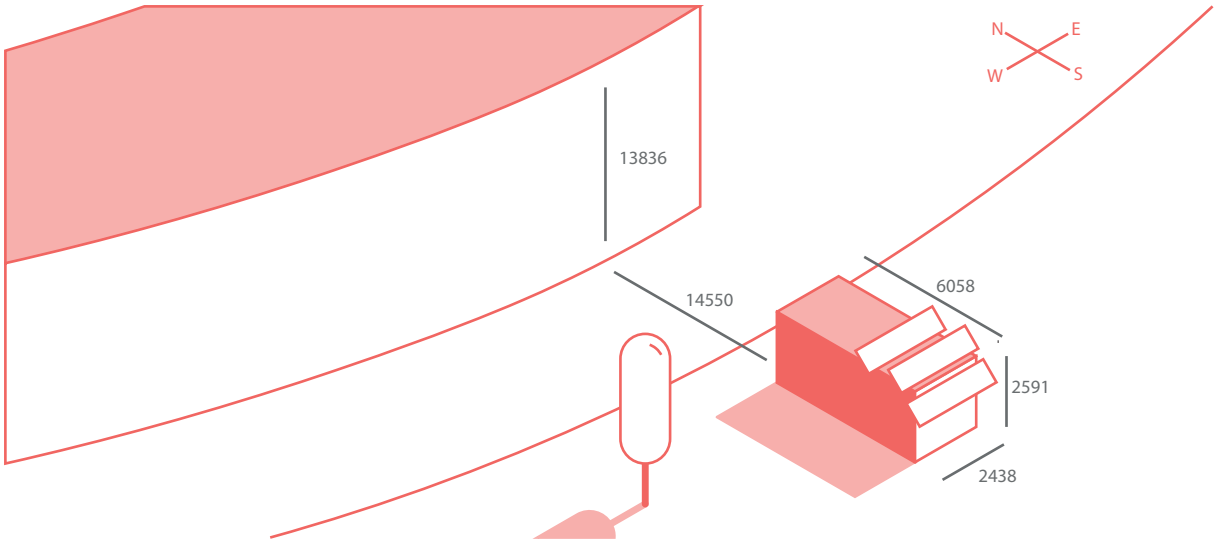

Figure 3.1: Schematic representation of the shipping container and its surroundings.

the surfaces of the shipping container have $5\ mm$ of thickness.

East facing wall and South facing door of the shipping container have also two extra pieces of synthetic canvas covering both the outer and inner surfaces (fig. 3.2(c)). Synthetic canvas are usually made of plasticized polyvinyl chloride (PVC-P) which is a flexible type of polyvinyl chloride (PVC) used in the fabrics industry. Each piece has $2\ mm$ of thickness, thermal conductivity of $0.17\ W \cdot m^{-1} \cdot K^{-1}$, density of $1400\ kg \cdot m^{-3}$ and specific heat capacity of $1400\ J \cdot m^{-1} \cdot K^{-1}$ [70]. The floor (fig. 3.2(d)) has also another inner layer made of medium density fiberboard (MDF). This layer has $10\ mm$ of thickness, thermal conductivity of $0.3\ W \cdot m^{-1} \cdot K^{-1}$, density of $750\ kg \cdot m^{-3}$ and specific heat capacity of $1700\ J \cdot m^{-1} \cdot K^{-1}$ [71]. The West facing wall has a canvas layer on the outer part of the corten steel surface (fig. 3.2(b)). All these properties are present in table 3.2 and the three types of shipping container surface configuration are illustrated in figure 3.2.

Table 3.2: Thermal properties, thickness and density of the shipping container surfaces' layers [69–71].

material	L thickness (mm)	k thermal conductivity $(W \cdot m^{-1} \cdot K^{-1})$	ρ density $(kg \cdot m^{-3})$	c_p specific heat $(J \cdot kg^{-1} \cdot K^{-1})$
corten steel [69]	5	39	7800	470
PVC-P [70]	2	0.17	1400	1400
MDF [71]	10	0.3	750	1700

The figure 3.3 shows the thermal behaviour of each surface by comparing the stored heat on the surfaces, $Q\ [Wh]$, the thermal inertia or thermal mass, $\lambda\ \left[J \cdot m^{-2} \cdot K^{-1}\right]$, and the overall heat transfer coefficient, $U\ \left[W \cdot m^{-2} \cdot K^{-1}\right]$.

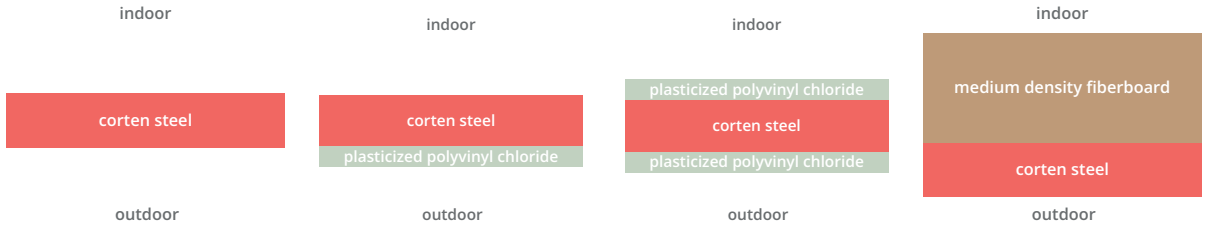

(a) North facing door and roof. (b) West facing wall. (c) East facing wall and South facing door. (d) Floor.

Figure 3.2: Types of shipping container surface configuration.

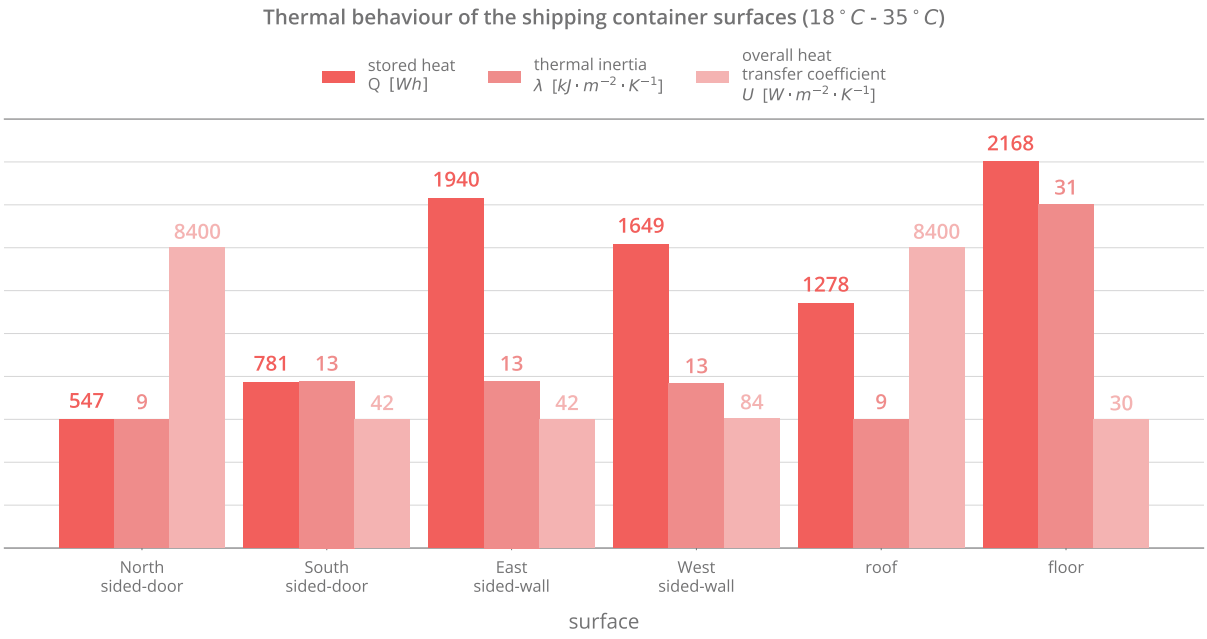

Figure 3.3: Thermal behaviour of the shipping container surfaces ($18°C$ to $35°C$).

Thermal inertia values, λ, were computed using equation 2.7 and the intermediate values are present in table B.1. This parameter gives an idea of the heat capacity for each type of surface per square meter, that is, it shows us the capacity of each surface has to store heat per square meter for later release. Looking at the results of the figure, we can conclude that all surfaces of the shipping container present typical values of low inertia constructions.

All heat stored on the shipping container surfaces, Q, is sensible heat and it is obtained using equation 2.1. This value gives a better sense of the total stored energy in each surface which complements the information given by the calculation of the thermal inertia, λ. Figure 3.3 shows that the greater the area and surface thickness, the higher the value of stored heat. It is also shown that shipping container surfaces have small heat storage capacity which confirms once more that the present shipping container has low inertia surfaces. Detailed values of calculations are present in table B.2.

Overall heat transfer coefficient values, $U\ \left[W \cdot m^{-2} \cdot K^{-1}\right]$, show us at which rate heat passes through the surface from outdoor to indoor per square meter of surface. It is important to preview the thermal delay and the temperature range reduction from outdoor conditions to indoor. Despite figure 3.3 showing

a huge difference between both North facing wall and roof and the rest of the surfaces, overall transfer coefficients of all surfaces have high values. This means that the shipping container is not well insulated and that outdoor conditions will be severely felt inside. Intermediate calculations can be seen in table B.3. This parameter can be calculated knowing thermal resistance, $R_i \ \left[K \cdot W^{-1}\right]$, and area, $A_i \left[m^2\right]$, of the materials that compose each surface (eq. 3.1).

$$U = \frac{1}{\sum R_i A_i} \tag{3.1}$$

Thermal resistance, $R_i \ \left[K \cdot W^{-1}\right]$, in an one-dimensional steady state system is given by the sum of thermal resistance for conduction, $R_{cond,i} \ \left[K \cdot W^{-1}\right]$, thermal resistance for convection, $R_{conv,i} \ \left[K \cdot W^{-1}\right]$, and thermal resistance for radiation, $R_{rad,i} \ \left[K \cdot W^{-1}\right]$. These three thermal resistances depend on material thermal conductivity , $k_i \ \left[W \cdot m^{-1} \cdot K^{-1}\right]$, convective heat transfer coefficient, $h_{conv,i} \ \left[W \cdot m^{-2} \cdot K^{-1}\right]$, radiative heat transfer coefficient, $h_{rad,i} \ \left[W \cdot m^{-2} \cdot K^{-1}\right]$, thickness of the surface, $L_i \ [m]$, and each surface area, $A_i \ \left[m^2\right]$ (eq. 3.2).

$$R_i = R_{cond,i} + R_{conv,i} + R_{rad,i} = \frac{L_i}{k_i A_i} + \frac{1}{h_{conv,i} A_i} + \frac{1}{h_{rad,i} A_i} \tag{3.2}$$

The overall thermal mass parameter (TMP) of the shipping container was computed using eq. (2.8) and its value is $77.3\, kJ \cdot m^{-2} \cdot K^{-1}$. According to section 2.6 this is a low thermal inertia enclosure ($TMP < 100\, kJ \cdot m^{-2} \cdot K^{-1}$) which implies clearly that we are in presence of a non-zero energy building.

3.1.2 Location and climate

The experiment took place in Instituto Superior Técnico (Taguspark) on the shipping container described in section 3.1.1. The shipping container is located outside the main building at $(38.7364377, -9.3026143)$ Oeiras, Portugal (fig. 3.4).

According to Peel et al. [72] the world climate classification can be made using the Köppen-Geiger climate classification present in table B.4. This criteria says that the South of Portugal has a temperate weather with dry hot Summer which means that the shipping container location is classified as a *Csa* by the Köppen-Geiger climate classification.

3.1.3 Phase change material (PCM) boards

The wallboards studied are the *DuPont Energain®* boards. These panels are made of a mixture of ethylene based polymer (40%) and paraffin wax (60%). The mixture is laminated on both sides with a $100\, \mu m$ aluminium thickness sheet and the edges are closed with a $75\, \mu m$ aluminium thickness tape, which increases the amount of energy transferred into the mixture and prevents melted paraffin leakage.

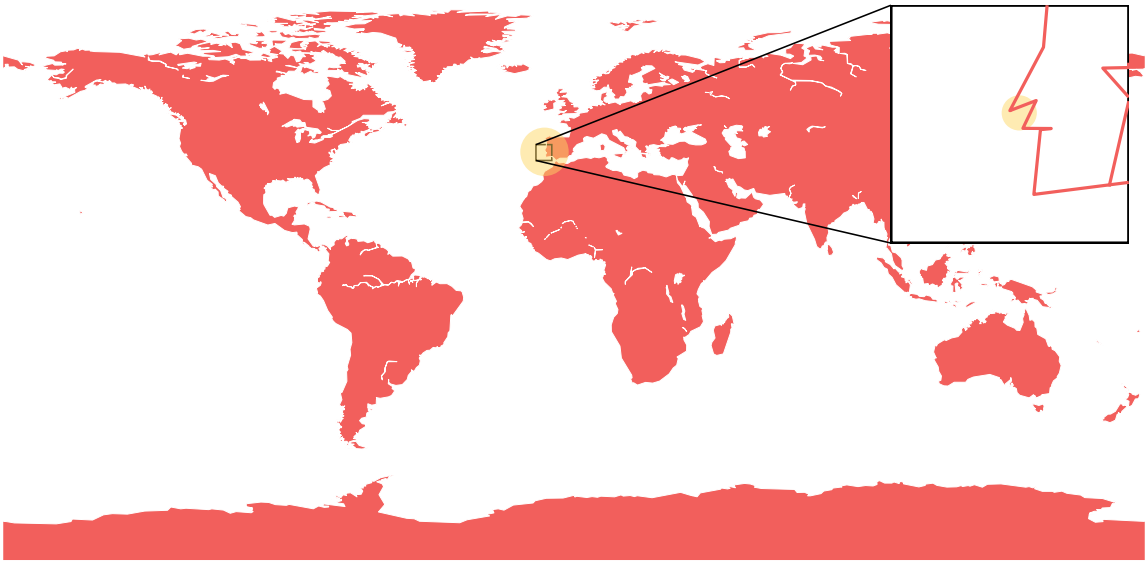

Figure 3.4: Location of the shipping container described in section 3.1.1.

The technical data sheet can be consulted in appendix A.

These energy-saving thermal mass systems have a total thickness of $5.2\,mm$, a width of $1000\,mm$ and a length of $1198\,mm$. Each panel weighs $5.391\,kg$ and has a volumetric mass density of $865.385\,kg \cdot m^{-3}$.

The paraffin wax inside these panels melts and solidifies around $22\,°C$ and $18\,°C$. The enthalpy vs temperature data was obtained from differential scanning calorimeter (DSC) measurements with a heating rate of $0.05\,°C \cdot min^{-1}$ by Tabares-Velasco et al. [45] and the results can seen in table 3.3 and figure 3.5.

Each wallboard has a total heat storage capacity per kilogram from $0°C$ to $30°C$ of $140\,kJ \cdot kg^{-1}$, a total heat storage capacity per square meter of $630\,kJ \cdot m^{-2}$ and can store $209.65\,Wh$ of heat. Half of the storage capacity of each unit is due to latent heat storage (see table 3.4).

Figure 3.6 compares stored heat between shipping container surfaces and thirty panels due to a temperature increase from $0\,°C$ to $30\,°C$. It can be seen that although the sum of stored heat on the shipping container surfaces is higher than on thirty PCM panels, adding those panels to the shipping container means an increase of $43\,\%$ in stored heat.

Table 3.3: Enthalpy vs temperature data for DuPont Energain PCM. Data obtained from differential scanning calorimeter (DSC) measurements with a heating rate of $0.05°C \cdot min^{-1}$ [45].

$T\,(°C)$	$H\,(J \cdot kg^{-1})$	$T\,(°C)$	$H\,(J \cdot kg^{-1})$
-9	0.001	12.5	81010
-7	5200	15	93760
-5	10800	17.5	109385
-4	13750	20	129635
-3	16850	22.5	157385
-2	20350	23.5	170985
-1	24750	24	177535
-0.2	30030	25	186185
0	31610	26	191185
1	37160	27	195535
2	40510	28	199485
2.5	42160	29	203135
4	47335	30	206335
5	50885	31.5	210535
7.5	60135	45	244960
10	70010	80	332460

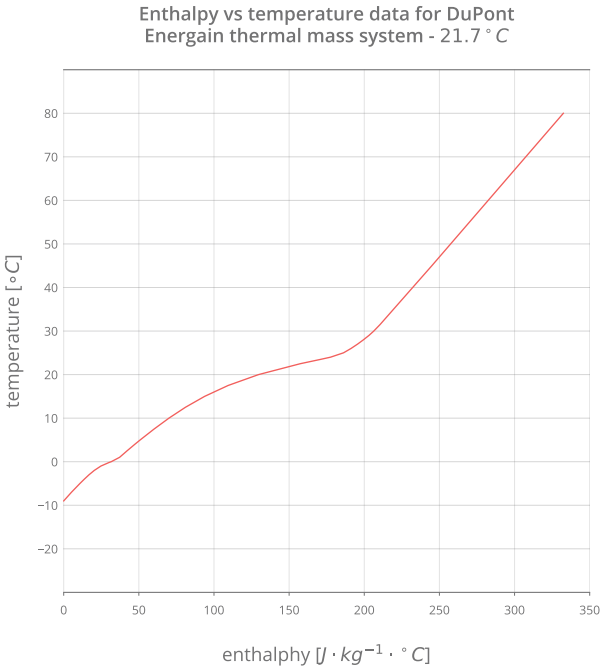

Figure 3.5: Enthalpy vs temperature data for DuPont Energain PCM.

Table 3.4: Heat storage capacity of DuPont Energain wallboards.

Heat storage capacity per quilogram $(kJ \cdot kg^{-1})$			Heat storage capacity per square meter $(kJ \cdot m^{-2})$			Heat storage capacity per panel $(Wh \cdot panel^{-1})$		
Latent	Sensible	Total	Latent	Sensible	Total	Latent	Sensible	Total
70	70	140	315	315	630	104.825	104.825	209.650

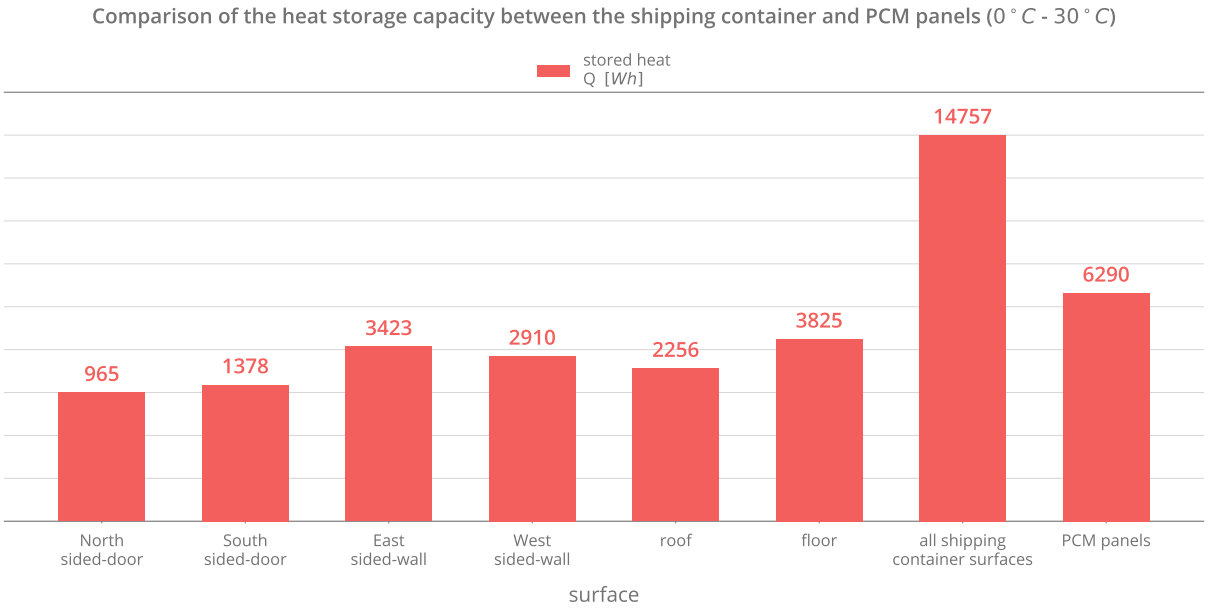

Figure 3.6: Comparison of the heat storage capacity between the shipping container and PCM panels $(0°C - 30°C)$.

3.2 Experimental set up

3.2.1 Structure and construction model

For the purpose of incorporating *DuPont Energain*® thermal mass units inside the shipping container, a totally new structure was designed and built within the scope of this thesis. Considering the air stratification inside the container and in order to take advantage of this process in terms of latent heat storage, installing the boards and consequently the structure near the inner part of the ceiling was decided as the best approach and disposition for the cooling system. This theory was confirmed by *EnergyPlus*® simulations.

Since it was intended to arrange these boards in a manner that could use the maximum width and length of the container, the structure was planned to support five layers of boards with two boards by width and three by length, giving a total of six boards per layer, thirty altogether. Given that it was supposed to study these boards in a way that would require them to be frequently mounted and dismounted, the system had to be flexible. Another constraint was allowing enough space for a person with a height of $1.90\,m$ to walk unobstructed and upright. The chosen method was the one used by tray clearing systems where PCM boards are arranged as food trays (fig. 3.7).

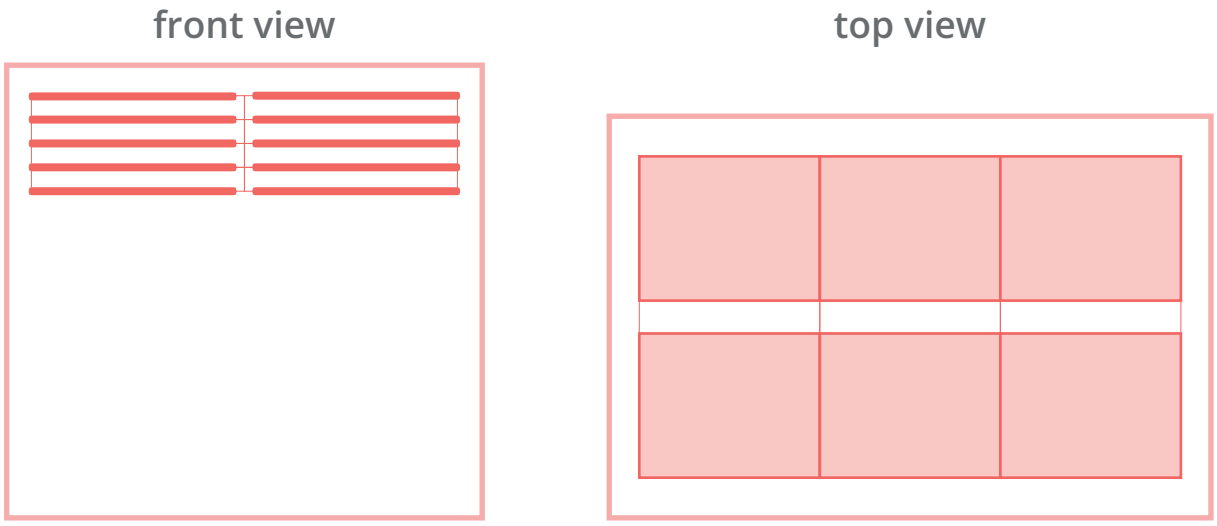

Figure 3.7: Schematic representation of PCM boards disposition within the wooden structure.

In order to build the schemed structure, five wooden bars were cut into twenty one wooden parts (fig. 3.8). These pieces were divided into two categories: central wooden parts (7) and side wooden parts (14) (fig. 3.9). In each piece, several rabbet cuts were made by milling. These cuts were planned to be equidistant between one another. However, as it was intended to do a parametric experimental study on the distance between PCM boards and how it would affect its effectiveness, three more rabbet cuts were added to the original model of wooden supports. So, two different board arrangements were considered: one with $84\,mm$ spacing and other with $62\,mm$ spacing.

(a) Wooden bar before milling.

(b) Wooden bar after milling.

Figure 3.8: Before and after milling pictures.

(a) Rabbet cuts on a central wooden piece.

(b) Rabbet cuts on a side wooden piece.

Figure 3.9: Central and side wooden pieces.

After milling, these wooden pieces were screwed into the shipping container ceiling. Moreover, to prevent the structure from shaking, more wooden stakes were added to its bottom. The final structure can be seen in figure 3.10.

After first trials, it was observed that PCM boards suffered from bulging when phase change occurred which could cause into boards to fall. To solve this situation, PVC tubes were cut into 72 pieces. These pieces had the role of supporting the boards and keeping them straight as the picture 3.11 shows.

Figure 3.10: Final wooden structure.

(a) Wooden structure and PCM boards: take 1.

(b) Wooden structure and PCM boards: take 2.

(c) Wooden structure and PCM boards: take 3.

Figure 3.11: Wooden structure and PCM boards.

3.2.2 Material and set up

For experimental tests, several devices and appliances were needed. Temperatures were measured using type *T* thermocouples. These thermocouples are very stable and appropriate to oxidizing atmospheres measuring from $-270°C$ to $370°C$ with an accuracy of $\pm 0.5°C$ [73]. Within the scope of this master thesis, twenty four thermocouples of this kind were made. From those, twelve were distributed with the purpose of measuring inner walls and doors temperatures, being installed in their respective geometric, upper and bottom center. Furthermore, ceiling and floor also had thermocouples installed in their geometric center. These locations were elected as a good reference for the location using a *Fluke TiR27* infrared camera (fig. 3.14(a)). An aluminium adhesive tape was used in order to protect these sensors from incident radiation and to resist high temperatures. With the aim of measuring mean outside and indoor temperatures, an outside and an inside (suspended) thermocouples were also carefully protected-installed by custom tubes. The remaining type *T* thermocouples were distributed by PCM boards so that their phase change was registered for further use (figs. 3.12(a) to 3.12(d)).

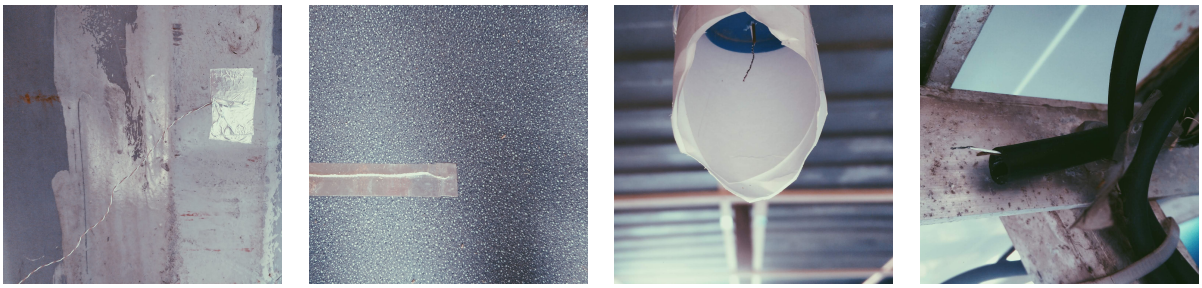

(a) Thermocouple-installed wall. (b) Thermocouple-installed floor. (c) Suspended thermocouple. (d) Thermocouple-installed outside.

Figure 3.12: Type T thermocouples installed at shipping container.

Data measured by these thermocouples was logged and saved on three devices: two *Omega DaqPro* 5300 (fig. 3.14(b)) and one *National Instruments NI cDaq* 9172 (fig. 3.14(c)). In thermocouples and data loggers calibration process, a *Newport True RMS Supermeter* model *HHM290* (fig. 3.14(c)) was used together with two type K thermocouples. Data loggers instructions were also judiciously followed. After their installation, the *Fluke TiR27* infrared camera was used to corroborate the validity of the previous calibration (fig. 3.13).

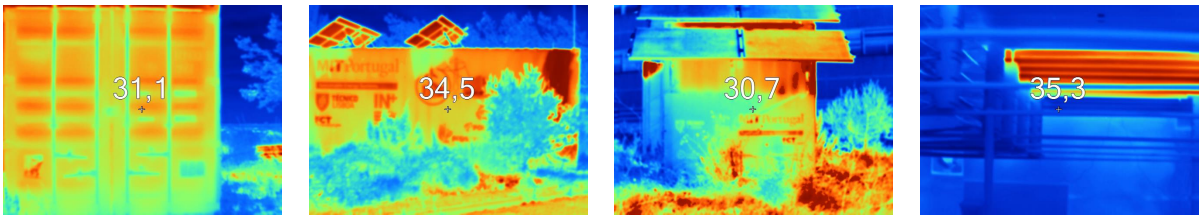

(a) North facing door infrared picture. (b) East facing wall infrared picture. (c) South facing door infrared picture. (d) PCM boards structure infrared picture.

Figure 3.13: Infrared pictures taken by the *Fluke TiR27* camera.

(a) Fluke TiR27. (b) Omega DaqPro 5300. (c) National Instruments NI cDaq 9172. (d) Newport True RMS Supermeter.

Figure 3.14: Temperatures data loggers and thermocouples calibrator.

Beyond these, a *Hobo* $U10-003$ data logger (figs. 3.15(a) to 3.15(c)) was installed in suspension so that mean indoor temperature and relative humidity were measured (figs. 3.15(a) to 3.15(c)). This data logger can measure these variables within the ranges of $-20°C$ to $70°C$ and 25% to 95% with an accuracy of $\pm 0.53°C$ (from $0°C$ to $50°C$) and $\pm 3.5\%$ (from 25% to 85% and from $15°C$ to $45°C$) or $\pm 5\%$ (from 25% to 95% and from $5°C$ to $55°C$), respectively [74]. The calibration process was the aforementioned.

In order to measure outside variables, a weather station located at Instituto Superior Técnico (Taguspark)

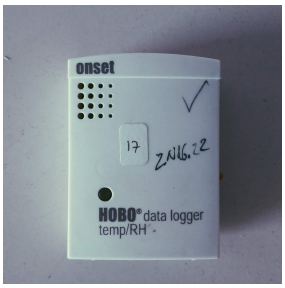

(a) Hobo U10-003.

(b) Hobo U10-003 suspended (1/2).

(c) Hobo U10-003 suspended (2/2).

(d) Davis Instruments Vantage Pro2 [75].

Figure 3.15: Hobo $U10-003$ data logger and Davis Instruments Vantage Pro2 weather station.

was used. This terminal was a *Davis Instruments Vantage Pro2* which measured outdoor dry-bulb temperature, dew point temperature, relative humidity, average wind speed and direction, pressure, solar radiation and solar energy (fig. 3.15(d)).

Experimental tests lasted three weeks from the 2^{nd} to the 24^{th} of August 2018. Data was saved into data loggers every minute after a three sample average. Experiments were performed with and without PCM boards with and without night ventilation in the shipping container. Temperatures measured were verified by Fluke infrared camera.

3.3 Modelling and simulation

In order to model and simulate the problem, several software were used. To model the heat balance in the shipping container, *EnergyPlus 8.9.0* was utilized. The geometry of the shipping container was created in *SketchUp Pro 2017 17.0.18899 64-bit*. Shadow groups of the photovoltaic panels and the Instituto Superior Técnico (Taguspark) building were also generated. The final geometry can be seen in figs. 3.16 and 3.17. For the purpose of converting the shipping container 3D model into an *EnergyPlus*® file (*.idf*), the plugin *OpenStudio v.2.5.2* was applied.

3.3.1 Conduction Finite Difference Solution Algorithm

EnergyPlus®employs heat balance equations by coupling them with a conduction transfer functions (CTF) solution algorithm. However, since this algorithm does not present results for surface internal layers (one-dimensional), when modelling phase change materials (PCM) or variable thermal conductivity materials, a conduction finite difference (CondFD) solution algorithm must be added to the model. Two different CondFD schemes are used by *EnergyPlus*® both based on an Adams-Moulton solution: (a) Crank-Nicholson (second-order in time semi-implicit scheme) and (b) fully implicit (first-order in time scheme). Both formulations can be seen in equation 3.3.

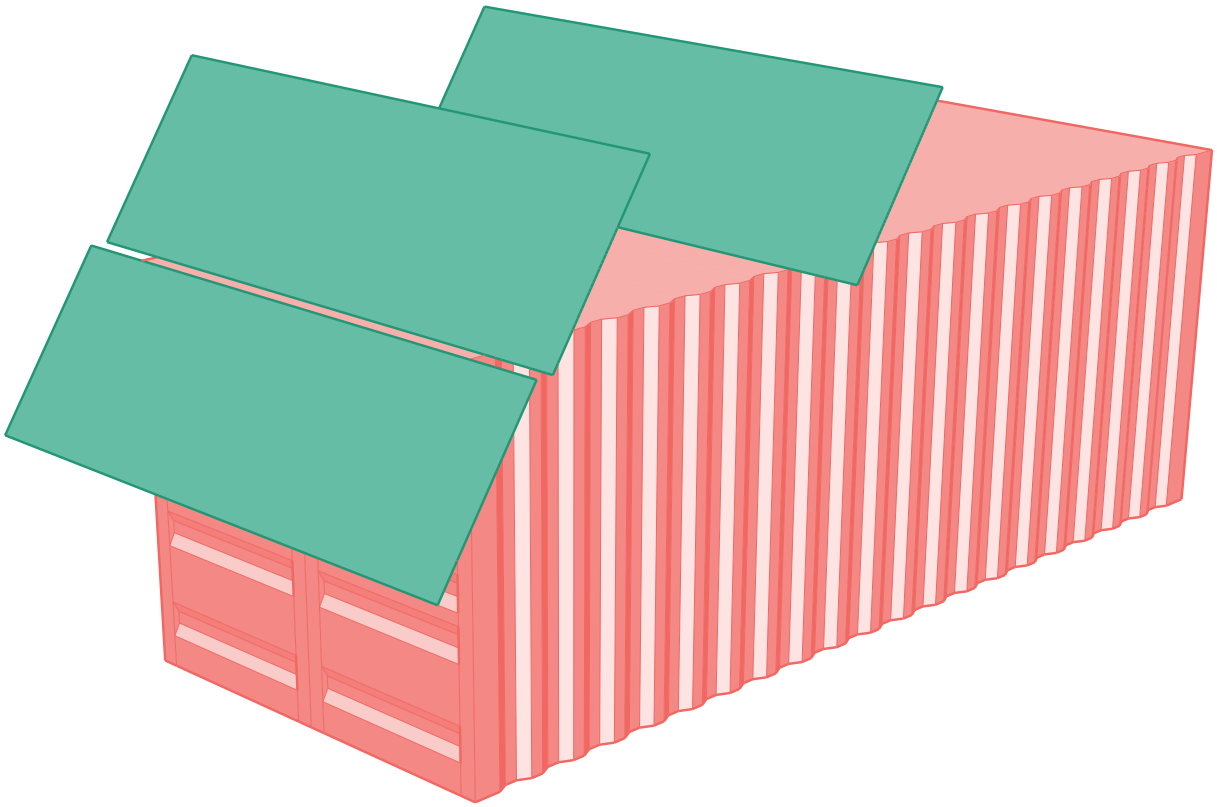

Figure 3.16: Shipping container SketchUp model's ISO view.

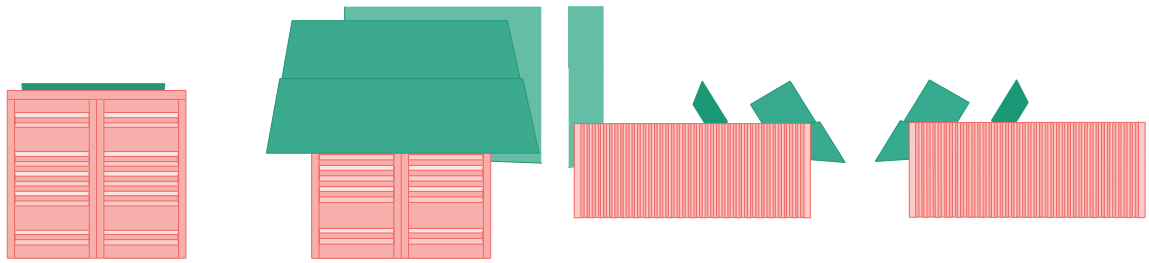

(a) Front view. (b) Back view. (c) Left view. (d) Right view.

Figure 3.17: Shipping container SketchUp model's views.

$$C_p \rho \Delta x \frac{T_i^{j+1} - T_i^j}{\Delta t} = \begin{cases} \frac{1}{2}\left[\left(k_W \frac{T_{i+1}^{j+1} - T_i^{j+1}}{\Delta x} + k_E \frac{T_{i-1}^{j+1} - T_i^{j+1}}{\Delta x}\right) + \left(k_W \frac{T_{i+1}^{j} - T_i^{j}}{\Delta x} + k_E \frac{T_{i-1}^{j} - T_i^{j}}{\Delta x}\right)\right], & \text{(a)} \\ k_W \frac{T_{i+1}^{j+1} - T_i^{j+1}}{\Delta x} + k_E \frac{T_{i-1}^{j+1} - T_i^{j+1}}{\Delta x}, & \text{(b)} \end{cases} \tag{3.3}$$

Where:

T node temperature

T_i temperature of the node being modelled

T_{i-1} temperature of the adjacent node (exterior of construction)

T_{i+1} temperature of the adjacent node (interior of construction)

T^{j} temperature in the previous time step

T^{j+1} temperature in the current time step

Δt calculation time step

Δx finite difference layer thickness

C_p specific heat of material

k_W thermal conductivity for interface between i and $i+1$ nodes

k_E thermal conductivity for interface between i and $i-1$ nodes

ρ volumetric mass density

A second equation (eq. 3.4) is used to obtain enthalpy values in function of temperatures. This data is introduced by the user on the *EnergyPlus®* *MaterialProperty:PhaseChange* object.

$$h_i = HFT(T_i) \tag{3.4}$$

The finite difference layer thickness, Δx, can be computed knowing the thermal diffusivity of a material, α, the calculation time step, Δt, (user input) and a space discretization constant, C, which is also defined by the user. This constant is determined as the inverse of the Fourier Number with a default value of 3 (3.5).

$$Fo = \frac{\alpha \Delta t}{\Delta x^2} \Longleftrightarrow \Delta x = \sqrt{\left(\frac{1}{Fo}\right) \alpha \Delta t} \Longleftrightarrow \Delta x = \sqrt{C \alpha \Delta t} \tag{3.5}$$

When PCM are being simulated, a third equation (3.6) must be added in order to update specific heat values for each iteration, using enthalpy-temperature data inputted by the user.

$$C_p = \frac{h_i^{j+1} - h_i^{j}}{T_i^{j+1} - T_i^{j}} \tag{3.6}$$

Moreover, if a variable thermal conductivity material is specified, its thermal conductivity must be updated as well, using equations 3.7 and 3.8 and data from *MaterialProperty:VariableThermalConductivity* object inserted by the user.

$$k_W = \frac{k_{i+1}^{j+1} - k_i^{j+1}}{2} \tag{3.7}$$

$$k_E = \frac{k_{i-1}^{j+1} - k_i^{j+1}}{2} \tag{3.8}$$

3.3.2 Model calibration

Since this work will simulate PCM boards, a conduction transfer functions (CTF) solution algorithm must be complemented by a conduction finite difference solution algorithm (CondFD), as previously mentioned. Therefore, using this Heat Balance Algorithm, it is essential to set the number of time steps per hour equal or greater than 20 and smaller or equal to 60 $(1' \leq \Delta t \leq 3')$.

In order to analyse the effect that the time step has on the accuracy of the results, the annual energy demand was measured and compared. These results can be seen in graph 3.18.

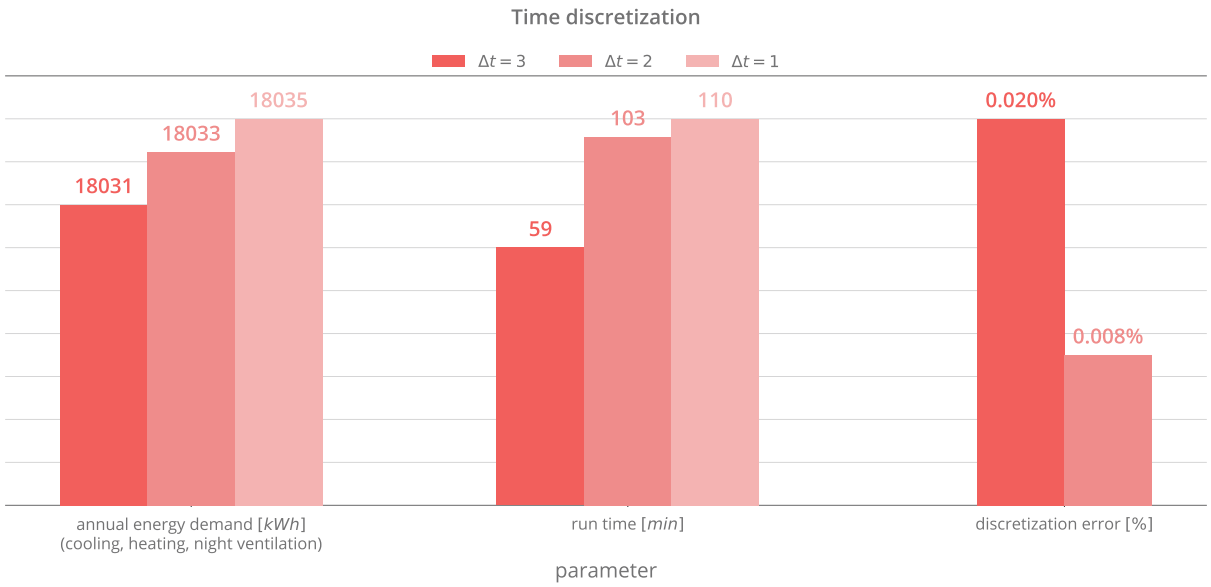

Figure 3.18: Time discretization.

As an overall trend, the higher the time step value the higher the annual energy demand and the higher the time the software takes to run the model. Discretization errors were considered as the difference between annual energy demand for a given time step and the annual energy demand with an $1'$ time step. It can be clearly seen that this error decreased slightly from $0.020\,\%$ to $0.008\,\%$ for $3'$ and $2'$ time steps respectively. Nonetheless, running time increased steeply with the increase of the number of time steps per hour and, for that reason, a $3'$ time step was chosen.

When using CondFD, there are two choices for the difference scheme: Crank-Nicholson and fully implicit. The graph 3.19 shows the results of the annual energy demand for the two methods for different number of nodes: 3 (default), 2 and 1.

If we look at annual energy demand over number of nodes for the two methods, we can see this remains constant. However, for the same number of nodes there is a minimal difference between them. On the

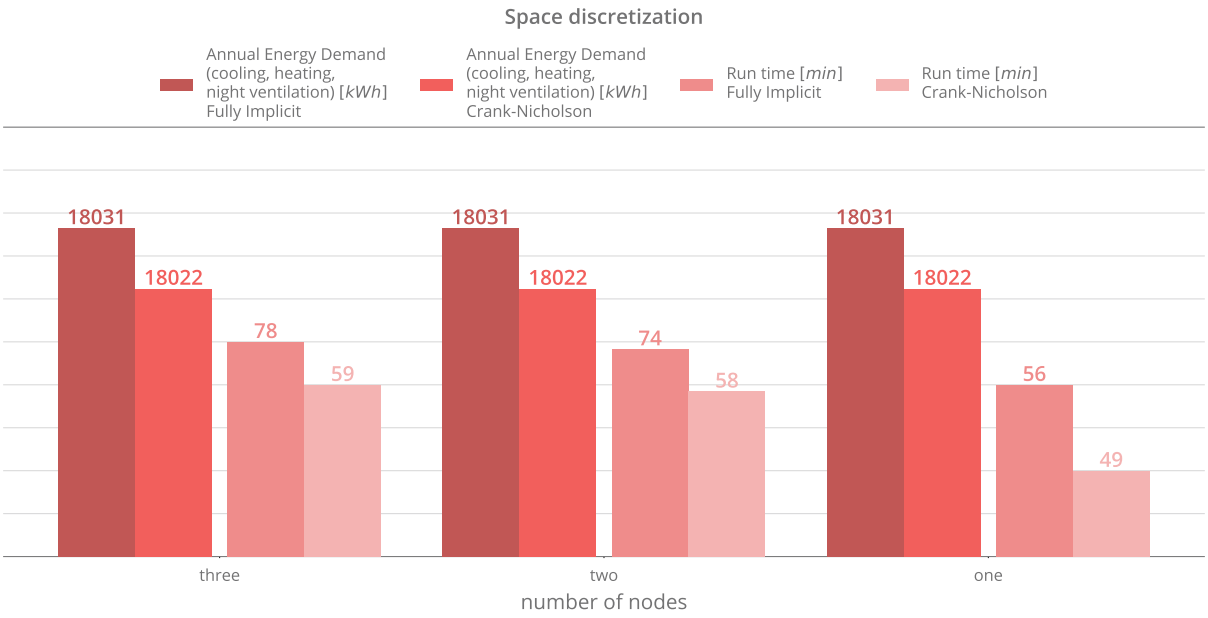

Figure 3.19: Space discretization.

other hand, running time decreases markedly with the decrease of number of nodes. It should also be noted that Crank-Nicholson running time is consistently smaller than the fully implicit's. However, according to Ozdenefe et al. [54], fully implicit scheme is more stable over time when incorporating PCM modules into *EnergyPlus*® model. For this reason, the fully implicit scheme with one node will be used in further simulations.

3.3.3 Weather File

Two different weather files were used within the scope of this thesis. One of those was the *epw* file which gathers Lisbon's real weather data from the year of 2005. This file is provided by *EnergyPlus*®itself and it can be found online [76]. The other weather file was obtained by editing this one with real data measured from June to September of 2018 on the weather station located at Instituto Superior Técnico - Taguspark. Outside dry-bulb temperature, outside dew point temperature, outside relative humidity, average wind speed, average wind direction and pressure are among the gauged variables inserted into the original weather file. To perform this operation, *Weather Statistics and Conversions* program was used. These files will serve different purposes. Although solar radiation was not one of the measured weather variables, data from cloudy days were inputted as well. The primary file will be used to run annual simulations on the *EnergyPlus*®model whereas the second will provide real weather data to validate this model.

3.3.4 Phase change material (PCM) boards

Although only *DuPont Energain®* thermal mass system with a $21.7\,°C$ melting point is experimentally tested, boards with different melting points should also be considered. *EnergyPlus®* allows the modelling of a phase change material by specifying the enthalpy-temperature curve and its thermal conductivity for different paraffin phases. This can be done by adding information into *MaterialProperty:PhaseChange* and *MaterialProperty:VariableThermalConductivity* objects respectively. For *DuPont Energain®* panels, this information is given by the manufacturer (section 3.1.3). To obtain the enthalpy-temperature curve for wallboards with different melting points a shift of these values was made (table 3.5 and fig. 3.20). The same criteria was applied to compute variable thermal conductivity values for several boards (table B.5).

Table 3.5: Enthalpy vs temperature values for PCM chosen.

	enthalpy $(J \cdot kg^{-1} \cdot ° C^{-1})$															
	31610	37160	40510	47335	50885	70010	93760	129635	177535	186185	191185	195535	199485	203135	206335	244960
PCM20	$-2°C$	$-1°C$	$0°C$	$2°C$	$3°C$	$8°C$	$13°C$	$18°C$	$22°C$	$23°C$	$24°C$	$25°C$	$26°C$	$27°C$	$28°C$	$43°C$
PCM22	$0°C$	$1°C$	$2°C$	$4°C$	$5°C$	$10°C$	$15°C$	$20°C$	$24°C$	$25°C$	$26°C$	$27°C$	$28°C$	$29°C$	$30°C$	$45°C$
PCM24	$2°C$	$3°C$	$4°C$	$6°C$	$7°C$	$12°C$	$17°C$	$22°C$	$26°C$	$27°C$	$28°C$	$29°C$	$30°C$	$31°C$	$32°C$	$47°C$
PCM26	$4°C$	$5°C$	$6°C$	$8°C$	$9°C$	$14°C$	$19°C$	$24°C$	$28°C$	$29°C$	$30°C$	$31°C$	$32°C$	$33°C$	$34°C$	$49°C$
PCM28	$6°C$	$7°C$	$8°C$	$10°C$	$11°C$	$16°C$	$21°C$	$26°C$	$30°C$	$31°C$	$32°C$	$33°C$	$34°C$	$35°C$	$36°C$	$51°C$
PCM30	$8°C$	$9°C$	$10°C$	$12°C$	$13°C$	$18°C$	$23°C$	$28°C$	$32°C$	$33°C$	$34°C$	$35°C$	$36°C$	$37°C$	$38°C$	$53°C$

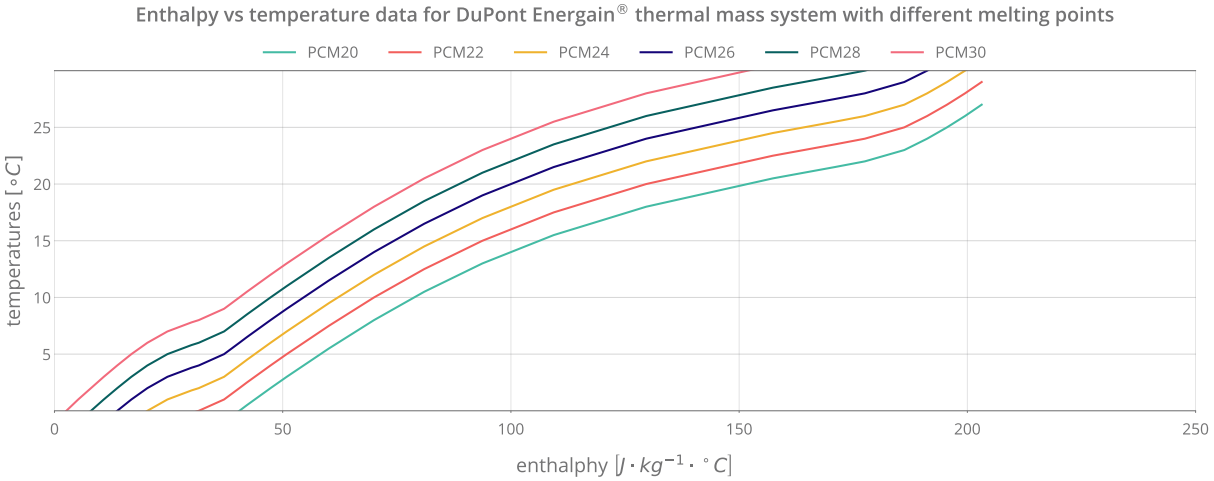

Figure 3.20: Enthalpy vs temperature for different PCM panels.

3.3.5 Internal gains

Inside the shipping container, there are several devices which need to be connected to the electric grid. The photovoltaic system above the shipping container is connected to two devices located inside the container (*Sunny Boy* and *Sunny Island*). Each of the devices has a total power of $3680\,W$ and $2200\,W$, respectively, and they are continuously turned on. There is also a lead battery connected to the

photovoltaic system used to store the photovoltaic panels' energy. This battery has $750\,amp \cdot h$ and $48\,V$ and is continuously turned on. Furthermore, there is a $20\,W$ light bulb but it was always turned off during the experiment. No people were inside the container during the experiment.

The previous setting represents the real conditions on the shipping container and it will be used to validate the model. A second scenario will be considered in simulations. All the photovoltaic system devices will have the same behaviour as in reality but lights will be turned on and one person will be inside the container. All the utilization schedules can be seen in figure 3.21.

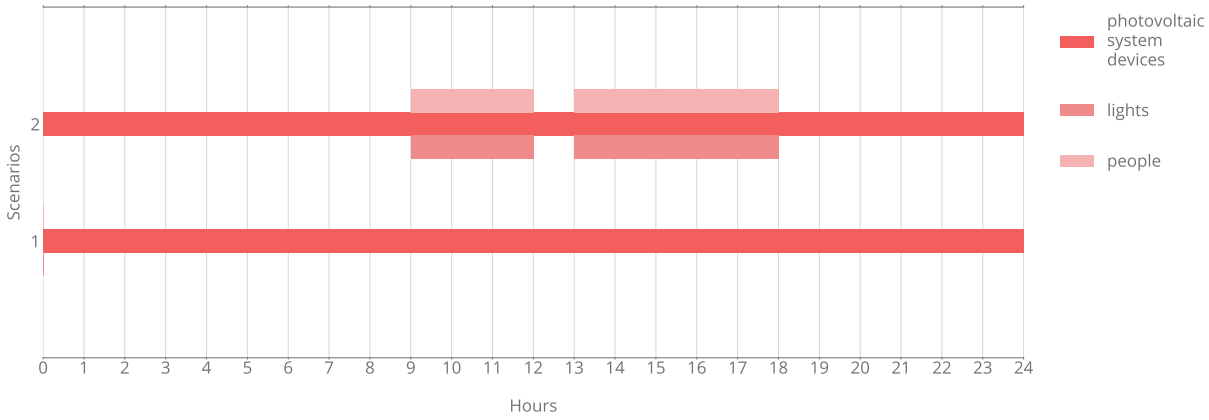

Figure 3.21: Internal gains schedule.

3.3.6 Airflow

The number of air changes per hour, $ACH\ \left[h^{-1}\right]$, of infiltration and natural ventilation in a room with two opposite openings can be obtained by multiplying an average value of wind speed, $v\ \left[m \cdot s^{-1}\right]$, by the smallest opening area, $A\ \left[m^2\right]$, and dividing by the room volume, $V\ \left[m^3\right]$ (see equation 3.9).

$$ACH = \frac{0.65 \times v \times A \times 3600}{V} \tag{3.9}$$

As the shipping container has an average wind speed in July and August of $2.82\,m \cdot s^{-1}$ and two opposite openings area of $0.0283\,m^2$ and 0.0381, then the container has a value of $5.628\,h^{-1}$ for the infiltration flow rate.

The shipping container has also a fan providing ventilation, promoting an air flow from outside to inside. The air intake is assumed to be at the outdoor conditions and a fraction of the heat from the fan is considered when the intake happens. In order for *EnergyPlus*® to be able to calculate the fan electrical consumption, the values for fan pressure rise and fan efficiency must be known. According to the software manual, the fan pressure rise, $\Delta p\ [Pa]$, should be calculated by multiplying the specific fan power, $SFP\ \left[dm^3 \cdot W^{-1} \cdot s^{-1}\right]$, and the fan efficiency, $\eta\ \left[W \cdot W^{-1}\right]$, by a factor of 1000. The specific fan power can be obtained by dividing the electrical power input, $P_e\ [W]$, by the volume flow, $\dot{Q}\ \left[dm^3 \cdot s^{-1}\right]$,

as the equation 3.10 suggests.

$$\Delta p = 1000 \times SFP \times \eta = 1000 \times \frac{P_e}{\dot{Q}} \times \eta \tag{3.10}$$

The fan of the container is a *Cata LHV 190* (00661000 - LHV 190 - EAN) [77] and it has a diameter of $190\,mm$, a maximum volume flow of $700\,m^3 \cdot h^{-1}$ and an electrical power input of $30\,W$. It is also assumed that the fan has a total efficiency of 0.8. These values translate into a fan pressure rise of $123.43\,Pa$.

The air changes per hour, $ACH\ \left[h^{-1}\right]$, of mechanical ventilation is given by equation 3.11, where $\dot{Q}\ \left[m^3 \cdot h^{-1}\right]$ and $V\ \left[m^3\right]$ stand for volume flow of the fan and the volume of the shipping container.

$$ACH = \frac{\dot{Q}}{V} \tag{3.11}$$

The maximum ACH of the shipping container fan is $21.1\,h^{-1}$. In addition and in order to study the effect of night ventilation on PCM panels effectiveness and air conditioning unit energy demand, other air flows will be modelled. Four scenarios will be considered: ventilation turned off, $5\,ACH$, $10\,ACH$ and $21.1\,ACH$. The *EnergyPlus*® inputs can be seen in table 3.6.

Table 3.6: Mechanical ventilation ACH and Δp values for the scenarios to be modelled in *EnergyPlus*®.

variable	scenario 1	scenario 2	scenario 3	scenario 4
$ACH\ \left[h^{-1}\right]$	—	5	10	21.1
$\Delta p\ [Pa]$	—	520.76	260.38	123.43

3.3.7 Thermal comfort

The ASHRAE Standard 55-2017 Thermal Comfort was used to determine the thermal comfort zones for Winter and Summer in the shipping container. The Predicted Mean Vote (PMV) was the model chosen to compute the set points for the HVAC system modelled for the container.

The container has an indoor average relative humidity of 61% and a mean radiant temperature of $25\,°C$ is considered. As there is no local air speed control in the container the air speed value used in the calculations is $0.1\,m \cdot s^{-1}$. The shipping container present in this study is not inhabited for any functions but, for the purpose of modelling an ideal office activity, it will be used. For that reason, activities such as typing, reading and writing while seated lead to a metabolic rate of 1.1. The clothing level considered will be 1.0 for typical Summer indoor clothing and 0.5 for typical Winter indoor clothing.

The figure 3.22 shows us the thermal comfort zones for Winter and Summer. Thus, temperature set point of used $18°C$ with relative and specific humidity falling within the ranges of $[30\%,\ 40\%]$ and $[3.81,\ 5.11]\ g_w \cdot kg_aC$ for Winter and a temperature set point of $27°C$ with relative and specific humidity falling within the ranges of $[60\%,\ 70\%]$ and $[13.42,\ 15.71]\ g_w \cdot kg_aC$ for Summer will be used for heating and cooling

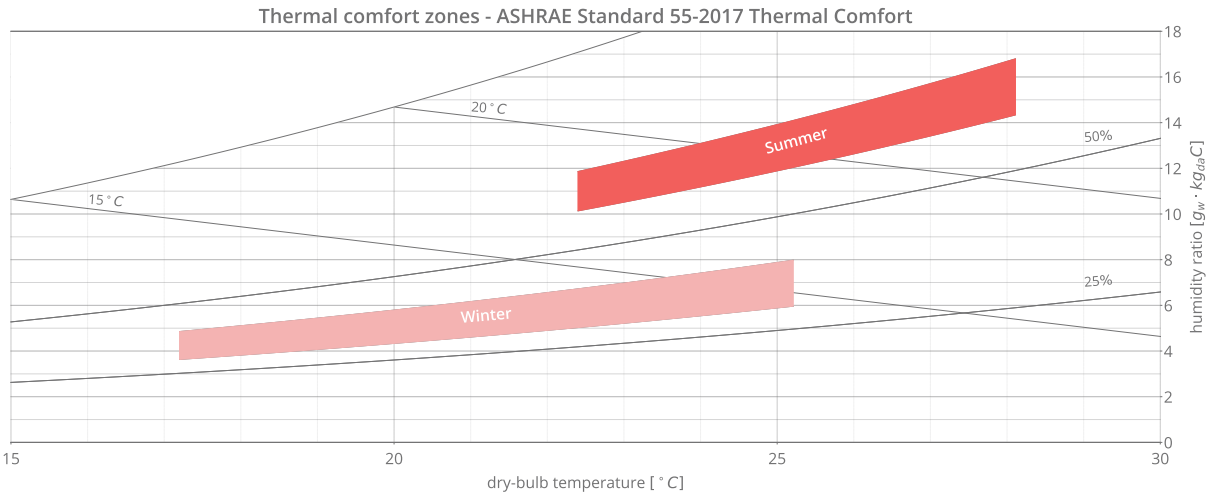

Figure 3.22: ASHRAE thermal comfort zones for Winter and Summer.

respectively.

3.3.8 HVAC system

For the purpose of obtaining cooling and heating needs in the shipping container to achieve thermal comfort as well as the costs of these needs, a fictitious HVAC system was designed. The HVAC modelled was a unitary system which contemplates a blow-through fan, a heating coil and a cooling coil. This system operates between $9\,a.m.\,-\,12\,p.m.$ and $1\,p.m.\,-\,6\,p.m.$, only if the set points computed in the previous section (3.3.7) are met.

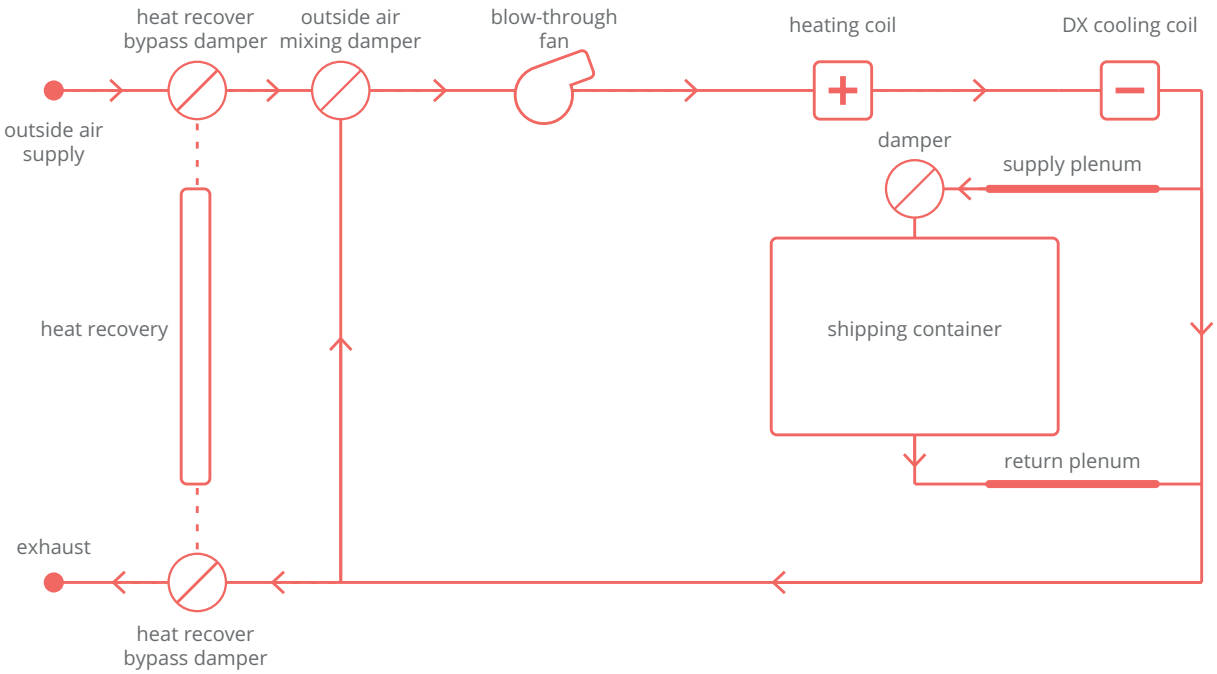

Figure 3.23: Schematic representation of the unitary HVAC system modelled.

In order to model the HVAC components, two *EnergyPlus*® objects were required in particular *HVACTemplate:Zone:Unitary* and *HVACTemplate:System:UnitarySystem*. The blow-through fan chosen has a supply delta pressure equal to $300\,Pa$, a motor efficiency of 0.8 and a total efficiency of 0.6. The direct expansion cooling and heating coils have coefficients of performance (COP) of 5 and 3, respectively. These components and respective specifications are widely common for residential and office HVAC system as studied by Alghoul [78]. The layout of the HVAC system modelled can be seen in figure 3.23.

3.3.9 Utility cost: tariff

To calculate the energy cost in the shipping container, it is necessary to input in the *EnergyPlus*® model the tariff costs of electricity using the *UtilityCost:Tariff* and *Schedule:Compact* objects. As table 3.7 shows, Instituto Superior Técnico (Taguspark campus) has a quadri-hourly rate electricity tariff which means the day is split up into four main periods: super off-peak, off-peak, peak and super peak. Moreover, these periods fall into distinct time ranges depending on wether it is Winter (from the 28^{th} of October to the 25^{th} of March) or Summer daylight saving time (from the 25^{th} of March to the 28^{th} of October) [79].

Table 3.7: Tariff costs of electricity in Instituto Superior Técnico - Taguspark (electricity bill).

period	Winter time $(hours)$	Summer time $(hours)$	price $\left(€ \cdot kW^{-1} \cdot h^{-1}\right)$
super peak	9 : 30 - 12 : 00	9 : 15 - 12 : 15	0.1129
	18 : 30 - 21 : 00		
peak	7 : 00 - 9 : 30	7 : 00 - 9 : 15	0.1011
	12 : 00 - 18 : 30	12 : 15 - 24 : 00	
	21 : 00 - 24 : 00		
off-peak	0 : 00 - 2 : 00	0 : 00 - 2 : 00	0.0713
	6 : 00 - 7 : 00	6 : 00 - 7 : 00	
super off-peak	2 : 00 - 6 : 00	2 : 00 - 6 : 00	0.0639

Chapter 4

Results and discussion

In this chapter, the results will be discussed. Firstly, an *EnergyPlus*® model will be validated comparing the experimental and simulation results. Secondly, on section 4.2, experimental outcomes with and without PCM will be assessed and contrasted with regard to thermal comfort. Additionally, with an already validated model, several tests will be performed for the purpose of obtaining cooling and heating needs for various scenarios. Finally, an economic analysis will be made considering the payback period.

4.1 Model validation

A model validation is essential to guarantee the current and forthcoming simulations will be in tune with real events. Consequently, it is essential to validate the *EnergyPlus*®model configured in section 3.3. In light of this, measured and predicted data was gathered and compared for two specific cases: a space without PCM (section 4.1.1) and a space with PCM (section 4.1.2). For both cases, the model was set up with conditions which emulate experimental settings. These can be easily seen in table 4.1. Some *EnergyPlus*® simulations runned *a priori* showed that it was best for PCM effectiveness to have have night ventilation turned on and, for that reason, it was a setting of the experimental scenario.

Table 4.1: Experimental and model set up for model validation.

Weather file	PCM panel	Fan airflow (ACH)	PCM panel thickness (mm)	PCM panel location	Number of PCM panels	Lights	People	HVAC
Oeiras - Csa	PCM 22	21.1	5.2	internal mass	30	○	○	○

○ - off | ● - on

4.1.1 Model validation - no PCM boards

The figure 4.1 shows some relevant weather data compiled over two days from the 8^{th} to the 10^{th} of August, 2018. This figure is divided into four subplots and, from top to bottom, those show pertinent in-

formation about temperatures, relative humidity, wind speed and direction and solar energy and radiation respectively.

Temperatures subplot compares indoor experimental and predicted values with outdoor data. Although measured and simulated temperatures exhibit very similar behaviour between each other with alike values, it can be clearly seen that there is a time gap where a difference between both indoor and outdoor temperatures takes shape. The maximum temperatures difference or maximum error (ME) registered has a value of $4.89°C$ and the mean average error (MAE) and the root mean square error (RMSE) were $1.00°C$ and $1.50°C$ respectively. Those magnitudes of error are quite reasonable considering that there was a temperatures measurement's uncertainty of $\pm 0.53°C$. However, NMBE and CVRMSE are all the more important when validating a model using predicted and measured temperatures, as explained in section 2.5. In this particular case, NMBE and CVRMSE were 1.9% and 6.65% which are within the acceptable range of $\pm 10\%$ and $\pm 30\%$. As a consequence, the *EnergyPlus*® model without PCM boards is validated.

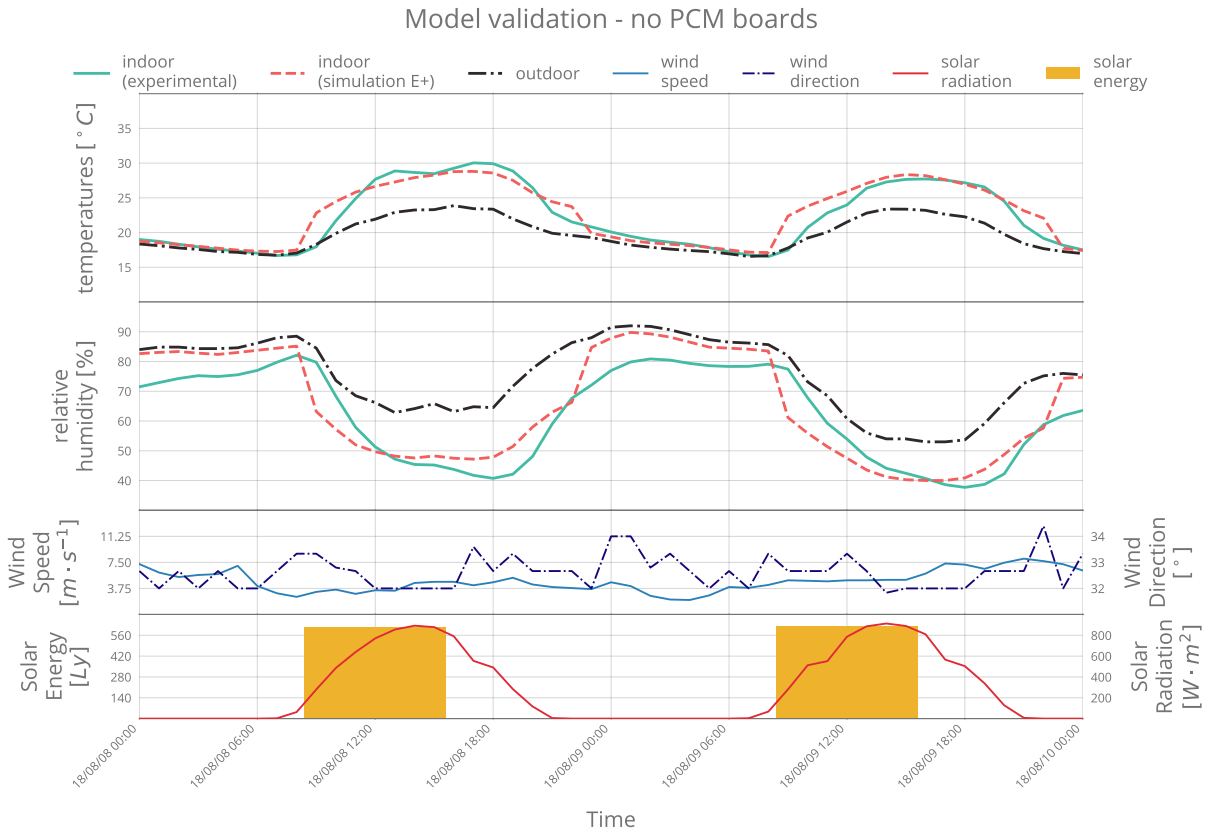

Figure 4.1: Model validation without PCM boards.

At the same time, on the second subplot, relative humidity relations do not stray too far from those seen in the previous subplot. Again, indoor experimental and simulated data draw near each other but a ME of 16.56% occurred. Over the two days, MAE and RMSE had values of 6.62% and 7.69% respectively. Since there was a relative humidity measurement's uncertainty of $\pm 3.50\%$, these magnitudes of error are once again acceptable. All model validation's information is summed up in table 4.2.

Table 4.2: Errors and validation indices for model validation without PCM boards.

temperatures					relative humidity			model validation
ME $(°C)$	MAE $(°C)$	RMSE $(°C)$	NMBE $(\%)$	CVRMSE $(\%)$	ME $(\%)$	MAE $(\%)$	RMSE $(\%)$	
4.89	1.00	1.50	1.90	6.65	16.56	6.62	7.69	●

○ - non validated model | ● - validated model

So that is possible to have additional information on the studied days' weather and to help to characterize it, a third and a forth subplots are shown. The third subplot demonstrates that over those two days wind blew with an average speed and direction of $4.81\,m \cdot s^{-1}$ and $32.6°$ respectively. On the other hand, the forth demonstrates that solar radiation profile for the two days have a Gaussian shape resulting in solar energy values approximately higher than $600\,Ly$. Therefore, the two experimenting days were days with a lower cloudiness index.

4.1.2 Model validation - with PCM boards

On a similar note, the figure 4.2 summarizes weather data for the case where thirty PCM boards are installed as internal mass of the shipping container. The experiment took place between the 11^{th} and 14^{th} of August, 2018. Information was displayed in accordance with the prior section (4.1.1).

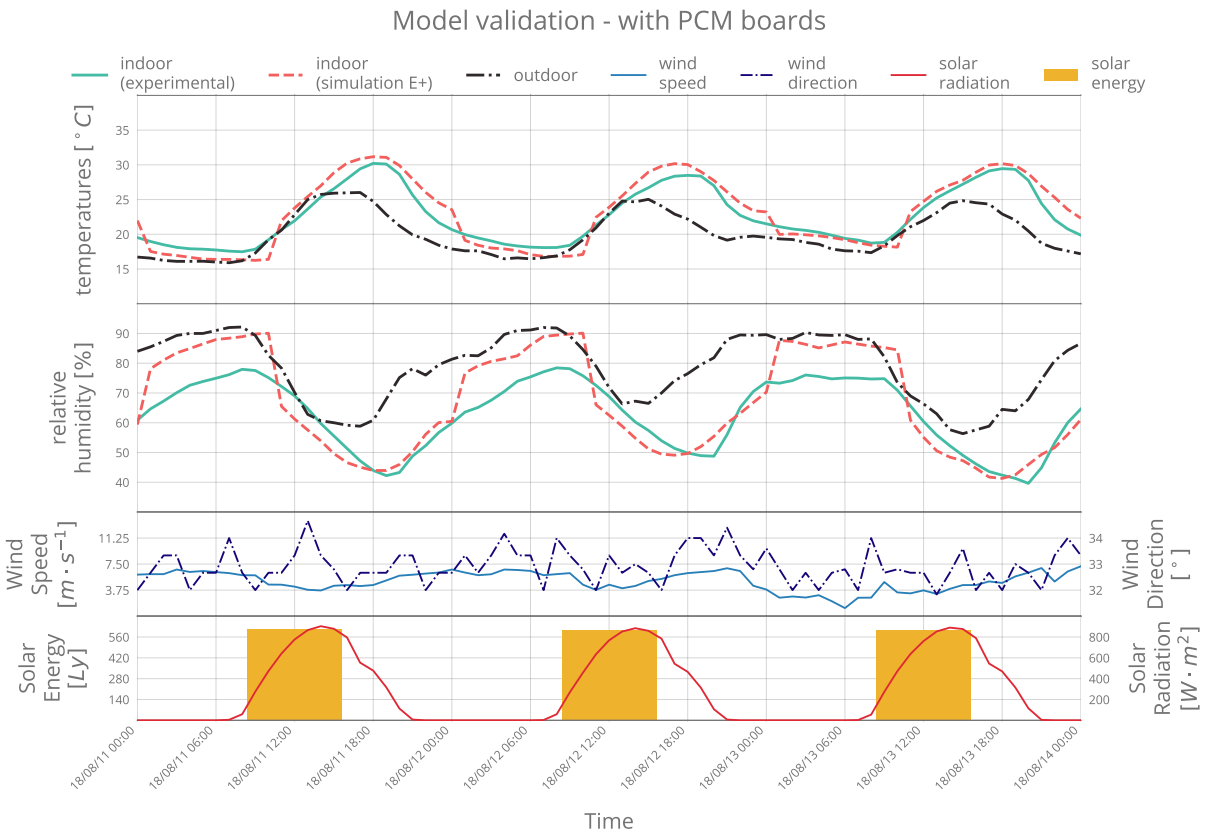

Figure 4.2: Model validation with PCM wallboards.

In the first subplot, it can be clearly seen that measured and predicted temperatures concord over time. The maximum error listed (ME) was $3.21°C$ while the mean average error (MAE) and the root mean square error (RMSE) were $1.40°C$ and $1.58°C$ respectively. Recalling that temperatures measurement's uncertainty has a value of $\pm 0.53°C$, those magnitudes of error are admissible. On the other hand, NMBE and CVRMSE were inside the respective adequate ranges ($\pm 10\%$ and $\pm 30\%$) rating 2.08% and 6.93%. Thus, the *EnergyPlus*® model with PCM boards is validated.

In addition, experimental and foreseen relative humidity were also analysed. The second subplot demonstrates a high agreement between them. The ME was 14.93% whereas MAE and RMSE were 7.22% and 8.53% respectively. Inasmuch as relative humidity measurement's uncertainty is $\pm 3.50\%$, those errors are reasonable. All the validation info is enumerated in table 4.3.

Table 4.3: Errors and validation indices for model validation with PCM boards.

temperatures					relative humidity			model validation
ME $(°C)$	MAE $(°C)$	RMSE $(°C)$	NMBE $(\%)$	CVRMSE $(\%)$	ME $(\%)$	MAE $(\%)$	RMSE $(\%)$	
3.21	1.40	1.58	2.08	6.93	14.93	7.22	8.53	●

○ - non validated model | ● - validated model

Over theses experimental days, wind speed blew $32.9°$ from North with an average speed of $5.06\, m \cdot s^{-1}$. Moreover, solar radiation once again has a Gaussian shape and solar energy is nearly larger than $600\, Ly$ for the three days. Therefore, it can be concluded that both experiments (with or without PCM) were made during days with alike climate.

4.2 Effect of PCM in thermal inertia and comfort

From the thermal comfort point of view, during the experiments with and without PCM panels inside the shipping container, it is expected that temperatures have often exceeded or failed to rise above what are considered the reasonable values.

The figure 4.3 shows these thermal parameters in the case of the container without PCM. As an overall trend, it is clear that indoor container temperatures follow the outdoor profile. Inner temperatures are well over the outer between $8\, a.m. - 10\, p.m.$ and occasionally fall below the outside temperatures during colder periods. Therefore, temperatures went up to a zone out of reach of the thermal comfort between $12\, p.m. - 7\, p.m.$ and between $2\, p.m. - 6\, p.m.$ on the first and second days respectively and, at the same time, they had dropped to a discomfort thermal zone between $3\, a.m. - 9\, a.m.$ and between $5\, a.m. - 9\, a.m.$. This means that, since the container has a low thermal inertia enclosure, it works as an amplifier of the external climate. The figure also compares peak temperatures delay, T_d, between indoor and outdoor temperatures. Over the two experimental days, it can be clearly seen that this delay has a value of 1 hour. In order to compute temperatures range reduction, T_{rr}, with comparable values, a shift time was chosen based on temperatures delay. It is seen that this temperatures difference was dramatically accentuated during $11\, a.m. - 8\, p.m.$ and that peak temperatures range reduction are $-6.16\, °C$ and $-4.34\, °C$ with a

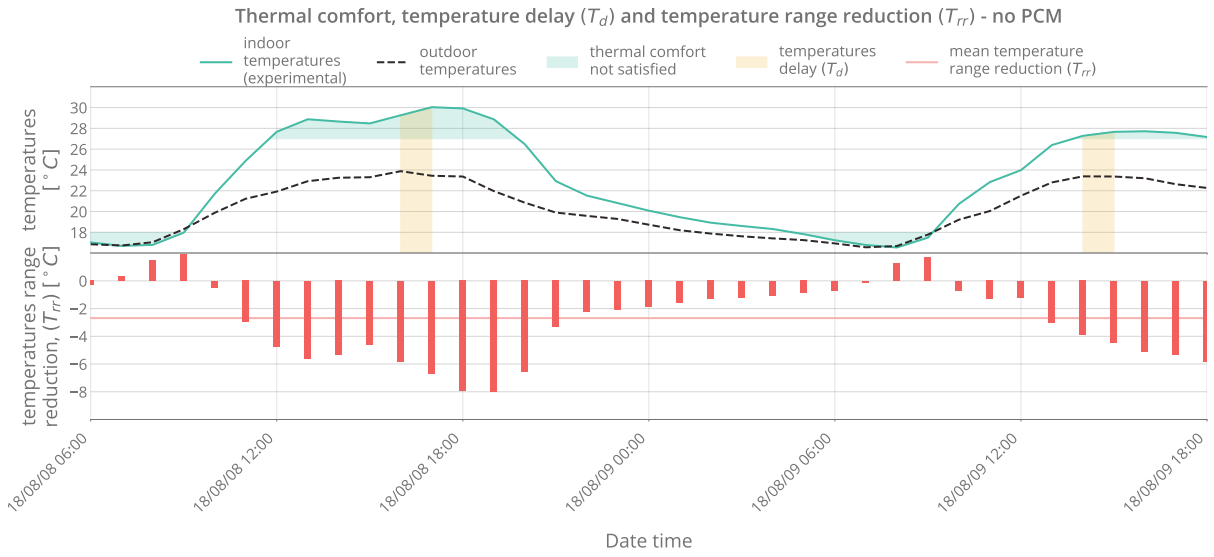

Figure 4.3: Thermal comfort, temperature delay (T_d) and temperature range reduction (T_{rr}). Experimental data measured without PCM.

mean temperature range reduction over the experiment of $-2.69\,°C$. These are negative values because outdoor temperatures caused an increase in indoor temperatures during warmer periods, which means the container was losing heat at a slower rate than the rate heat was being transferred to its inside.

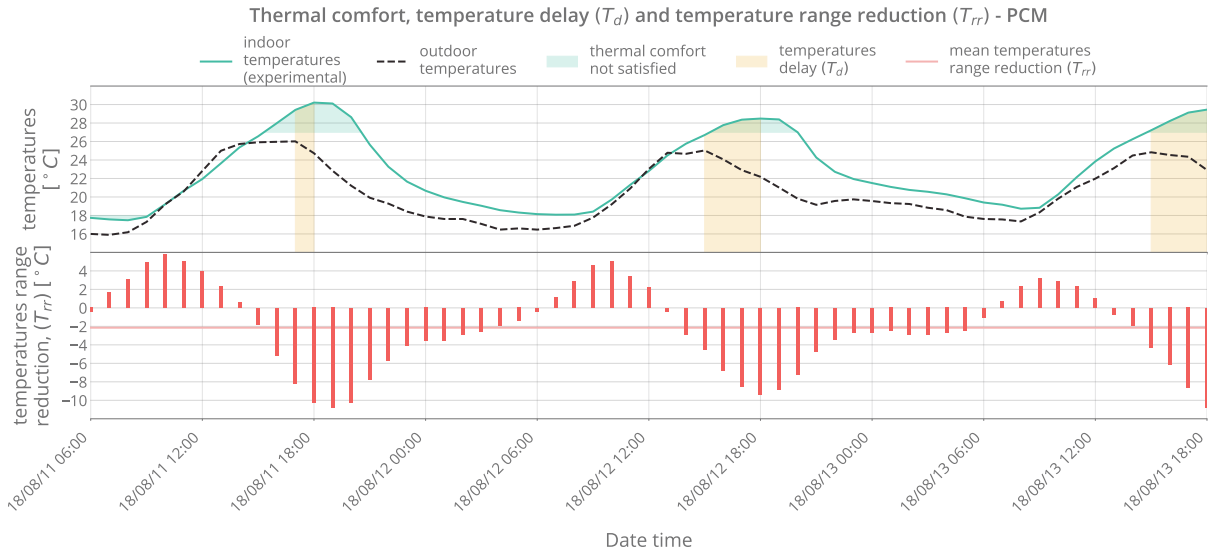

Figure 4.4: Thermal comfort, temperature delay (T_d) and temperature range reduction (T_{rr}). Experimental data measured with thirty PCM panels.

The figure 4.4 shows the same parameters in the case of the container with thirty PCM panels acting as internal mass. It can be seen that inner temperatures are beyond reach of the thermal comfort zone during $4\,a.m. - 9\,a.m.$, $4\,p.m. - 8\,p.m.$ and $3\,p.m. - 8\,p.m.$ intervals. This translates into a time percentage out of the thermal comfort zone with PCM of $19\,\%$. Peak temperatures delay, T_d, are equal on the first day and 2 hours higher on the second and third days compared with peak temperatures delay without PCM. Using this value, the shift time chosen to compute temperatures range reduction has a value of 3 hours.

It can be seen that this temperatures difference is enormously higher within the range of $4\,p.m.-10\,p.m.$. Peak temperatures range reduction on the three days are $-4.19\,°C$, $-3.45\,°C$ and $-4.62\,°C$ and a mean temperature range reduction of $-2.14\,°C$ was registered. These results show that adding PCM panels inside the shipping container causes a reduction in the absolute value of temperatures range reduction which is due to an improvement of the container thermal inertia.

In conclusion, experimental results show that installing PCM inside the shipping container as internal mass improves its thermal inertia and thermal comfort. Although the average temperatures range reduction did not experience a large improvement ($0.55°C$), minimum indoor temperatures and temperatures delay demonstrated that PCM boards were effective. Comparing both graphs, we can see that temperatures delay was two hours higher with PCM than without it. This was thanks to its sensible and latent heat storage capacity that was able to absorb excess heat being transferred into the container. At the same time, minimum indoor temperatures suffered a change in its behaviour. Despite this drop in outdoor temperatures at times when no PCM are installed, indoor temperatures are levelled out on $18°C$ when PCM were incorporated. This is due to the fact that all the excess heat absorbed by PCM during hotter periods is being released when outside temperatures reach PCM's solidification point ($18°C$). All this contributed to an amelioration of the thermal comfort inside the container. During experiments without PCM, thermal discomfort was felt for eleven hours over two days, whereas with PCM this period was only fourteen hours during the three days. Therefore, incorporating PCM boards inside the container translated into a thermal comfort time period improvement of 25%, avoiding or softening overheating problems. Table 4.4 sums the facts just described.

Table 4.4: A thermal comfort comparison of the shipping container with and without PCM.

Average indoor and outdoor peak temperatures difference $(°C)$		Temperatures range reduction $(°C)$		Thermal discomfort $(\%)$		Peak temperatures delay $(hours)$	
no PCM	PCM	no PCM	PCM	no PCM	PCM	no PCM	PCM
5.25	4.09	−2.69	−2.14	44	19	1	3

4.3 Sensitivity analysis on PCM boards

The aim of this section is to understand how several parameters affect the effectiveness of PCM boards. In this way, numerous sensitivity analysis will be made and the *EnergyPlus*® models' outcomes will be analysed. Paraffin melting point, night ventilation airflow, number of PCM boards used, their location and thickness are among the tests performed. It should be pointed out that *EnergyPlus*® models used in this section were validated beforehand (see section 2.5).

4.3.1 Paraffin melting point

In this section, paraffin melting point will be tested for the purpose of gauging the influence it has on PCM efficiency. For this reason, six PCM boards with melting point temperatures of about $19.7°C$, $21.7°C$, $23.7°C$, $25.7°C$, $27.7°C$ and $29.7°C$ were simulated. In the validated *EnergyPlus*® model, both their enthalpy-temperatures curves and variable thermal conductivity values were input for each test performed, according to section 3.3.4. Moreover, a Lisbon's weather file was used for these simulations as well as lights, people and an HVAC system, as mentioned earlier on subsections 3.3.5 and 3.3.8. Other than that, night ventilation airflow, number of PCM boards, their location and thickness remained with the same values used on the experimental setting.

Table 4.5: Model set up for paraffin melting point's sensitivity analysis.

Weather file	PCM panel	Fan airflow (ACH)	PCM panel thickness (mm)	PCM panel location	Number of PCM panels	Lights	People	HVAC
Lisbon	PCM22-30	21.1	5.2	internal mass	30	●	●	●

○ - off | ● - on

Total energy demand for the current study is shown in figure 4.5. The annual cooling and heating needs derive from the HVAC system considered. Overall, cooling needs represent the largest share in annual energy demand whereas heating arise as the smallest. It can be clearly seen that including PCM boards inside the container reduces the total annual energy demand whatever it is the melting point considered. Furthermore, over paraffin melting point, the biggest change derives from cooling needs since it shows a slight increase from $20°C$ to $26°C$. From $26°C$, no relevant energy demand changes are observed. Yet, the best scenario where the smallest amount of energy was expended occurs by $20°C$.

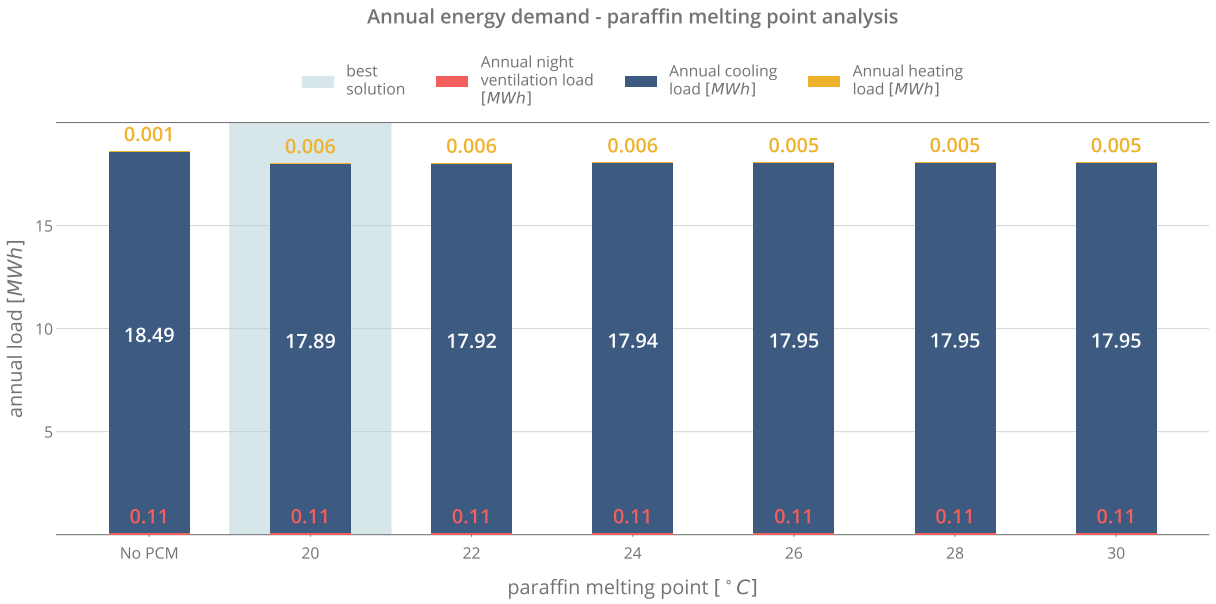

Figure 4.5: Annual HVAC cooling, HVAC heating and night ventilation energy demand for different PCM melting points.

The figure 4.6 compares the annual cooling and heating energy demands for the several melting temperatures in comparison with the case without PCM panels inside the container.

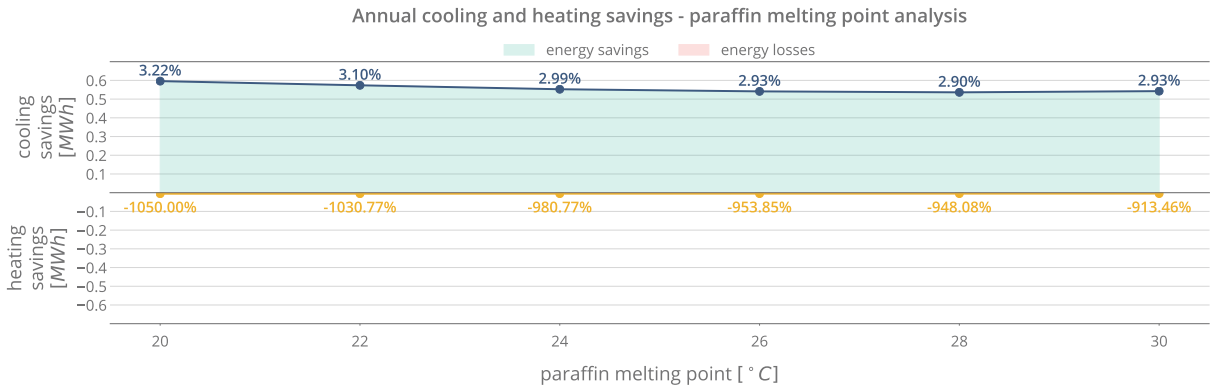

Figure 4.6: Annual HVAC cooling and heating energy savings for different PCM melting points.

As an overall trend, it can be noticed that PCM acts as a cooling system. Although it drops the amount of HVAC cooling needs by 3%, heating demand registers a negligibly increase. Nevertheless, as it was already pointed out, a melting temperature of $20°C$ stands out as the case with the highest cooling needs savings around $0.596\,MWh$ (3.22%). This result contradicts some previous studies in which higher melting points came up as the best option for warmer climates [65].

From an energy costs point of view, the outlook does not change considerably as figure 4.7 suggests. From $20°C$ to $26°C$, there is a slight cost decrease and above $26°C$ energy costs remain more or less the same. However, an annual cost slump between the case without PCM boards and the others is perceptible. Cooling costs stick out as the biggest slice in annual energy costs and heating constitutes less than 0.03%.

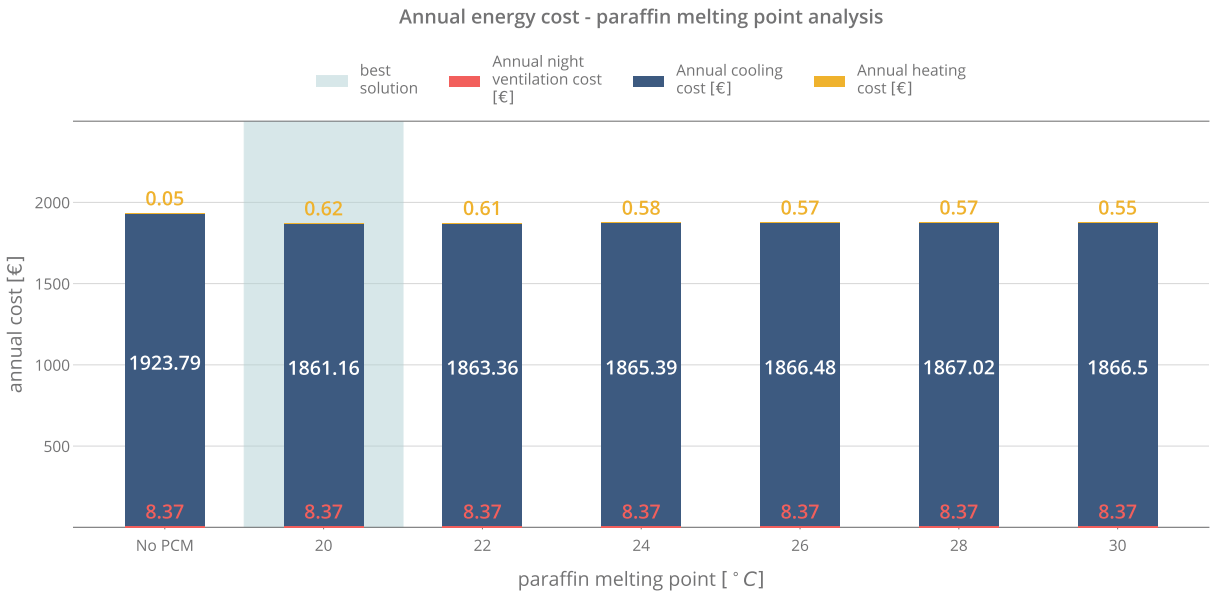

Figure 4.7: Annual HVAC cooling, HVAC heating and night ventilation energy costs for different PCM melting points.

Figure 4.8 makes a parallel between cooling and heating energy costs for the different temperatures considered and the case without PCM boards inside the container. It clearly shows that the annual electricity bill of this low thermal inertia space benefits from incorporating PCM. Despite heating costs revealing a slightly rise of $0.50€$, it is almost negligible when balancing with cooling savings in the order of $60€$. Therefore, as long as no other investment and maintenance costs are contemplated installing PCM makes a good investment.

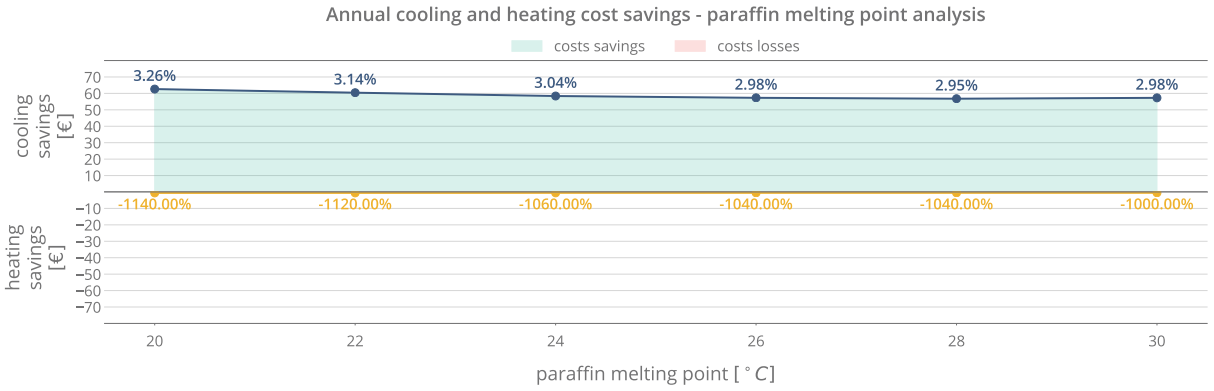

Figure 4.8: Annual HVAC cooling and heating energy costs savings for different PCM melting points.

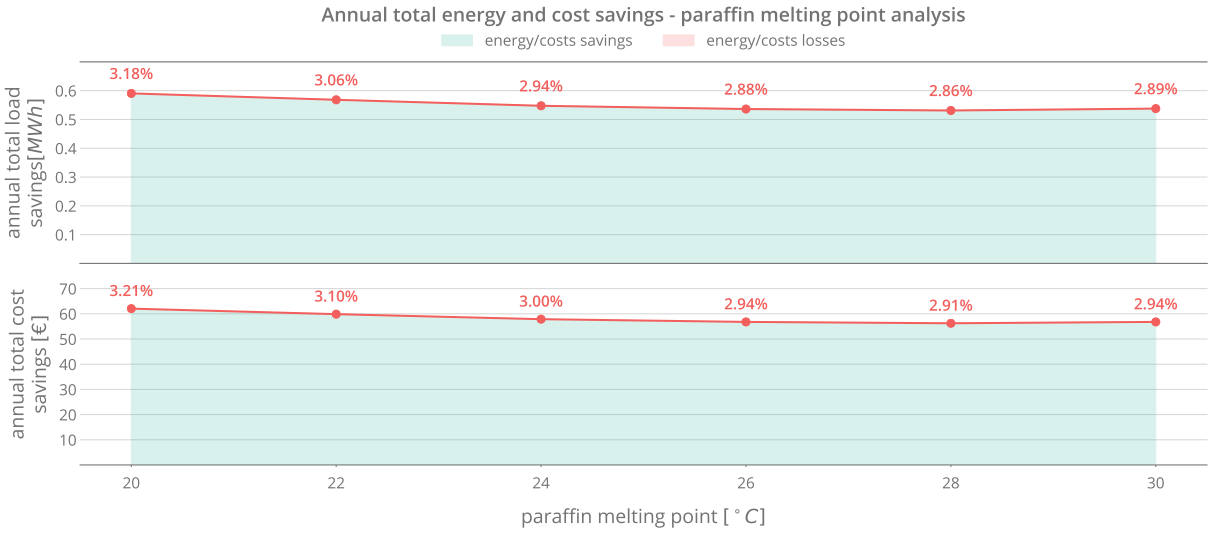

Figure 4.9: Total (HVAC cooling, HVAC heating and night ventilation) annual energy and costs savings for different PCM melting points.

All this information is added together in figure 4.9. In general, since heating HVAC system needs are nearly trifling, all the energy savings comes from cooling savings. In terms of energy, in this particular case, this indicates PCM acts as an effective cooling system, reducing energy needs in about $0.591\,MWh$ annually. For the best scenario ($20°C$), this corresponds to a drop in $62.06€$ spent annually in electricity provided to the HVAC system. It was also concluded that lower melting temperatures appear as the best option for the shipping container studied. This implies that latent heat storage starts off sooner than if PCM with higher fusion temperatures was chosen. Given that, further simulations will be

made using $20°C$ PCM boards.

4.3.2 Night ventilation

As previous studies mentioned [49], night ventilation constitutes a useful way to drop indoor mean temperatures and therefore induce a release of the latent heat stored during the day into PCM boards. Moreover, in the scope of this thesis, the same conclusion was achieved during several experimental tests with and without night ventilation. However, it was not possible to experimentally control the air changes per hour of the fan. Therefore, in this section a parametric study on this variable was made simulating $0\,ACH$, $5\,ACH$, $10\,ACH$, $15\,ACH$ and $21.1\,ACH$. Besides that, all the remaining inputs were the same used in section 4.3.1 and can be seen in table 4.6.

Table 4.6: Model set up for night ventilation's sensitivity analysis.

Weather file	PCM panel	Fan airflow (ACH)	PCM panel thickness (mm)	PCM panel location	Number of PCM panels	Lights	People	HVAC
Lisbon	PCM20	$0-21.1$	5.2	internal mass	30	●	●	●

○ - off | ● - on

The figure 4.10 puts in parallel the three types of energy loads with and without PCM over the forced ventilation. As an overall trend, the higher the night ventilation ACH value, the smaller the cooling needs for both cases. The order of magnitude of the energy needs for acclimatization rounds $18\,MWh$. Almost 99% of the energy spent annually comes from cooling needs making it the uppermost energy demander.

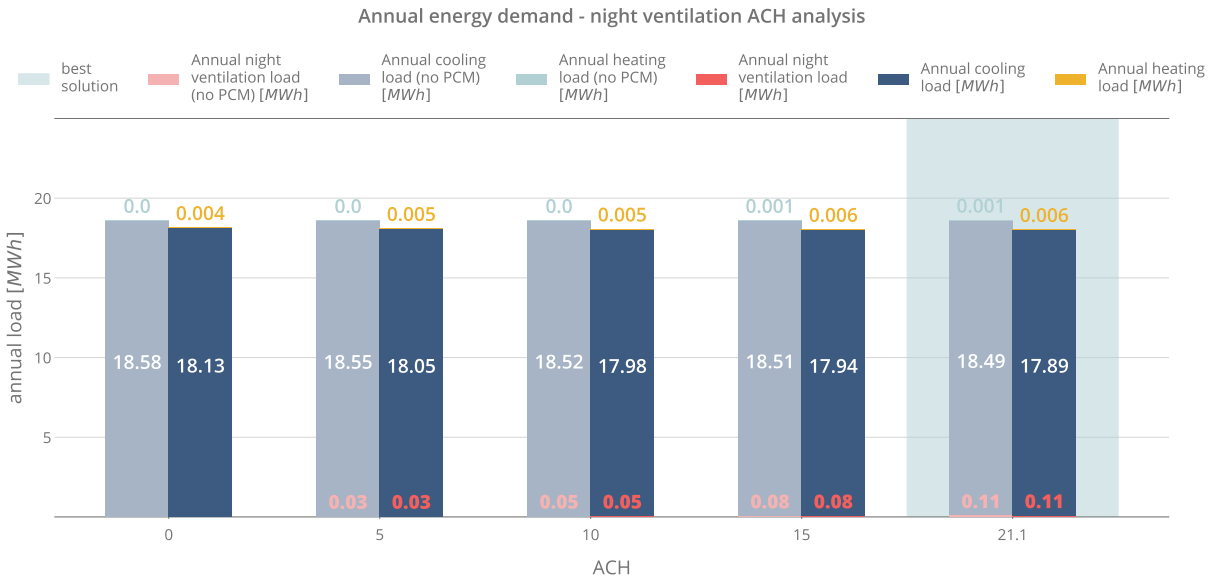

Figure 4.10: Annual HVAC cooling, HVAC heating and night ventilation energy demand for different rate values of night ventilation.

Nevertheless, rising the ACH value makes PCM more cooling effective when compared with the case without PCM as it can be seen in figure 4.11. While in the case of $0\,ACH$ the cooling energy difference

between no PCM and PCM was only $456\,kWh$, by $21.1\,ACH$ the cooling energy savings rise to $596\,kWh$. This is due to the fact that night ventilation brings colder outside air that induces a temperatures drop on PCM panels which causes the release of stored sensible and latent heat. Despite that, heating needs seem not to benefit from increasing ACH when PCM are installed, as during colder weather no or minimum phase change occurs on these boards.

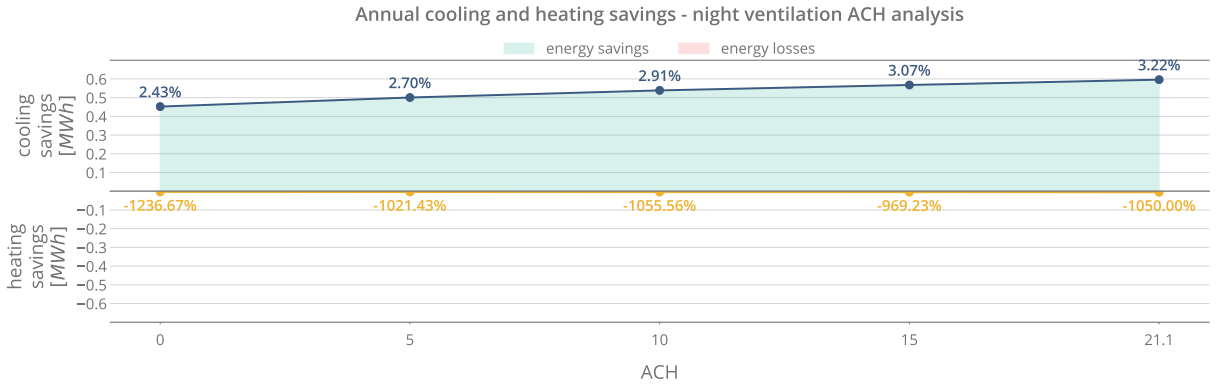

Figure 4.11: Annual HVAC cooling and heating energy savings for different rate values of night ventilation.

In respect of costs, the electricity bill of the shipping container follows its energy demand. In figure 4.12, it can be noticed that the higher the ACH value, the lower the cooling and the higher the heating and ventilation costs, either with or without PCM. Nonetheless, cooling shows up as the most costly, making the others almost insignificant. Consequently, cooling costs variation sets the pace of the total annual energy costs, spending more than $1860€$.

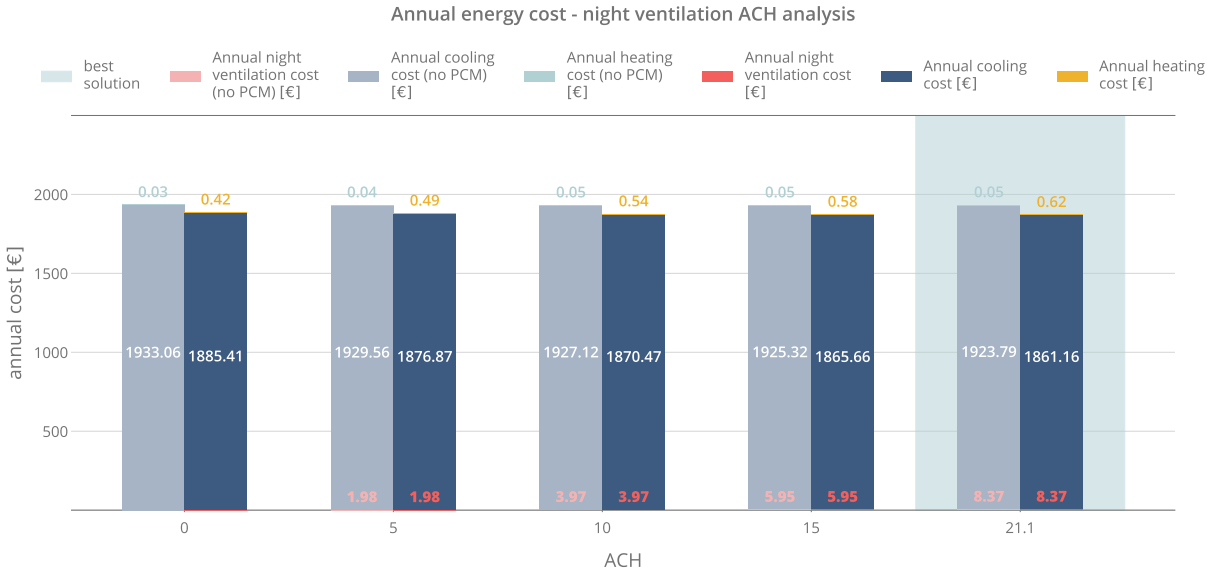

Figure 4.12: Annual HVAC cooling, HVAC heating and night ventilation energy costs for different rate values of night ventilation.

Figure 4.13 demonstrates that it is more profitable rising the value of night ventilation ACH in terms of cooling rather than in heating. By $21.1\,ACH$, installing PCM boards with a $20°C$ melting point saved up

about 62.63€ in cooling costs while in heating more than 0.57€ were spent.

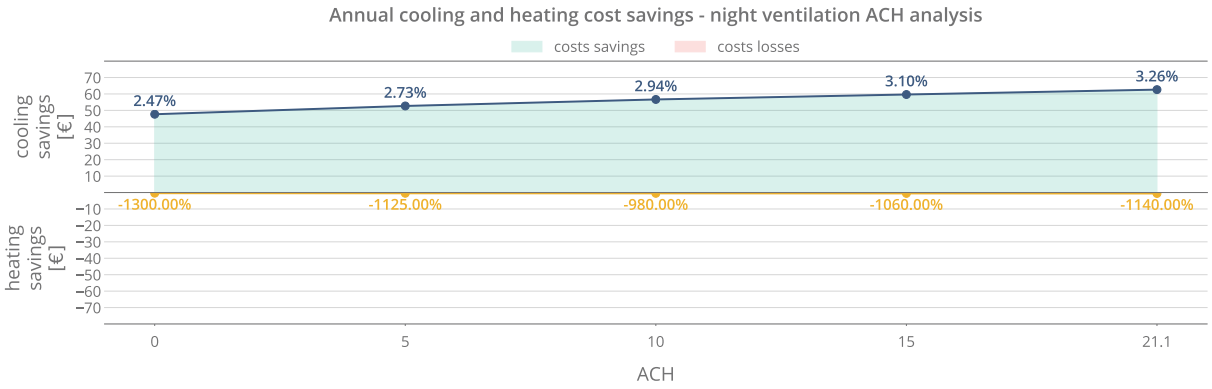

Figure 4.13: Annual HVAC cooling and heating energy costs savings for different rate values of night ventilation.

As a global trend (fig. 4.13), promoting a growth of the night ventilation inside the shipping container causes an improvement on PCM boards effectiveness. Annually, more than $591\,kWh$ and 62.06€ could be economized when PCM together with a high night ventilation airflow are set. In spite of that, it must be borne in mind no benefit comes from having night ventilation turned on during colder days since PCM do not reach the melting point and, for this reason, there is no latent heat release to be improved by night ventilation.

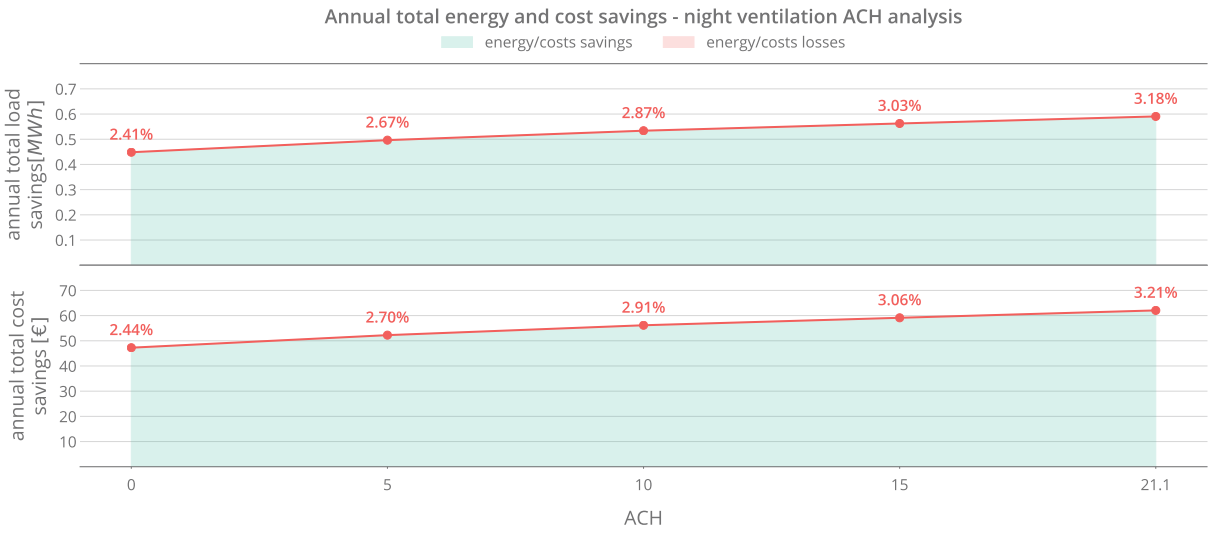

Figure 4.14: Total (HVAC cooling, HVAC heating and night ventilation) annual energy and costs savings for different rate values of night ventilation.

4.3.3 Number of PCM boards

Experimental tests were only run with 0 or 30 PCM boards. For this reason, a sensitivity analysis on the number of PCM boards will be made in this section. A quantity of 0, 6, 12, 18, 24, 30, 36, 42 and 48 boards are among the studied cases. Although it is not physically possible to install 100 boards, this

scenario was also included in the tests performed. This allowed to observe how doubling the number of boards will affect a shipping container twice the original size with approximately the same amount of HVAC energy needs. All the other inputs are present in table 4.7.

Table 4.7: Model set up for PCM boards number's sensitivity analysis.

Weather file	PCM panel	Fan airflow (ACH)	PCM panel thickness (mm)	PCM panel location	Number of PCM panels	Lights	People	HVAC
Lisbon	PCM20	21.1	5.2	internal mass	$0-100$	●	●	●

○ - off | ● - on

The figure 4.15 shows night ventilation, cooling and heating HVAC energy demand over the amount of PCM boards. It can be clearly seen that over the x axis cooling needs fall moderately from $18.49\,MWh$ to $16.9\,MWh$. The highest number of PCM boards modelled (100) has the lowest value of cooling energy load. In terms of heating needs, despite the fact that no load was registered from 0 to 24 boards, from 30 a marginal increase was noticeable. However, it should be pointed out that cooling needs lead as the highest energy demander, representing more than 99%. In this particular case, using 48 PCM boards pops out as the best choice since 100 is physically impossible. Night ventilation, as expected, levels out at $110\,kWh$ annually.

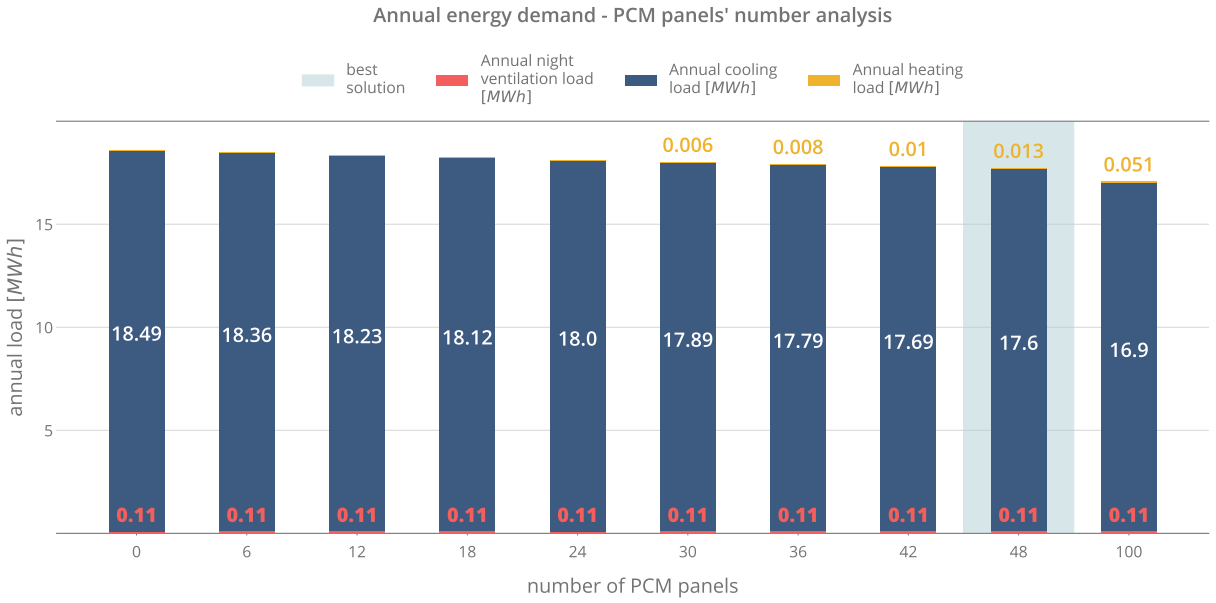

Figure 4.15: Annual HVAC cooling, HVAC heating and night ventilation energy demand for different number of PCM panels.

The figure 4.16 relates cooling and heating loads with and without PCM. It can be seen that rising the number of panels inside the container increases the amount of cooling energy saved in comparison with the case without PCM boards. Accordingly to this, during Summer, adding PCM boards implies adding latent heat storage units which prevents overheating and so, cooling needs fall. On the other hand, annexing more PCM pieces increases the amount of energy it is needed in order to warm the surroundings. Thus, during colder days the heating needs have an upward trend over the quantity of

PCM boards. However, these warming needs are minor.

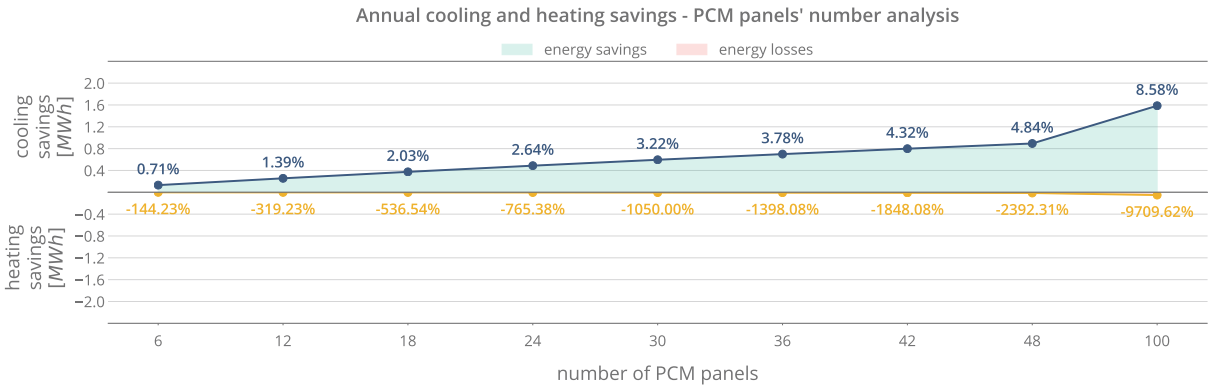

Figure 4.16: Annual HVAC cooling and heating energy savings for different number of PCM panels.

Costs reinforces the same idea. Chilling costs have a falling trend as figure 4.17 suggests. From 0 to 48 boards, the cooling price varies from 1923.79€ to 1829.72€. However, having 100 units of PCM inside the container would mean a refrigeration price of 1756.29€. In opposition, heating costs rise from 0.05€ to 5.35€ over the amount of panels.

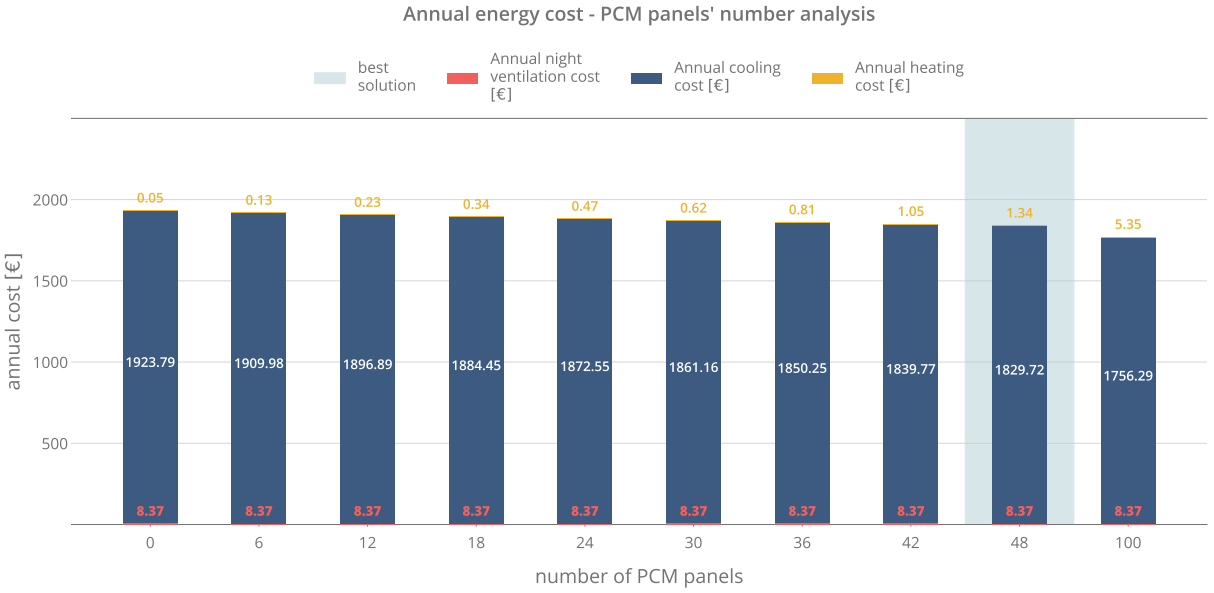

Figure 4.17: Annual HVAC cooling, HVAC heating and night ventilation energy costs for different number of PCM panels.

Cooling and heating costs are shown in figure 4.18. Similar to energy savings, the higher the number of boards incorporated into the shipping container, the larger the amount of money saved in cooling and the higher the costs spent in heating, in comparison with the case without PCM. Nevertheless, the order of magnitude spent in heating is 72 times lower than the magnitude of money saved with cooling. When only acclimatization costs are taken into account, six units of PCM saves more than 13€ per year whereas forty eight pieces of the same material saves more than 94.07€. At the same time, using 100 boards shoots this saving up to 167.50€.

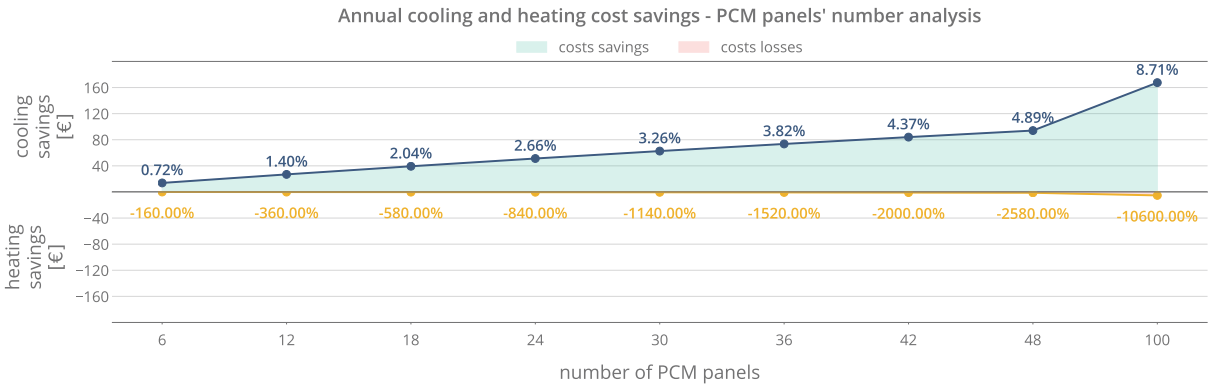

Figure 4.18: Annual HVAC cooling and heating energy costs savings for different number of PCM panels.

As an overall trend (fig. 4.18), PCM saves energy that would be required by a HVAC system to achieve a certain level of thermal comfort. In total, more than $882\,kWh$ would be economized if 48 units were installed in the container and that would mean 92.78€ savings contrasting with the case without PCM. Making a parallel with the real set up experimented, 48 units would cause $291\,kWh$ and 30.72€ energy and costs savings, respectively. It should be noted that if possible it would have been better removing or decreasing the number of PCM boards installed during colder days, though it has an almost imperceptible impact.

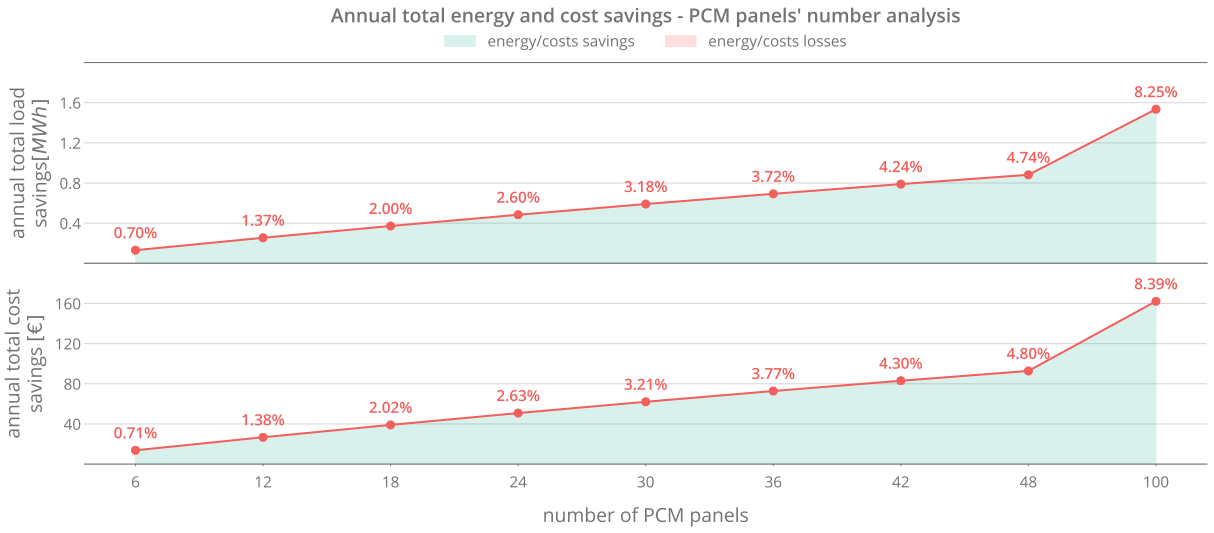

Figure 4.19: Total (HVAC cooling, HVAC heating and night ventilation) annual energy and costs savings for different number of PCM panels.

4.3.4 PCM boards location

The experimental set up only allowed to test PCM as internal mass. So, in order to study the effect a change in PCM location can bring to the overall thermal comfort and energy consumed, a parametric analysis on this matter was done. Eight different scenarios were considered such as no PCM, using

PCM as internal mass, in both West and East sided-walls ($15.7\,m^2$), North and South-doors ($6.3\,m^2$), in roof ($14.8\,m^2$) and, finally, in floor ($14.8\,m^2$). Since the different scenarios had equally different amounts of PCM, internal mass was modelled with 6, 12 and 13 boards. The extra inputs remained identical (see table 4.8).

Table 4.8: Model set up for PCM location's sensitivity analysis.

Weather file	PCM panel	Fan airflow (ACH)	PCM panel thickness (mm)	PCM panel location	Number of PCM panels	Lights	People	HVAC
Lisbon	—	21.1	—	no PCM	—	●	●	●
Lisbon	PCM20	21.1	5.2	internal mass	6	●	●	●
Lisbon	PCM20	21.1	5.2	North sided-door	6	●	●	●
Lisbon	PCM20	21.1	5.2	South sided-door	6	●	●	●
Lisbon	PCM20	21.1	5.2	internal mass	13	●	●	●
Lisbon	PCM20	21.1	5.2	East sided-wall	13	●	●	●
Lisbon	PCM20	21.1	5.2	West sided-wall	13	●	●	●
Lisbon	PCM20	21.1	5.2	internal mass	12	●	●	●
Lisbon	PCM20	21.1	5.2	roof	12	●	●	●
Lisbon	PCM20	21.1	5.2	floor	12	●	●	●

○ - off | ● - on

Figure 4.20 shows clearly that in terms of energy the HVAC system demands, installing PCM as internal mass is the most beneficial option. As it was concluded in the previous section (see section 4.3.3), the higher the amount of PCM as internal mass, the smaller the amount needed for cooling by the HVAC system. This analysis confirms that since the best option from all those presented had the highest amount of boards (13) used as internal mass, requiring $18.21\,MWh$.

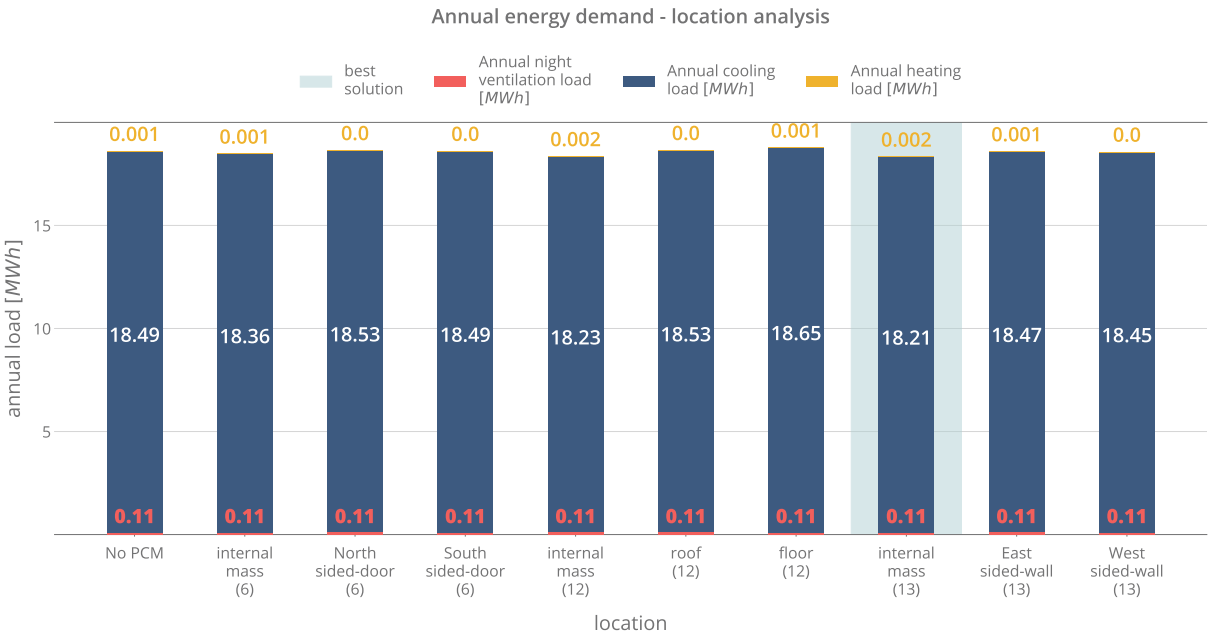

Figure 4.20: Annual HVAC cooling, HVAC heating and night ventilation energy demand when PCM panels are located in different places.

In some cases, cooling needs are higher with than without PCM. Among these we have the North and South sided-doors ($18.53\,MWh$ and $18.49\,MWh$), roof ($18.53\,MWh$) and floor ($18.65\,MWh$). On the other hand, apart from the floor case, these same scenarios work best as heating systems. This means that during colder days, installing PCM in doors and roof raised the amount of sensible heat PCM store during the day, though this amount was insignificant.

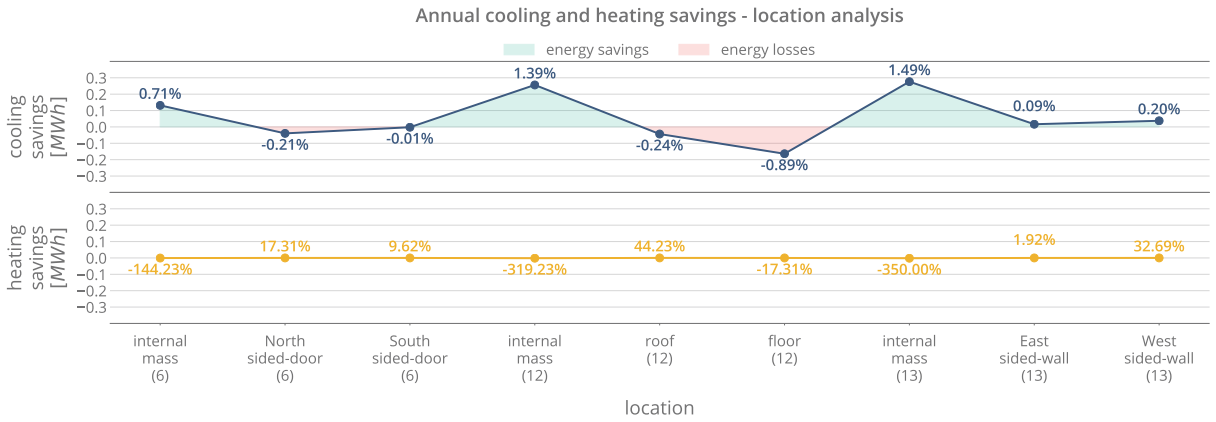

Figure 4.21: Annual HVAC cooling and heating energy savings when PCM panels are located in different places.

The reason for internal mass PCM working better than the others as a cooling system comes from the fact it had both surfaces uncovered. This made it easier for boards to drop their temperatures, release the latent heat stored and consequently be more effective. Furthermore, PCM internal mass was incorporated near the ceiling which took advantage of air stratification. Hotter air has smaller values of volumetric mass density (ρ) and therefore it goes up. This fact made it easier for PCM to absorb latent heat. Figure 4.21 corroborates this theory.

From the costs point of view, this panorama does not change. PCM internal mass cases stayed as the best options available, being the case with the largest quantity of boards the most profitable one (1894.78€). The worst scenario is when a PCM floor is installed costing 1940.80€, 17.01€ more than the case without PCM (1923.79€). All this info is shown in figures 4.22 and 4.23.

Overall, contemplating figure 4.24 the most effective scenarios are those where PCM is installed as internal mass and the higher units quantity the higher the cooling effectiveness. Keeping this and the previous section (4.3.3) in mind, the best option so far is using 48 units of PCM internal mass.

4.3.5 PCM board thickness

Since thermal mass systems available experimentally had only $5.2\,mm$ of thickness, an additional sensitivity analysis on this variable was made. Tests performed included thickness values of $5.2\,mm$, $10\,mm$, $20\,mm$, $30\,mm$, $40\,mm$ and $50\,mm$. It should be noted that 48 units of PCM were used on these simulations. All the other parameters were maintained as table 4.9 suggests.

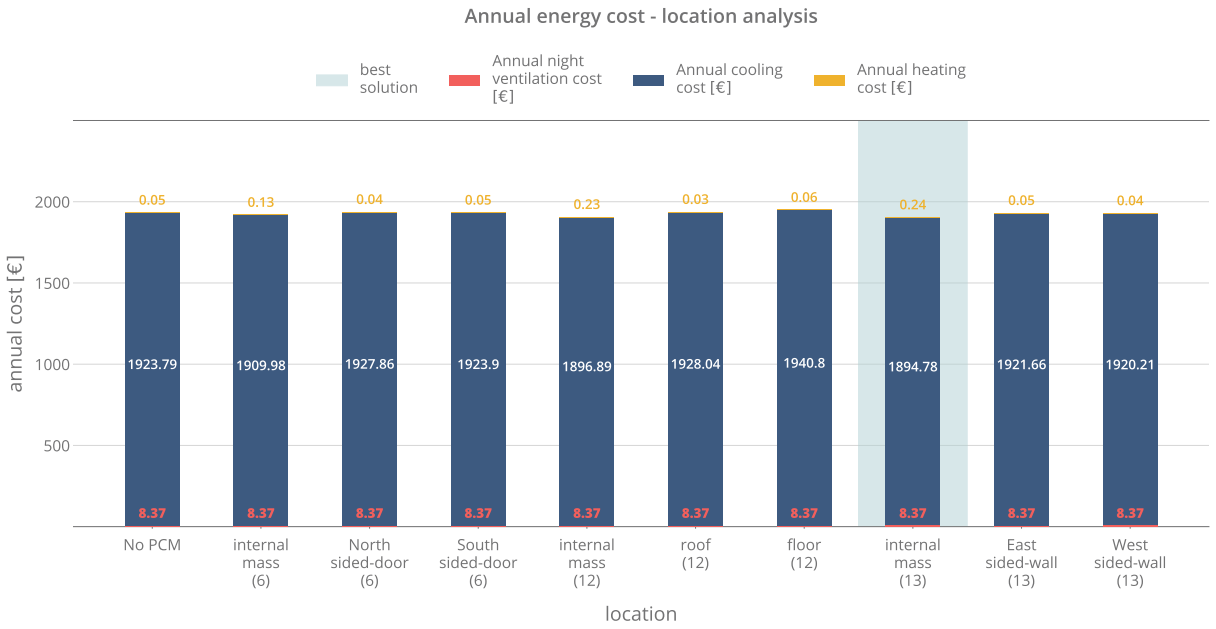

Figure 4.22: Annual HVAC cooling, HVAC heating and night ventilation energy costs when PCM panels are located in different places.

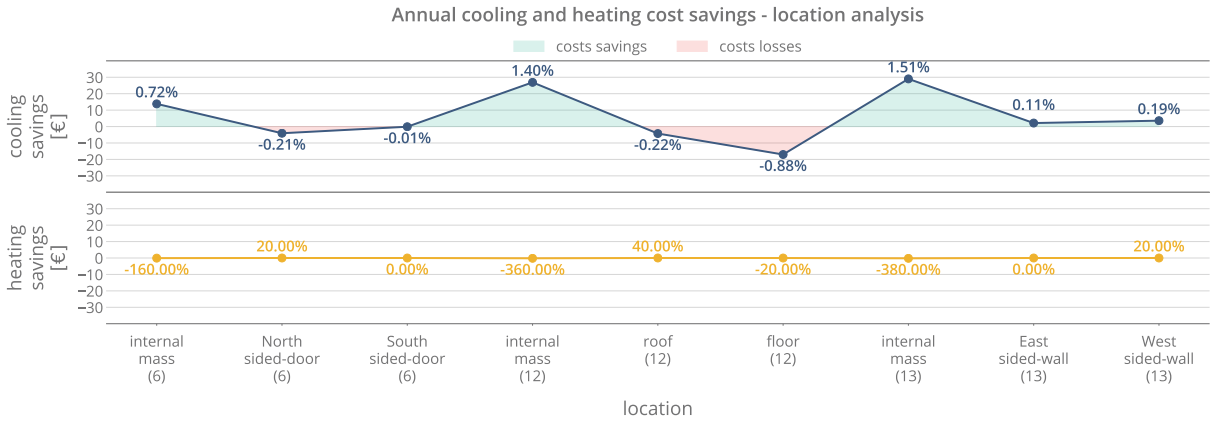

Figure 4.23: Annual HVAC cooling and heating energy costs savings when PCM panels are located in different places.

Table 4.9: Model set up for PCM boards thickness's sensitivity analysis.

Weather file	PCM panel	Fan airflow (ACH)	PCM panel thickness (mm)	PCM panel location	Number of PCM panels	Lights	People	HVAC
Lisbon	PCM20	21.1	$5.2 - 50$	internal mass	48	●	●	●

○ - off | ● - on

Annual energy loads for night ventilation, cooling and heating are shown in figure 4.25. As an overall trend, rising the thickness decreases cooling needs while heating needs stay almost unchanged. Although the best option seems to be when $50\,mm$ thickness PCM were used, it should be pointed out that it would mean a 1000% increase in PCM weight. If 48 units with a thickness of $5.2\,mm$ have a mass of $258.8\,kg$, having a proportional mass quantity in PCM boards with a thickness of $50\,mm$ would mean a

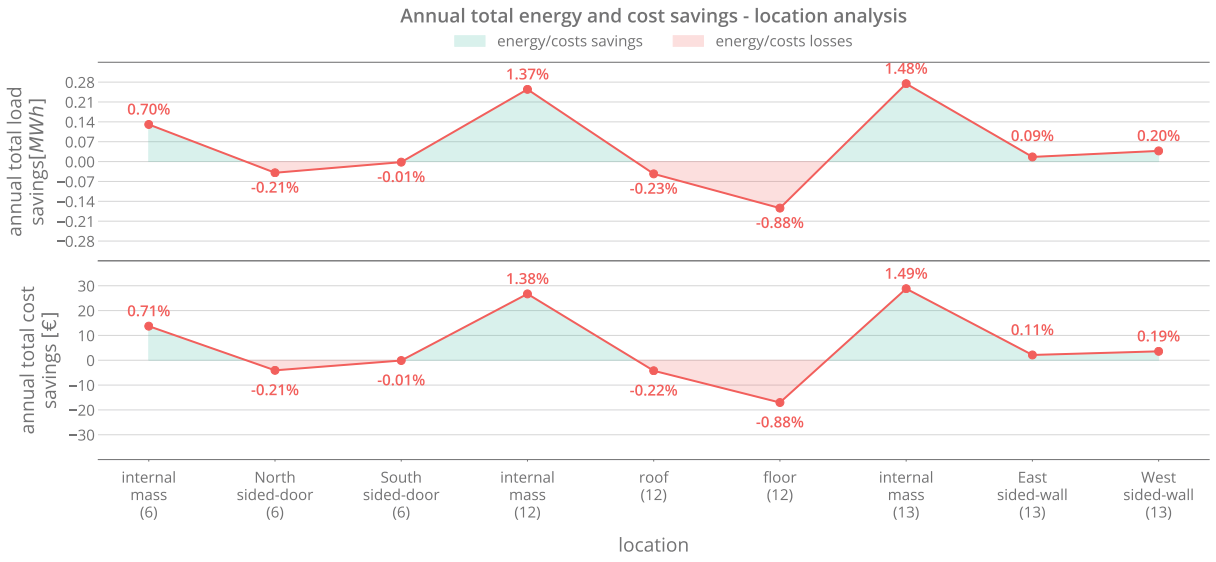

Figure 4.24: Total (HVAC cooling, HVAC heating and night ventilation) annual energy and costs savings when PCM panels are located in different places.

total system mass of $2588\,kg$. Due to this thickness-mass commitment, the best option was using PCM panels with a thickness of $10\,mm$. Rising board thickness also increases the heat storage capacity. In this particular case, each board now has $280\,kJ \cdot kg^{-1}$ both sensible and latent heat storage capacity and the total cooling thermal mass system has $13440\,kJ \cdot kg^{-1}$. For this reason, only $16.84\,MWh$ are required by the HVAC system opposing to the PCM free case.

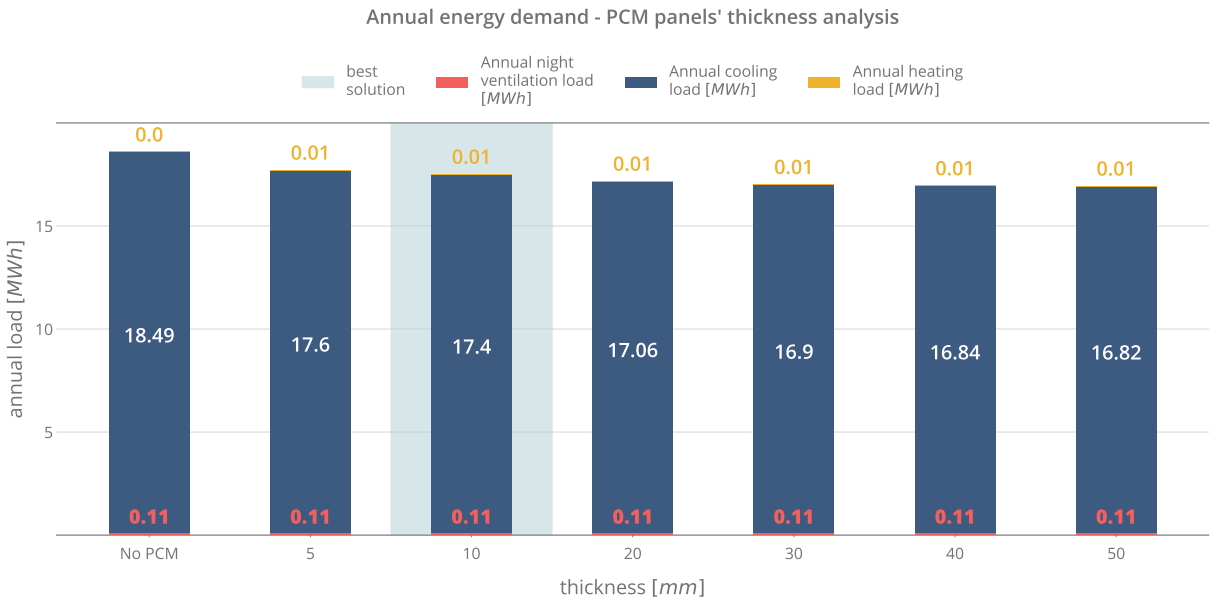

Figure 4.25: Annual HVAC cooling, HVAC heating and night ventilation energy demand when PCM panels are located in different places.

Considering figure 4.26, cooling and heating savings are plotted. It can be clearly seen adding PCM brings benefits as a cooling system whereas it demands more heating energy by the HVAC system.

However, it was almost negligible. From $5\,mm$ to $30\,mm$ of thickness, refrigeration load savings had a rapid increase but by $40\,mm$ it levelled out around $1.651\,MWh$. This means that raising thickness values above $50\,mm$ if possible does not translate into a proportional increase in cooling savings. A reason for this is the fact that increasing excessively the thickness of the boards will make the PCM in the center layer less available for latent heat storage. For this reason, rising thickness above $40\,mm$ becomes unprofitable in the sense that a bigger amount of material and therefore more expensive is bought and the latent heat storage stays identical as if a $40\,mm$ thickness board was used. Not to mention the costs of the structure to support the weight of such boards.

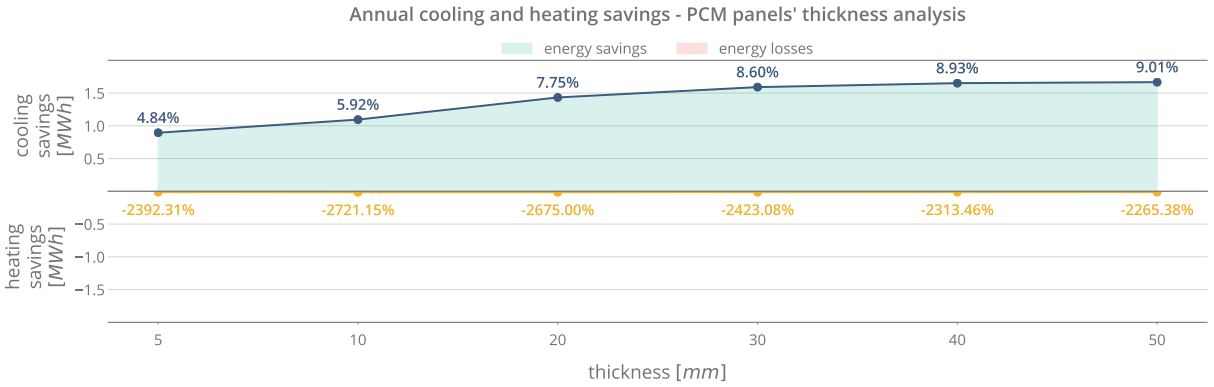

Figure 4.26: Annual HVAC cooling and heating energy savings for PCM panels with different thicknesses.

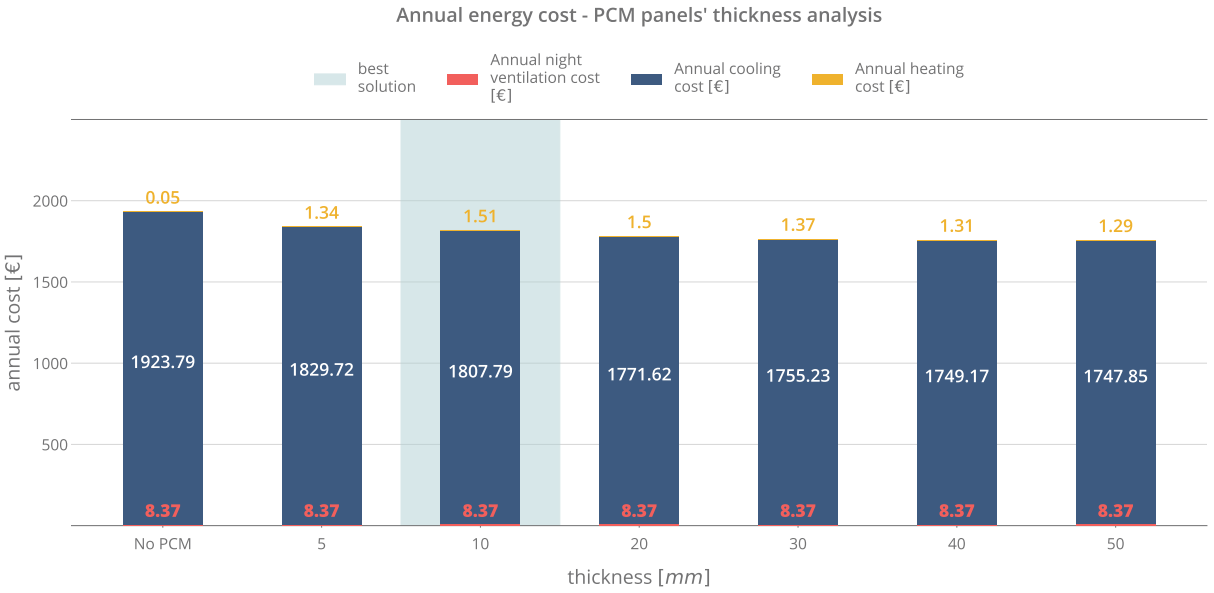

Figure 4.27: Annual HVAC cooling, HVAC heating and night ventilation energy costs for PCM panels with different thicknesses.

Costs also followed the same trend. Although the less expensive scenario (1747.85€) was using 48 units with $50\,mm$ of thickness, it was not physically possible and so the case with $10\,mm$ of thickness (1807.79€) was the best option available (fig. 4.27). Looking into figure 4.28 this meant a cooling saving and a heating loss of 116€ and -1.46€. Again, cooling prices demonstrate a considerable increase from

$5\,mm$ to $30\,mm$ and from $40\,mm$ it stays around 175€. In this particular case, the best option saves more than 116€ in cooling when compared with the case without PCM.

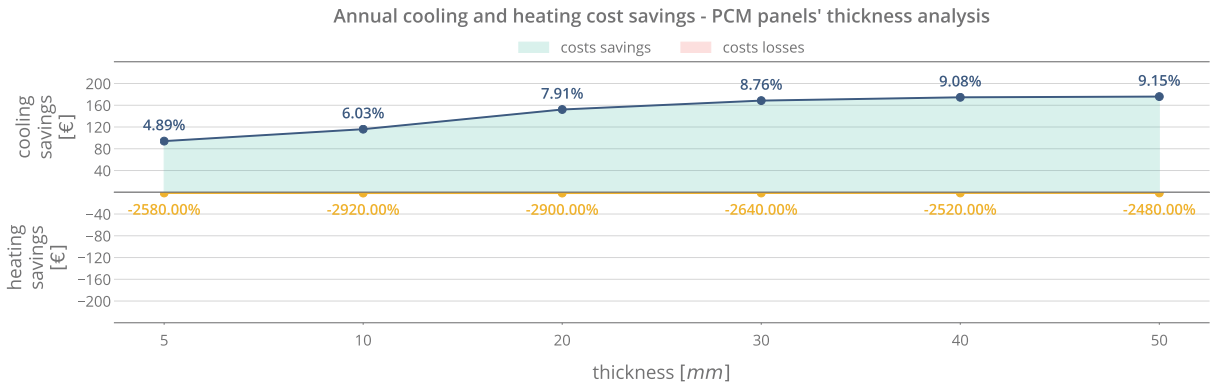

Figure 4.28: Annual HVAC cooling and heating energy costs savings for PCM panels with different thicknesses.

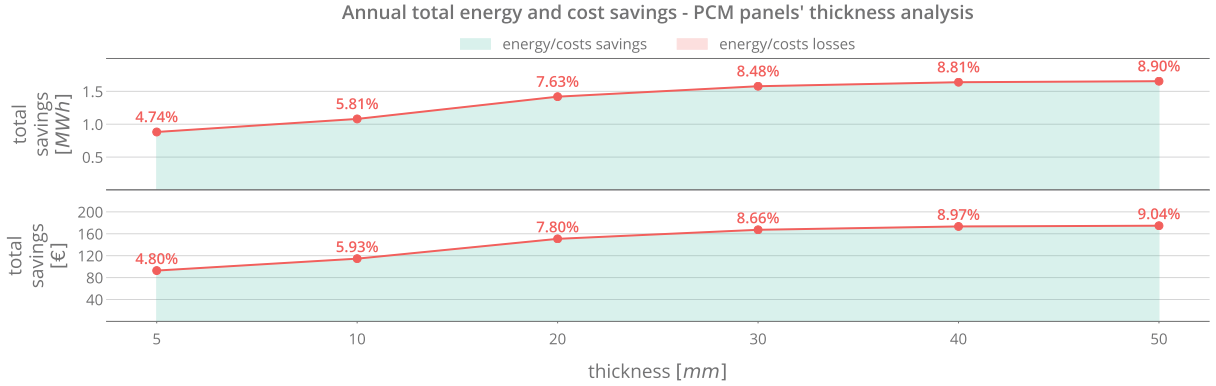

Figure 4.29: Total (HVAC cooling, HVAC heating and night ventilation) annual energy and costs savings for PCM panels with different thicknesses.

In conclusion, rising PCM thickness is energy and cost advantageous until an optimum value where part of the PCM becomes inaccessible. In this particular case, although there was a scenario where $1.655\,MWh$ and 174.70€ savings could be achieved, it constituted an unrealistic one. Consequently, the case with $10\,mm$ of thickness was considered the best with energy and HVAC costs savings around $1.08\,MWh$ and 114.54€, respectively (fig. 4.28).

4.4 Economic analysis

For the purpose of understanding if buying these boards is a profitable investment, a simple economic analysis will be made considering their payback period. Two different scenarios will be chosen such as the experimental scenario and the best option for this particular case. The respective settings for each one are shown in table 4.10.

The payback period is computed using the net present value (NPV) concept. This principle brings all

Table 4.10: Scenarios of the economic analysis.

Scenario	PCM panel	Fan airflow (ACH)	PCM panel thickness (mm)	PCM panel location	Number of PCM panels	Lights	People	HVAC
experimental	PCM22	21.1	5.2	internal mass	30	●	●	●
ideal	PCM20	21.1	10	internal mass	48	●	●	●

○ - off | ● - on

the investments and future cash-flows into the present. If the result is positive the project is valuable and if not the project should not be done. In this particular case, the NPV will be estimated knowing the initial investment, I_0 [€], and the present value, PV [€]. Considering that cash-flows, C [€], are annuities coming from annual electricity savings, the PV can be calculated knowing their inflation rate, g, the respective rate of return, r, and the time period in years in which these cash-flows are generated, t. The payback period is obtained solving equation 4.1 in respect to the time period, t, by imposing $NPV \geq 0$.

$$NPV = I_0 + PV = I_0 + \frac{C}{r-g} - \frac{C}{r-g} \times \left(\frac{1+g}{1+r}\right)^t \tag{4.1}$$

Inflation rate of electricity prices, g, and the rate of return, r were computed using the average value of the past ten years. This data can be seen in table 4.11.

Table 4.11: Return rate of treasury bonds [80], r, and inflation rate of consumer price in electricity sector [81], g.

variable	2007	2008	2009	2010	2011	2012	2013	2014	2015	2016	2017	average value $(\bar{r}, \bar{g})$
r	4.4%	4.5%	4.2%	5.4%	10.2%	10.5%	6.3%	3.8%	2.4%	3.2%	3.1%	5.27%
g	3.6%	4.0%	2.1%	4.4%	6.7%	8.7%	2.2%	2.2%	0.2%	0.4%	0.6%	3.19%

Initial investment was estimated using two different approaches for each scenario: a prototype price and price based on their raw materials costs. *DuPont Energain®* thermal mass system has a prototype price of $40\,£/m^2$ [82]. Since the best option has double thickness, its price would be duplicated for $80\,£/m^2$. In the case of the price based in raw materials, market prices for aluminium (alloy 8011), ethylene based polymer (polyethylene glycol 200 - $H\,(OCH_2CH_2)_n \cdot OH$) and paraffin wax with a melting point of $21.7°C$ (n-heptadecane - $C_{17}H_{36}$) were conferred. Nonetheless, according to Sharma et al. [13] and since the best option uses a fatty acid PCM with a $20°C$ melting point, a polyethylene glycol 600 $(H\,(OC_2H_2)_n \cdot OH)$ was the obvious option. The corresponding market prices and respective currency conversion [83] can be seen in table 4.12.

Knowing aluminium foils' thickness $(100\,\mu m)$, area $(1.198\,m^2)$ and mass volumetric density $(2710\,kg{\cdot}m^{-3})$ [88], it is possible to compute its weight $(0.649\,kg)$. Since each panel has a mass of $5.391\,kg$, the remaing 88% of material is constituted by polyethylene glycol (PEG) 200 and paraffin wax. The respective quantities and prices for each material can be seen in table 4.13. In final estimated prices, a 50% net

Table 4.12: Market prices for alloy 8011 [84], polyethylene glycol 200 [85], n-heptadecane [86] and polyethylene glycol 600 [87].

alloy 8011 [84]		polyethylene glycol 200 [85]		n-heptadecane [86]		polyethylene glycol 600 [87]	
$\$/kg$	$€/kg$	$\$/kg$	$€/kg$	$\$/kg$	$€/kg$	$\$/kg$	$€/kg$
2.70	2.32	1.35	1.16	1.00	0.86	1.35	1.16

margin was considered in order to account for production maintenance, labour costs, machinery costs and of course a proper profit margin.

Table 4.13: Prototype and estimated prices.

scenario	prototype price	estimated price				
	final price $(€ \cdot m^{-2})$ [89]	alloy $(€ \cdot unit^{-1})$	PEG 200 $(€ \cdot unit^{-1})$	PCM $(€ \cdot unit^{-1})$	net margin $(\%)$	final price $(€ \cdot m^{-2})$
experimental	45.20	1.51	2.20	2.45	50	7.71
ideal	90.40	1.51	4.71	7.06	50	16.62

Going back to equation 4.1, we now already know the initial investment for the several studied scenarios and their respective annual cash-flows, rate of return and inflation rate. As table 4.14 shows, the experimental setting gives a total initial investment of $1358.00€$ which requires 32 years with annual electricity savings of $59.87€$ to refund its investment. On the other hand, the optimal scenario needs 78 years to depreciate the capital invested. However, when we look into the estimated price in a few years of a consolidated product in the market, those 32 and 78 years have an enormous slump to 5 and 8 years, respectively, which makes this PCM boards a highly attractive asset.

Table 4.14: Payback period values for the different scenarios.

scenario		initial investment I_0 (€)	rate of return r $(\%)$	inflation rate g $(\%)$	annual electricity savings C (€)	payback period t $(years)$
experimental	(prototype)	1358.00	5.27	3.19	59.87	32
	(estimated)	231.25	5.27	3.19	59.87	5
ideal	(prototype)	4339.20	5.27	3.19	114.54	78
	(estimated)	797.63	5.27	3.19	114.54	8

Comparing the payback period in both experimental (fig. 4.30) and ideal (fig. 4.31) scenarios, it can be seen that although the experimental amortizes three years earlier the investment, the ideal is more worthwhile in long term. By 14 years after the purchase and PCM installation, the ideal scenario would save $537.00€$, more $110.00€$ than in the experimental setting. Nonetheless, any of these cases are lucrative in the short and long term.

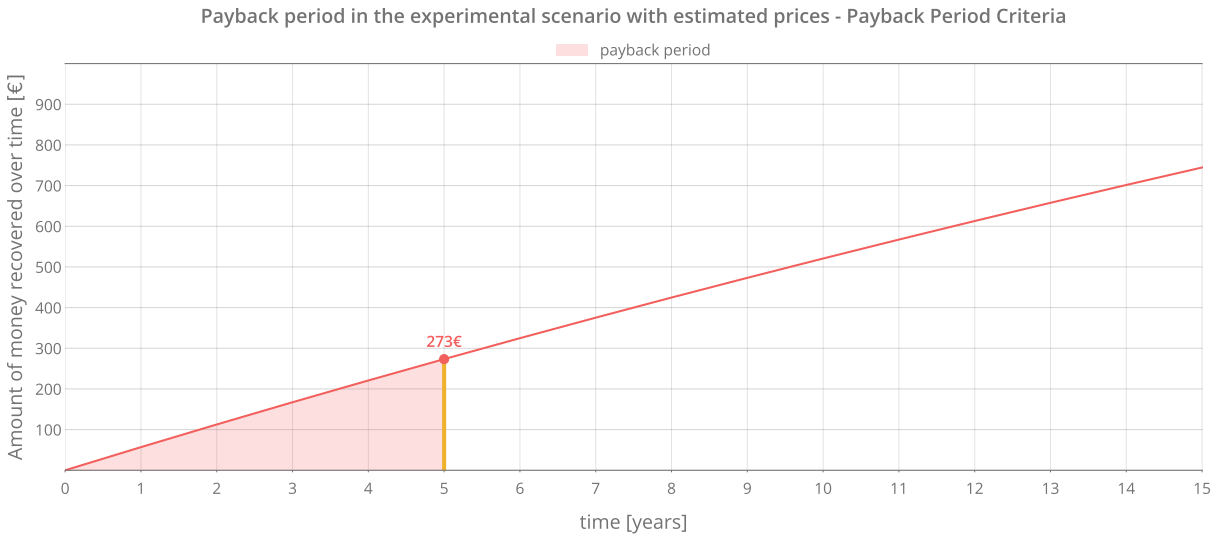

Figure 4.30: Payback period for the experimental scenario with estimated price.

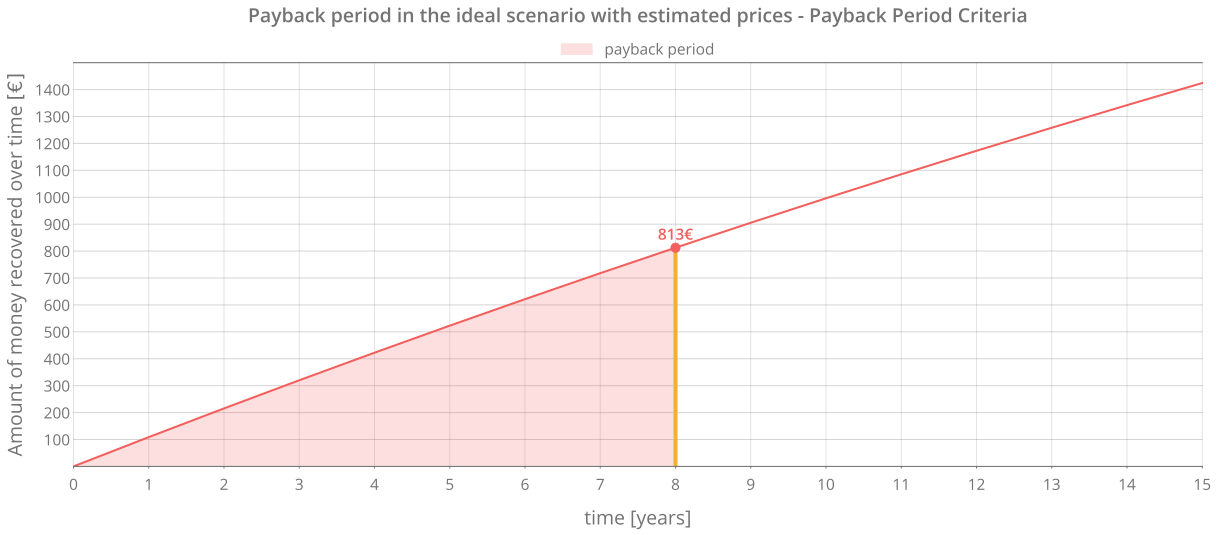

Figure 4.31: Payback period for the ideal scenario with estimated price.

4.5 Results overview

Summing up and looking up previous experimentally validated numerical and economic results (table 4.15), several conclusions can be consummated.

Firstly, as others studies had already mentioned [46], choosing proper PCM for an established place depends on its melting point, its quantity and its installation location. In this particular case, incorporating PCM in a low thermal inertia enclosure brings indubitable benefits in terms of cooling and heating energy demands, required to achieve a certain thermal comfort level.

However, when considering different PCM melting point values, it was demonstrated that lower ranges suited better the case-study of this work, which is an opposite conclusion to the outcome from previous

studies [65].

Furthermore, experimental and simulation tests verified the conclusion of Jiao et al. [49] that night ventilation increases the effectiveness of PCM, by aiding its latent heat stored release, and the higher the ACH provided the higher the improvement.

Increasing PCM thickness also increases its latent heat storage capacity [48], although this capacity converges for a certain value due to having unreachable inner PCM layers. In this sense, a PCM thickness-mass commitment must exist in order to come out the best solution for each specific case.

Moreover, the PCM location in the experimental set up revealed to be the best way to make the most of PCM boards. Using PCM as internal mass near ceiling took advantage of air stratification and night ventilation airflow. Nonetheless, incorporating it in walls also exhibited energy demand improvements.

In terms of number of boards used, the higher the amount the greater the latent heat storage capacity and, for this reason, the bigger the value of cooling energy demand savings.

Table 4.15: Simulation results overview.

Test number	PCM panel	Fan airflow (ACH)	PCM panel thickness (mm)	PCM panel location	Number of PCM panels	Energy savings (MWh)	Energy savings $(\%)$	Cost savings (€)	Cost savings $(\%)$
#1	PCM20	21.1	5.2	internal mass	30	0.591	3.18	62.06	3.21
#2	PCM22	21.1	5.2	internal mass	30	0.568	3.06	59.87	3.10
#3	PCM24	21.1	5.2	internal mass	30	0.548	2.94	57.87	3.00
#4	PCM26	21.1	5.2	internal mass	30	0.536	2.88	56.79	2.94
#5	PCM28	21.1	5.2	internal mass	30	0.531	2.86	56.25	2.91
#6	PCM30	21.1	5.2	internal mass	30	0.538	2.89	56.79	2.94
#7	PCM20	0	5.2	internal mass	30	0.448	2.41	47.26	2.45
#8	PCM20	5	5.2	internal mass	30	0.496	2.67	52.24	2.71
#9	PCM20	10	5.2	internal mass	30	0.534	2.87	56.16	2.91
#10	PCM20	15	5.2	internal mass	30	0.563	3.03	59.13	3.06
#11	PCM20	21.1	5.2	internal mass	30	0.591	3.18	62.06	3.21
#12	PCM20	21.1	5.2	internal mass	6	0.131	0.70	13.73	0.71
#13	PCM20	21.1	5.2	internal mass	12	0.255	1.37	26.72	1.38
#14	PCM20	21.1	5.2	internal mass	18	0.372	2.00	39.05	2.02
#15	PCM20	21.1	5.2	internal mass	24	0.484	2.60	50.82	2.63
#16	PCM20	21.1	5.2	internal mass	30	0.591	3.18	62.06	3.21
#17	PCM20	21.1	5.2	internal mass	36	0.692	3.72	72.78	3.77
#18	PCM20	21.1	5.2	internal mass	42	0.789	4.24	83.02	4.30
#19	PCM20	21.1	5.2	internal mass	48	0.882	4.74	92.78	4.80
#20	PCM20	21.1	5.2	internal mass	100	1.535	8.25	162.2	8.40
#21	PCM20	21.1	5.2	internal mass	6	0.131	0.70	13.73	0.71
#22	PCM20	21.1	5.2	North sided-door	6	−0.039	−0.21	−4.06	−0.21
#23	PCM20	21.1	5.2	South sided-door	6	−0.002	−0.01	−0.11	−0.01
#24	PCM20	21.1	5.2	internal mass	12	0.255	1.37	26.72	1.38
#25	PCM20	21.1	5.2	roof	12	−0.043	−0.23	−4.23	−0.22
#26	PCM20	21.1	5.2	floor	12	−0.164	−0.88	−17.02	−0.88
#27	PCM20	21.1	5.2	internal mass	13	0.274	1.48	28.82	1.49
#28	PCM20	21.1	5.2	East sided-wall	13	0.016	0.09	2.13	0.11
#29	PCM20	21.1	5.2	West sided-wall	13	0.038	0.20	3.59	0.19
#30	PCM20	21.1	5.2	internal mass	48	0.882	4.74	92.78	4.80
#31	PCM20	21.1	10	internal mass	48	1.080	5.81	114.54	5.93
#32	PCM20	21.1	20	internal mass	48	1.419	7.63	150.72	7.80

Table 4.15: Simulation results overview.

Test number	PCM panel	Fan airflow (ACH)	PCM panel thickness (mm)	PCM panel location	Number of PCM panels	Energy savings (MWh)	Energy savings $(\%)$	Cost savings (€)	Cost savings $(\%)$
#33	PCM20	21.1	30	internal mass	48	1.578	8.48	167.24	8.66
#34	PCM20	21.1	40	internal mass	48	1.639	8.81	173.36	8.97
#35	PCM20	21.1	50	internal mass	48	1.655	8.90	174.70	9.04

Chapter 5

Conclusions

5.1 Achievements

The aim of this thesis was to study the effect that the incorporation of PCM on a low thermal inertia building had in terms of its thermal mass, energy demand required to achieve thermal comfort by a HVAC system and respective costs. The main goal was accomplished and it showed that *DuPont Energain*® thermal mass boards are effective cooling systems when incorporated inside low thermal inertia buildings during Summer season. Experimental tests showed that thirty boards of this type installed as internal partitions in a shipping container are capable of delaying peak temperatures for three hours and improving the time that thermal comfort temperatures are met by 25%. This tangible and useful result is an accomplishment that must be highlighted. Nevertheless, although in the end it turned out to be a successful set up, the wooden structure built in the scope of this thesis had to be upgraded several times in order to sustain these boards effectively. This is due to the fact that these boards were not originally designed to be used as suspended pieces since they have a large shape change when the melting process occurs.

Nonetheless, software applications such as *EnergyPlus*® continue to prove being accurate enough to simulate this type of latent heat storage systems due to their recent supplements of PCM modules such as *MaterialProperty:PhaseChange* and *MaterialProperty:VariableThermalConductivity* and a CondFD solution algorithm. Moreover, a parametric study on these boards showed that a cooling system with forty eight units installed as internal mass with a melting temperature of $20°C$, a thickness of $10\,mm$ and a night ventilation that provides $21.1\,ACH$ is the best solution in this case. It saved more than 114€ and $5.5\,MWh$, demanding $18.60\,MWh$ and 17.52€ in total in terms of energy required to grant thermal comfort. Since these parameters affect the effectiveness of PCM, they should be taken into account when choosing the best PCM system for a certain building.

Finally, a simple economic analysis on the profitability of these boards demonstrated that although their current price is not permissive of a short payback period (38 years), in the future with a mass production

of these materials and the respective market price reduction, this technology should become more investment-attractive (5 years).

5.2 Future Work

As future work, and for a better and more accurate perception of the real impact that these boards can induce in a low thermal inertia building, two shipping containers should be used side by side, one with PCM and the other without. Additionally and if possible, melting temperatures, boards thickness, quantity and different spacing between them are among the experimental sensitivity analysis that could be done.

Furthermore and according to the knowledge obtained with this work, a boost in the container thermal mass could also be experimental and numerically tested by installing an outer insulation layer of extruded polystyrene with a thickness of $40\,mm$ in the container's enclosure. An *EnergyPlus*® model should be set so that its outcome could be compared both with the real experiment and the case without insulation. This will allow to perceive if this layer could prevent solar radiation from overheating the interior of the container and consequently enhance PCM boards effectiveness.

Bibliography

[1] Gi, K., Sano, F., Hayashi, A., Tomoda, T. and Akimoto, K. “A global analysis of residential heating and cooling service demand and cost-effective energy consumption under different climate change scenarios up to 2050”. *Mitigation and Adaptation Strategies for Global Change* 23.1 (2018), pages 51–79.

[2] Clarke, L., Eom, J., Marten, E. H., Horowitz, R., Kyle, P., Link, R., Mignone, B. K., Mundra, A. and Zhou, Y. “Effects of long-term climate change on global building energy expenditures”. *Energy Economics* 72 (2018), pages 667–677.

[3] Ürge-Vorsatz, D., Cabeza, L. F., Serrano, S., Barreneche, C. and Petrichenko, K. “Heating and cooling energy trends and drivers in buildings”. *Renewable and Sustainable Energy Reviews* 41 (2015), pages 85–98.

[4] Schrag, D. P. “The Timescales of Climate Change”. *ReVista (Cambridge)* 18.3 (2018), pages 2–82.

[5] Soares, N., Costa, J. J., Gaspar, A. R. and Santos, P. “Review of passive PCM latent heat thermal energy storage systems towards buildings’ energy efficiency”. *Energy and buildings* 59 (2013), pages 82–103.

[6] Wang, X., Zhang, Y., Xiao, W., Zeng, R., Zhang, Q. and Di, H. “Review on thermal performance of phase change energy storage building envelope”. *Chinese science bulletin* 54.6 (2009), pages 920–928.

[7] Dincer, I. and Rosen, M. A. *Thermal Energy Storage: Systems and Applications*. 2nd edition.

[8] Lane, G. *Solar heat storage: Latent heat materials*. 1st edition. Volume 1. Jan. 1983.

[9] Farid, M. M., Khudhair, A. M., Razack, S. A. K. and Al-Hallaj, S. “A review on phase change energy storage: materials and applications”. *Energy conversion and management* 45.9-10 (2004), pages 1597–1615.

[10] Al-Saadi, S. N. and Zhai, Z. J. “Modeling phase change materials embedded in building enclosure: A review”. *Renewable and Sustainable Energy Reviews* 21 (2013), pages 659–673.

[11] Chandra, S., Kumar, R., Kaushik, S. and Kaul, S. “Thermal performance of a non-air-conditioned building with PCCM thermal storage wall”. *Energy Conversion and Management* 25.1 (1985), pages 15–20.

[12] Akeiber, H., Nejat, P., Majid, M. Z. A., Wahid, M. A., Jomehzadeh, F., Famileh, I. Z., Calautit, J. K., Hughes, B. R. and Zaki, S. A. “A review on phase change material (PCM) for sustainable passive cooling in building envelopes”. *Renewable and Sustainable Energy Reviews* 60 (2016), pages 1470–1497.

[13] Sharma, A., Tyagi, V. V., Chen, C. and Buddhi, D. “Review on thermal energy storage with phase change materials and applications”. *Renewable and Sustainable energy reviews* 13.2 (2009), pages 318–345.

[14] Zhou, D., Zhao, C.-Y. and Tian, Y. “Review on thermal energy storage with phase change materials (PCMs) in building applications”. *Applied energy* 92 (2012), pages 593–605.

[15] Jankowski, N. R. and McCluskey, F. P. “A review of phase change materials for vehicle component thermal buffering”. *Applied Energy* 113 (2014), pages 1525–1561.

[16] Angayarkanni, S. and Philip, J. “Thermal conductivity measurements in phase change materials under freezing in presence of nanoinclusions”. *Journal of Applied Physics* 118.9 (2015), page 094306.

[17] Hawes, D., Feldman, D. and Banu, D. “Latent heat storage in building materials”. *Energy and buildings* 20.1 (1993), pages 77–86.

[18] Memon, S. A., Cui, H., Zhang, H. and Xing, F. “Utilization of macro encapsulated phase change materials for the development of thermal energy storage and structural lightweight aggregate concrete”. *Applied Energy* 139 (2015), pages 43–55.

[19] Jacob, R. and Bruno, F. “Review on shell materials used in the encapsulation of phase change materials for high temperature thermal energy storage”. *Renewable and Sustainable Energy Reviews* 48 (2015), pages 79–87.

[20] Waqas, A. and Din, Z. U. “Phase change material (PCM) storage for free cooling of buildings—a review”. *Renewable and sustainable energy reviews* 18 (2013), pages 607–625.

[21] Shi, X., Memon, S. A., Tang, W., Cui, H. and Xing, F. “Experimental assessment of position of macro encapsulated phase change material in concrete walls on indoor temperatures and humidity levels”. *Energy and Buildings* 71 (2014), pages 80–87.

[22] Schossig, P., Henning, H.-M., Gschwander, S. and Haussmann, T. “Micro-encapsulated phase-change materials integrated into construction materials”. *Solar Energy Materials and Solar Cells* 89.2-3 (2005), pages 297–306.

[23] Jamekhorshid, A., Sadrameli, S. and Farid, M. “A review of microencapsulation methods of phase change materials (PCMs) as a thermal energy storage (TES) medium”. *Renewable and Sustainable Energy Reviews* 31 (2014), pages 531–542.

[24] Kenisarin, M. and Mahkamov, K. “Solar energy storage using phase change materials”. *Renewable and sustainable energy reviews* 11.9 (2007), pages 1913–1965.

[25] Shilei, L., Guohui, F., Neng, Z. and Li, D. “Experimental study and evaluation of latent heat storage in phase change materials wallboards”. *Energy and buildings* 39.10 (2007), pages 1088–1091.

[26] Shilei, L., Neng, Z. and Guohui, F. “Impact of phase change wall room on indoor thermal environment in winter”. *Energy and buildings* 38.1 (2006), pages 18–24.

[27] Athienitis, A., Liu, C., Hawes, D., Banu, D. and Feldman, D. “Investigation of the thermal performance of a passive solar test-room with wall latent heat storage”. *Building and environment* 32.5 (1997), pages 405–410.

[28] Kuznik, F. and Virgone, J. “Experimental investigation of wallboard containing phase change material: Data for validation of numerical modeling”. *Energy and Buildings* 41.5 (2009), pages 561–570.

[29] Lai, C.-m. and Hokoi, S. “Thermal performance of an aluminum honeycomb wallboard incorporating microencapsulated PCM”. *Energy and Buildings* 73 (2014), pages 37–47.

[30] Ahmad, M., Bontemps, A., Sallée, H. and Quenard, D. “Thermal testing and numerical simulation of a prototype cell using light wallboards coupling vacuum isolation panels and phase change material”. *Energy and buildings* 38.6 (2006), pages 673–681.

[31] Cabeza, L. F., Castellon, C., Nogues, M., Medrano, M., Leppers, R. and Zubillaga, O. “Use of microencapsulated PCM in concrete walls for energy savings”. *Energy and buildings* 39.2 (2007), pages 113–119.

[32] Entrop, A. G., Brouwers, H. and Reinders, A. H. “Experimental research on the use of microencapsulated Phase Change Materials to store solar energy in concrete floors and to save energy in Dutch houses”. *Solar energy* 85.5 (2011), pages 1007–1020.

[33] Alawadhi, E. M. “Thermal analysis of a building brick containing phase change material”. *Energy and Buildings* 40.3 (2008), pages 351–357.

[34] Castell, A., Martorell, I., Medrano, M., Pérez, G. and Cabeza, L. F. “Experimental study of using PCM in brick constructive solutions for passive cooling”. *Energy and Buildings* 42.4 (2010), pages 534–540.

[35] Zhang, C., Chen, Y., Wu, L. and Shi, M. “Thermal response of brick wall filled with phase change materials (PCM) under fluctuating outdoor temperatures”. *Energy and Buildings* 43.12 (2011), pages 3514–3520.

[36] Silva, T., Vicente, R., Soares, N. and Ferreira, V. “Experimental testing and numerical modelling of masonry wall solution with PCM incorporation: a passive construction solution”. *Energy and Buildings* 49 (2012), pages 235–245.

[37] Weinlaeder, H., Koerner, W. and Heidenfelder, M. “Monitoring results of an interior sun protection system with integrated latent heat storage”. *Energy and Buildings* 43.9 (2011), pages 2468–2475.

[38] Manz, H., Egolf, P., Suter, P. and Goetzberger, A. “TIM–PCM external wall system for solar space heating and daylighting”. *Solar energy* 61.6 (1997), pages 369–379.

[39] Weinläder, H., Beck, A. and Fricke, J. “PCM-facade-panel for daylighting and room heating”. *Solar Energy* 78.2 (2005), pages 177–186.

[40] Bontemps, A., Ahmad, M., Johannès, K. and Sallée, H. “Experimental and modelling study of twin cells with latent heat storage walls”. *Energy and Buildings* 43.9 (2011), pages 2456–2461.

[41] Pedersen, C. O. “Advanced zone simulation in EnergyPlus: incorporation of variable properties and phase change material (PCM) capability”. *Building simulation*. 2007, pages 1341–1345.

[42] Shrestha, S. S., Miller, W. A., Stovall, T. K., Desjarlais, A. O., Childs, K. W., Porter, W. D., Bhandari, M. S. and Coley, S. J. *Modeling PCM-enhanced insulation system and benchmarking EnergyPlus against controlled field data*. Technical report. Oak Ridge National Laboratory (ORNL); Building Technologies Research and Integration Center, 2011.

[43] Tardieu, A., Behzadi, S., Chen, J. J. and Farid, M. M. “Computer simulation and experimental measurements for an experimental PCM-impregnated office building”. *Proceedings of the building simulation 2011: 12th conference of international building performance simulation association*. Volume 1. 2011, pages 56–63.

[44] Evola, G., Papa, N., Sicurella, F. and Wurtz, E. “Simulation of the behaviour of phase change materials for the improvement of thermal comfort in lightweight buildings”. *Proceedings of Building Simulation*. 2011, pages 1299–1306.

[45] Tabares-Velasco, P. C., Christensen, C. and Bianchi, M. “Verification and validation of EnergyPlus phase change material model for opaque wall assemblies”. *Building and Environment* 54 (2012), pages 186–196.

[46] Evola, G., Marletta, L. and Sicurella, F. “A methodology for investigating the effectiveness of PCM wallboards for summer thermal comfort in buildings”. *Building and Environment* 59 (2013), pages 517–527.

[47] Sage-Lauck, J. and Sailor, D. “Evaluation of phase change materials for improving thermal comfort in a super-insulated residential building”. *Energy and Buildings* 79 (2014), pages 32–40.

[48] Soares, N., Gaspar, A., Santos, P. and Costa, J. “Multi-dimensional optimization of the incorporation of PCM-drywalls in lightweight steel-framed residential buildings in different climates”. *Energy and buildings* 70 (2014), pages 411–421.

[49] Jiao, F. and Xu, P. “Simulation and feasibility analysis of PCM based passive cooling technique in residential house”. *Procedia Engineering* 121 (2015), pages 1969–1976.

[50] Marin, P., Saffari, M., Gracia, A. de, Zhu, X., Farid, M. M., Cabeza, L. F. and Ushak, S. “Energy savings due to the use of PCM for relocatable lightweight buildings passive heating and cooling in different weather conditions”. *Energy and Buildings* 129 (2016), pages 274–283.

[51] Yang, C., Susman, G. and Dowson, M. “EnergyPlus model of novel PCM cooling system validated with installed system data”. *Proceedings of SimBuild* 6.1 (2016).

[52] Saffari, M., Gracia, A. de, Ushak, S. and Cabeza, L. F. “Economic impact of integrating PCM as passive system in buildings using Fanger comfort model”. *Energy and Buildings* 112 (2016), pages 159–172.

[53] Jamil, H., Alam, M., Sanjayan, J. and Wilson, J. “Investigation of PCM as retrofitting option to enhance occupant thermal comfort in a modern residential building”. *Energy and Buildings* 133 (2016), pages 217–229.

[54] Ozdenefe, M. and Dewsbury, J. “Thermal performance of a typical residential Cyprus building with phase change materials”. *Building Services Engineering Research and Technology* 37.1 (2016), pages 85–102.

[55] Lei, J., Yang, J. and Yang, E.-H. “Energy performance of building envelopes integrated with phase change materials for cooling load reduction in tropical Singapore”. *Applied Energy* 162 (2016), pages 207–217.

[56] Nghana, B. and Tariku, F. “Phase change material’s (PCM) impacts on the energy performance and thermal comfort of buildings in a mild climate”. *Building and Environment* 99 (2016), pages 221–238.

[57] Auzeby, M., Wei, S., Underwood, C., Tindall, J., Chen, C., Ling, H. and Buswell, R. “Effectiveness of using phase change materials on reducing summer overheating issues in UK residential buildings with identification of influential factors”. *Energies* 9.8 (2016), page 605.

[58] Zhou, D., Tian, Y., Qu, Y. and Chen, Y. “Thermal analysis of phase change material board (PCMB) under weather conditions in the summer”. *Applied Thermal Engineering* 99 (2016), pages 690–702.

[59] Ramakrishnan, S., Wang, X., Alam, M., Sanjayan, J. and Wilson, J. “Parametric analysis for performance enhancement of phase change materials in naturally ventilated buildings”. *Energy and Buildings* 124 (2016), pages 35–45.

[60] Mi, X., Liu, R., Cui, H., Memon, S. A., Xing, F. and Lo, Y. “Energy and economic analysis of building integrated with PCM in different cities of China”. *Applied Energy* 175 (2016), pages 324–336.

[61] Long, X., Zhang, W., Li, Y. and Zheng, L. “Thermal performance improvement of lightweight buildings integrated with phase change material: An experimental and simulation study”. *Advances in Mechanical Engineering* 9.6 (2017), page 1687814017702082.

[62] Soares, N., Reinhart, C. F. and Hajiah, A. “Simulation-based analysis of the use of PCM-wallboards to reduce cooling energy demand and peak-loads in low-rise residential heavyweight buildings in Kuwait”. *Building Simulation*. Volume 10. 4. Springer. 2017, pages 481–495.

[63] Alam, M., Sanjayan, J., Zou, P. X., Ramakrishnan, S. and Wilson, J. “A comparative study on the effectiveness of passive and free cooling application methods of phase change materials for energy efficient retrofitting in residential buildings”. *Procedia engineering* 180 (2017), pages 993–1002.

[64] Devaux, P. and Farid, M. M. “Benefits of PCM underfloor heating with PCM wallboards for space heating in winter”. *Applied energy* 191 (2017), pages 593–602.

[65] Kharbouch, Y., Mimet, A., El Ganaoui, M. and Ouhsaine, L. “Thermal energy and economic analysis of a PCM-enhanced household envelope considering different climate zones in Morocco”. *International Journal of Sustainable Energy* 37.6 (2018), pages 515–532.

[66] *SAP 2009 – Fabric energy efficiency & thermal mass*. MPA – The Concrete Centre. Feb. 2010.

[67] *20’ General Purpose Container. Singamas website.* 2018. URL: http://www.singamas.com/en-us/products/detail/12 (visited on 17/04/2018).

[68] *Contentores Standard. Nippon Express Portugal website.* 2018. URL: https://www.nipponexpress.pt/servicos/informacao-util/dimensoes-dos-contentores/contentores-standard#top (visited on 17/04/2018).

[69] *EN 1.8967 (S355K2W) Weathering Steel. Material Properties Database website.* 2018. URL: https://www.makeitfrom.com/material-properties/EN-1.8967-S355K2W-Weathering-Steel (visited on 12/04/2018).

[70] *Plasticized (Flexible) Polyvinyl Chloride (PVC-P). Material Properties Database website.* 2018. URL: https://www.makeitfrom.com/material-properties/Plasticized-Flexible-Polyvinyl-Chloride-PVC-P (visited on 12/04/2018).

[71] *Medium Density Fiberboard (MDF). Material Properties Database website.* 2018. URL: https://www.makeitfrom.com/material-properties/Medium-Density-Fiberboard-MDF (visited on 12/04/2018).

[72] Peel, M. C., Finlayson, B. L. and McMahon, T. A. “Updated world map of the Köppen-Geiger climate classification”. *Hydrology and earth system sciences discussions* 4.2 (2007), pages 439–473.

[73] *Type T Thermocouple. Thermocouple Info website.* 2018. URL: https://www.thermocoupleinfo.com/type-t-thermocouple.htm (visited on 17/04/2018).

[74] *HOBO Temperature Relative Humidity Data Logger: U10-003. Onset website.* 2018. URL: https://www.onsetcomp.com/products/data-loggers/u10-003 (visited on 17/04/2018).

[75] *Davis 6152 Wireless Vantage Pro2 Weather Station. eBay website.* 2018. URL: https://www.ebay.com/p/Davis-6152-Wireless-Vantage-Pro2-Weather-Station/2292303308 (visited on 11/04/2018).

[76] *Weather Data by Location: All Regions - Europe WMO Region 6 - Portugal - Lisboa 085360 (INETI). EnergyPlus site.* 2018. URL: https://energyplus.net/weather-location/europe_wmo_region_6/PRT//PRT_Lisboa.085360_INETI (visited on 15/04/2018).

[77] *Cata LHV 190. Cata website.* 2018. URL: http://www.cata.es/es/catalogo/a%C3%A9ration/wall-extraction/lhv/153/ (visited on 15/04/2018).

[78] Alghoul, S. “A Comparative Study of Energy Consumption for Residential HVAC Systems Using EnergyPlus”. *American Journal of Mechanical and Industrial Engineering* 2.2 (2017), pages 98–103.

[79] *Clock Changes in Lisbon, Portugal (Lisboa) in 2017. Time and date website*. 2018. URL: https://www.timeanddate.com/time/change/portugal/lisbon?year=2018 (visited on 17/04/2018).

[80] *Pordata: Return rate of treasury bonds. Pordata site.* 2018. URL: https://www.pordata.pt/en/Portugal/Return+rate+of+treasury+bonds-2803 (visited on 14/09/2018).

[81] *Pordata. Inflation Rate (Growth Rate - Consumer Price Index): total and individual consumption by purpose. Pordata site.* 2018. URL: https://www.pordata.pt/en/Portugal/Inflation+Rate+(Growth+Rate+++Consumer+Price+Index)+total+and+individual+consumption+by+purpose-2315 (visited on 14/09/2018).

[82] *Phase Change Materials: And the Arup thermal calculator. Robert Matthews SelfBuild site.* 2018. URL: https://irp-cdn.multiscreensite.com/e3960383/files/uploaded/2014%20K%20Phase%20change%20materials.pdf (visited on 11/07/2018).

[83] *US dollar (USD). European Central Bank site.* 2018. URL: https://www.ecb.europa.eu/stats/policy_and_exchange_rates/euro_reference_exchange_rates/html/eurofxref-graph-usd.en.html (visited on 18/09/2018).

[84] *Alloy 8011. Alibaba site.* 2018. URL: https://www.alibaba.com/product-detail/2018-Hotsale-Aluminum-Foil-Jumbo-Roll_1613063452.html?spm=a2700.7724857.normalList.1.344c690eKR9Nrs (visited on 14/09/2018).

[85] *Polyethylene Glycol 200 (PEG 200). Alibaba site.* 2018. URL: https://www.alibaba.com/product-detail/Factory-price-PEG-200-400-600_60251067131.html?spm=a2700.7724838.2017115.97.16dd6e71GjHGPB (visited on 14/09/2018).

[86] *N-heptadecane, paraffin wax. Alibaba site.* 2018. URL: https://www.alibaba.com/product-detail/high-quality-best-price-629-78_60746572829.html?spm=a2700.7724838.2017115.30.316db5e52ZtRNv (visited on 14/09/2018).

[87] *Polyethylene Glycol 600 (PEG 600). Alibaba site.* 2018. URL: https://www.alibaba.com/product-detail/Factory-price-PEG-200-400-600_60251067131.html?spm=a2700.7724838.2017115.51.52383747Zbg4tT (visited on 14/09/2018).

[88] *Aluminum 8011 Alloy (UNS A98011). Azo Materials site.* 2018. URL: https://www.azom.com/article.aspx?ArticleID=8782 (visited on 18/09/2018).

[89] *Pound sterling (GBP). European Central Bank site.* 2018. URL: https://www.ecb.europa.eu/stats/policy_and_exchange_rates/euro_reference_exchange_rates/html/eurofxref-graph-gbp.en.html (visited on 18/09/2018).

Appendix A

Technical Datasheets

A.1 DuPont Energain Datasheet

DUPONT™ ENERGAIN®

Energy-saving thermal mass systems

THERMAL MASS PANEL

Descriptive properties		Unit	Value
Thickness		mm	5.2
Width		mm	1000
Length		mm	1198
Area weight		kg/m²	4.5
Aluminium thickness (sheet)		µm	100
Aluminium thickness (edges)		µm	75
Thermal properties	**Test Method**		
Paraffin loading	Comparative test by DSC	%	60
Melt point (paraffin)	DSC method (1°C/min)	°C	21.7
Latent heat storage capacity (0°C - 30°C)	DSC method (1°C/min)	kJ/kg	> 70
Total heat storage capacity (Temperature range 0°C to 30°C)	DSC method (1°C/min)	kJ/kg	~ 140
Physical properties			
Aluminium sheet delamination force	Internal DuPont test method	N/cm	> 20
Conductivity solid	BS EN 12667-2001	W/(m.K)	0.18
Conductivity liquid	BS EN 12667-2001	W/(m.K)	0.14
Flash Point (paraffin)	ASTM D56	°C	148

PRODUCT DESCRIPTION

The panel is a fine mixture of ethylene based polymer (40%) designed by DuPont and paraffin wax (60%) laminated on both sides with a 100 µm aluminium sheet. The edges are closed with a 75 µm aluminium tape.

REACTION TO FIRE

Single-flame source test	EN 11925-2	Class E
Surface spread of flame test	BS476-7	Class 1

DURABILITY

Predicted to be durable for the life-time of a building

Chemically inert with most materials

ALUMINIUM TAPE

Descriptive Properties	Unit	Value
Thickness	µm	75
Width	mm	50

DuPont patented technology

All values correspond to average results obtained in our laboratories and outside institutes and are indicative.
The right is reserved to make changes at any time without notice.

DuPont de Nemours (Luxembourg) S.à r.l.
Rue Général Patton
L-2984 Luxembourg
Tel: 00352 3666 5885
Fax: 00352 3666 5021
E-mail: energain@lux.dupont.com
www.energain.dupont.com

12/2011

Appendix B

Tables

Table B.1: Thermal inertia or thermal mass of the shipping container surfaces using equation 2.7.

surface	material	L length (m)	ρ density $(kg \cdot m^{-3})$	c_p specific heat capacity $(J \cdot kg^{-1} \cdot K^{-1})$	λ thermal inertia $(J \cdot m^{-2} \cdot K^{-1})$
North sided-door	corten steel	0.0025	7800	470	9165
South sided-door	PVC-P	0.002	1400	1400	13085
	corten steel	0.0025	7800	470	
East sided-wall	PVC-P	0.002	1400	1400	13085
	corten steel	0.0025	7800	470	
West sided-wall	corten steel	0.0035	7800	470	12831
Roof	corten steel	0.0025	7800	470	9165
Floor	MDF	0.010	750	1700	31080
	corten steel	0.005	7800	470	

Table B.2: Stored sensible heat on the shipping container surfaces using equation 2.1 with $T_i = 18°C$ and $T_f = 35°C$ and the values in table 3.2.

surface	material	m mass (kg)	c_p specific heat capacity $(J \cdot kg^{-1} \cdot K^{-1})$	Q stored heat (Wh)
North sided-door	corten steel	246.357	470	546.777
South sided-door	PVC-P	35.374	1400	780.641
	corten steel	246.357	470	
East sided-wall	PVC-P	87.899	1400	1939.75
	corten steel	612.155	470	
West sided-wall	PVC-P	43.950	1400	1649.2
	corten steel	612.155	470	
Roof	corten steel	576.007	470	1278.41
Floor	MDF	110.771	1700	1649.2
	corten steel	576.007	470	

Table B.3: Overall heat transfer coefficient of shipping container's surfaces.

surface	layer	U_i $(W \cdot m^{-2} \cdot K^{-1})$	U $(W \cdot m^{-2} \cdot K^{-1})$
North sided-door Roof	corten steel	8400	8400
West sided-wall	corten steel	8400	84.149
	PVC-P	85	
East wall South door	PVC-P	85	42.286
	corten steel	8400	
	PVC-P	85	
Floor	MDF	30	29.893
	corten steel	8400	

Table B.5: Variable thermal conductivity for PCM chosen.

	thermal conductivity $\left(W \cdot m^{-1} \cdot K^{-1}\right)$		
	solid phase		liquid phase
	0.18	0.18	0.14
PCM20	$15.5°C$	$18°C$	$19.7°C$
PCM22	$17.5°C$	$20°C$	$21.7°C$
PCM24	$19.5°C$	$22°C$	$23.7°C$
PCM26	$21.5°C$	$24°C$	$25.7°C$
PCM28	$23.5°C$	$26°C$	$27.7°C$
PCM30	$25.5°C$	$28°C$	$29.7°C$

Table B.4: Table of The Köppen-Geiger climate classification adapted from *"Updated world map of the Köppen-Geiger climate classification"* [72].

1^{st}	2^{nd}	3^{rd}	description	criteria*
A			Tropical	$T_{cold} \geq 18$
	f		Rainforest	$P_{dry} \geq 60$
	m		Monsoon	$100 - \frac{MAP}{25} < P_{dry} < 60$
	w		Savannah	$(P_{dry} < 60) \wedge \left(P_{dry} < 100 - \frac{MAP}{25}\right)$
B			Arid	$MAP < 10 \times P_{threshold}$
	W		Desert	$MAP < 5 \times P_{threshold}$
	S		Steppe	$MAP \geq 5 \times P_{threshold}$
		h	Hot	$MAT \geq 18$
		k	Cold	$MAT < 18$
C			Temperate	$(T_{hot} > 10) \wedge (0 < T_{cold} < 18)$
	s		Dry Summer	$\left(P_{s_{dry}} < 40\right) \wedge \left(P_{s_{dry}} < \frac{P_{w_{wet}}}{3}\right)$
	w		Dry Winter	$P_{w_{dry}} < \frac{P_{s_{wet}}}{10}$
	f		Without dry season	$\left[\left(P_{s_{dry}} \geq 40\right) \vee \left(P_{s_{dry}} \geq \frac{P_{w_{wet}}}{3}\right)\right] \wedge \left(P_{w_{dry}} \geq \frac{P_{s_{wet}}}{10}\right)$
		a	Hot Summer	$T_{hot} \geq 22$
		b	Warm Summer	$(T_{hot} < 22) \wedge (T_{mon_{10}} \geq 4)$
		c	Cold Summer	$(T_{hot} < 22) \wedge (1 \leq T_{mon_{10}} < 4)$
D			Cold	$(T_{hot} > 10) \wedge (T_{cold} \leq 0)$
	s		Dry Summer	$\left(P_{s_{dry}} < 40\right) \wedge \left(P_{s_{dry}} < \frac{P_{w_{wet}}}{3}\right)$
	w		Dry Winter	$P_{w_{dry}} < \frac{P_{s_{wet}}}{10}$
	f		Without dry season	$\left[\left(P_{s_{dry}} \geq 40\right) \vee \left(P_{s_{dry}} \geq \frac{P_{w_{wet}}}{3}\right)\right] \wedge \left(P_{w_{dry}} \geq \frac{P_{s_{wet}}}{10}\right)$
		a	Hot Summer	$T_{hot} \geq 22$
		b	Warm Summer	$(T_{hot} < 22) \wedge (T_{mon_{10}} \geq 4)$
		c	Cold Summer	$(T_{hot} < 22) \wedge (1 \leq T_{mon_{10}} < 4)$
		d	Very cold Winter	$(T_{hot} < 22) \wedge (T_{mon_{10}} < 4) \wedge (T_{cold} < -38)$
E			Polar	$T_{hot} < 10$
	T		Tundra	$T_{hot} > 0$
	F		Frost	$T_{hot} \leq 0$

MAP = mean annual precipitation | MAT = mean annual temperature | T_{hot} = temperature of the hottest month | T_{cold} = temperature of the coldest month | $T_{mon_{10}}$ = number of months where the temperature is above 10 | P_{dry} = precipitation of the driest month | $P_{s_{dry}}$ = precipitation of the driest month in Summer | $P_{w_{dry}}$ = precipitation of the driest month in Winter | $P_{s_{wet}}$ = precipitation of the wettest month in Summer | $P_{w_{wet}}$ = precipitation of the wettest month in Winter | $P_{threshold}$ = varies according to the following rules: if 70% of MAP occurs in winter $\rightarrow$ $P_{threshold} = 2 \times MAT$; if 70% of MAP occurs in Summer $\rightarrow$ $P_{threshold} = 2 \times MAT + 28$; otherwise $\rightarrow$ $P_{threshold} = 2 \times MAT + 14$ | Summer (Winter) is defined as the warmer (cooler) six month period of ONDJFM and AMJJAS.